Politecnico di Torino

Corso di Laurea Magistrale in Ingegneria Meccanica
(Mechanical Engineering)
A.a. 2023/2024

Sessione di Laurea di Ottobre 2024

FE-modelling of flexible pipes in aftertreatment system for trucks and buses

Relatori
Andrei Tchernov
Prof. Carlo Rosso
Prof. Mårten Olsson

Candidato
Paolo Bellieni

Abstract

Exhaust flexible pipes are components characterised by a complex dynamic behaviour. Friction is generated by internal contacts in the interlock and entails a dynamic softening phenomenon as the excitation amplitude increases.

Due to their complex geometry, the modelling is complicated. The purpose of the thesis is to improve the dynamic model by investigating different Finite Element formulations. Shell, connector, and thin-walled pipe elements are implemented in Abaqus, and numerical modal analysis is run.
The models are adjusted in order to fit the first two experimental eigenfrequencies identified by running frequency sweeps in shaker tests. Depending on the method, either manual or automatic parametric optimization in Heeds is performed.

The results from different models are compared among themselves and in relation to the measurements, and their corresponding pros and cons are stated.
Since the pipe elements turn out to be the most efficient and applicable way of modelling for the first case-study of an U-shaped bellow, the method is adopted for other single components and a dual bellow assembly as validation.
The model succeeds in fitting the eigenfrequencies for another bellow and its implementation in the complete pipe-assembly allows for coherent results with experimental tests. The match is not reached for a welded flexible hose.

New measurements on the shaker table are performed with the aim of capturing the dynamic behaviour of flexible hose, but different results are obtained by using different ways of attaching the accelerometer. The comparison between frequency sweeps at different constant acceleration amplitudes evidences a softening phenomenon due to non-linear behaviour, which strongly affects the response of the component.

Keywords: Exhaust flexible pipes, Finite Element Method, Modal Analysis, Equivalent thin-walled pipe elements, Shaker test, Non-linear dynamics.

Preface

This Master's thesis has been carried out at the Scania Research and Development centre in Södertälje during the spring of 2024 as final part of the Master's degree programme in Mechanical Engineering at Politecnico di Torino and during the exchange period in Solid Mechanics track at KTH Royal Institute of Technology.
The thesis has been presented at the Scania Research and Development centre in the presence of the examiner from KTH. It is also going to be discussed at Politecnico di Torino during the autumn.

List of Figures

IV

VI

List of Tables

X

Nomenclature

$\bar{\gamma}_y$ Average shear deformation of the beam $[-]$

χ_y Rotation of the beam cross-section [rad]

ϵ^o Elongation of the beam $[-]$

κ Timoshenko's shear coefficient $[-]$

κ_z Curvature of the beam $[-]$

ν_p Poisson's ratio of equivalent pipe element $[-]$

ρ Density of the material of flexible pipe $[\frac{\text{kg}}{\text{m}^3}]$

ρ_i Density of equivalent pipe element of inner part $[\text{kg/m}^3]$

ρ_p Density of equivalent pipe element $[\text{kg/m}^3]$

ρ_s Density of equivalent pipe element of the straight part of bellow $[\text{kg/m}^3]$

θ Rotation around beam axis [rad]

A Cross-sectional area of the beam $[\text{m}^2]$

A_p Cross-sectional area of equivalent pipe element $[\text{m}^2]$

b_c Bending stiffness of the single connector element $[\frac{\text{Nm}}{\text{rad}}]$

b_T Bending stiffness of the flexible pipe $[\frac{\text{Nm}}{\text{rad}}]$

c Torsion stiffness of half convolution $[\frac{\text{Nm}}{\text{rad}}]$

c_c Torsion stiffness of the single connector element $[\frac{\text{Nm}}{\text{rad}}]$

c_i Torsion stiffness of equivalent pipe element of inner part $[\frac{\text{Nm}}{\text{rad}}]$

c_T Torsion stiffness of the flexible pipe $[\frac{\mathrm{Nm}}{\mathrm{rad}}]$

D Diameter of the U-shaped bellow [m]

E Young's modulus of the material of flexible pipe [GPa]

E_p Young's modulus of equivalent pipe element [GPa]

G Shear modulus of the beam material $[\frac{\mathrm{N}}{\mathrm{m}^2}]$

G_p Shear modulus of equivalent pipe element [GPa]

h Height of the convolution [m]

I_p Area moment of inertia of equivalent pipe element $[\mathrm{m}^4]$

I_z Second moment of inertia of the beam $[\mathrm{m}^4]$

J Mass moment of inertia per unit length of equivalent pipe element [kgm]

k Axial stiffness of half convolution $[\frac{\mathrm{N}}{\mathrm{m}}]$

k_c Axial stiffness of the single connector element $[\frac{\mathrm{N}}{\mathrm{m}}]$

k_i Axial stiffness of equivalent pipe element of inner part $[\frac{\mathrm{N}}{\mathrm{m}}]$

K_p Polar area moment of inertia of equivalent pipe element $[\mathrm{m}^4]$

k_T Axial stiffness of the flexible pipe $[\frac{\mathrm{N}}{\mathrm{m}}]$

L Length of the flexible pipe [m]

m Distributed moment load [N]

m Mass of the flexible pipe [kg]

m_c Mass of the single connector element [kg]

m_e Mass of the end-caps [kg]

M_z Bending moment in beam cross-section [Nm]

n Number of convolutions on the bellow [-]

n_c Number of connector elements $[-]$

N_x Axial force in beam cross-section [N]

q_x Distributed load along beam axis $[\frac{N}{m}]$

q_y Distributed load perpendicular to beam axis $[\frac{N}{m}]$

R Rotary inertia of the beam $[\frac{kg}{m^2}]$

R_c Meridional radius of the convolution crown [m]

R_m Mean radius of the bellow [m]

R_r Meridional radius of the convolution root [m]

$R_{m,i}$ Mean radius of the inner part [m]

$R_{m,s}$ Mean radius of the equivalent pipe element of the straight part of bellow [m]

S Shear stiffness of the beam [N]

s Thickness of the bellow [mm]

s_p Wall thickness of equivalent pipe element of bellow [m]

s_s Wall thickness of equivalent pipe element of the straight part of bellow [m]

t_c Transverse stiffness of the single connector element $[\frac{N}{m}]$

t_T Transverse stiffness of the flexible pipe $[\frac{Nm}{rad}]$

u Displacement along the beam [m]

V_y Shear force in beam cross-section [N]

w Displacement perpendicular to the beam [m]

w_b Perpendicular displacement of the beam due to bending [m]

Acronyms

FRF Frequency response function

FEM Finite element method

FE Finite element

DOF Degree of freedom

SDOF Single degree of freedom

MDOF Multiple degree of freedom

CAD Computer-aided design

ASME American Society of Mechanical Engineers

EJMA Expansion Joints Manufacturing Association

SHERPA Simultaneous Hybrid Exploration that is Robust, Progressive, and Adaptive

Contents

Chapter 1

Introduction

1.1 Introduction and historical notes

"Although invented about hundreds of years ago, exhaust metal bellows play today an important role in modern automotive engineering and emissions control"[1].

Flexible pipes, hoses, or expansion joints are mechanical components that are widely used in various industrial applications for different purposes. Even if the field of application changes, the main purpose remains the same. In the presence of axial and angular movements, high internal pressure, and hot or cold fluid flow; flexible pipes are included in larger installations in order to provide greater flexibility and reduce the risk of failure.

In the last sixty years, various researchers have conducted studies on the application of metal flexible pipes in different industries using analytical, numerical, and experimental approaches. They are concerned above all with piping apparatuses in the automotive sector and offshore oil industries, as shown in Figs. 1.1.1a and 1.1.1b, respectively, but also in heat exchangers, power plants, and the chemical sector.
Only automotive flexible pipes, with a special consideration for heavy trucks, are debated in this thesis. In order to have a broader framework about various fields of application, it is suggested to glance at the recent review made by S.D. Wankhede and S.H. Gawande which represents an exhaustive summary of the investigations of the bellows up to the last years[2].

In the heavy truck industry, flexible pipes play an important role, especially in the connection between the engine and exhaust after-treatment system. Here, the components are linked by piping systems exposed to external excitation due to the closeness of the engine and road irregularities.

The presence of flexible pipes facilitates these connections thanks to tolerances and decouples the load transferred between parts by reducing the transmission of vibrations and allowing for a general low level of vibration. At the same time, high temperatures and gas corrosion entail the need for a specific design in order to maintain the same level of performance during their working lives.
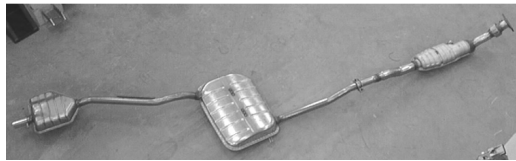
(a) **Automobile exhaust system[3].**
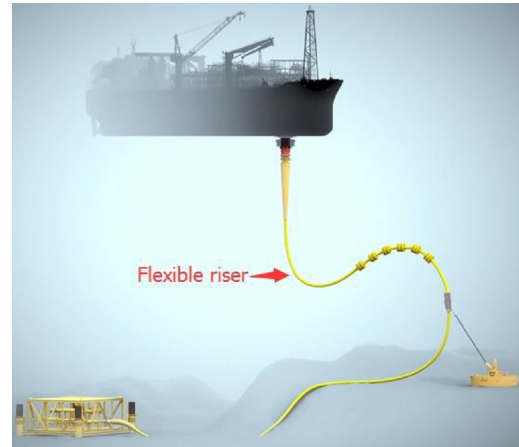
(b) **Flexible risers in offshore oil industries[4].**

Figure 1.1.1: **Applications of flexible pipes in different industries.**

Furthermore, in the last few years, after-treatment design has been affected by new emission legislations Euro 6[5], starting in 2014, and Euro 7[6], forecasted for 2026, which tighten up the exhaust emission limits for buses and trucks. It directly affects the choice of flexible pipes that need to be gas-tight in order to guarantee more robustness and reliability in avoiding leakages of exhaust gases.

In this scenario, the role of simulations turns out to be fundamental in the development of new design solutions, allowing for a decrease in the amount of physical testing as well as the time required. Due to the complex structure, it is not obvious which is the most efficient method of simulating the behaviour, and different finite element formulations are considered in different simulation procedures.

Of all the cases, the dynamic behaviour turns out to be complicated to simulate because of the complex geometry and non-linear behaviour, that arises from contacts among the parts and internal friction. High temperatures and ageing phenomena contribute to making the problem difficult, but these aspects are not included in this work.

An important research project on this topic was conducted by G. Broman, M. Hermann, and A. Jönsson[1]. This procedure inspired the extended investigation of J. Wall[3] who investigated the entity of the non-linear behaviour.

Experimental modal analysis is used as a reference for the development of reliable simulations. Due to the difficulty of testing in operating conditions, tests are usually performed on shaker tables without considering the effects of temperature and internal pressure. Both new and aged components can be used, although this thesis includes only the first type.

1.2 Purpose and structure of the work

After defining appropriate guidelines for the simulation of exhaust flexible pipes for static and fatigue load cases, this work arises from the need to improve the dynamic model of exhaust flexible pipes used in the Strength Simulation group from Emission Solutions Development in Scania CV AB.

Different finite element formulations have been investigated in order to develop a simple yet reliable method of modelling.
The main purpose is to predict the dynamic behaviour of different flexible pipes and larger systems with higher accuracy and increase overall simulation reliability.

The report consists of different chapters. Following the introduction, a state of the art review includes a description of how flexible pipes are composed and recalls different methodologies, evidencing pros and cons. The theory behind vibration mechanics is presented together with the Finite Element Method by considering the different finite element formulations.
The case studies are then presented, and the methodology motivates the procedure followed in the investigation. Experimental setups are also shown, and the related measurements are reported.
Different methodologies of modelling are proposed, and the analysis procedure is presented. The corresponding results are shown for each component and then discussed. In the last part, the conclusions are drawn and the future work is defined.

Chapter 2

State of the art

2.1 Exhaust flexible pipes: terminology and structure

The term flexible pipes can be misleading because it is used to indicate a vast category of components that are rather different. By referring to catalogues from manufacturer companies[7], it is possible to make a distinction between flexible hoses and expansion joints.
Flexible connectors or hoses, as shown in Fig. 2.1.1a, are used in the presence of high-frequency, low-amplitude vibrations, but they are not designed to compress, compensate for pipe expansion, or correct major misalignments in exhaust piping. They are constructed from a single ply of small corrugations.

(a) **Flexible hoses from manufacturing company[9].**

(b) **Expansion joints from manufacturing company[10].**

Figure 2.1.1: **Components from manufacturing company.**

Expansion joints or bellows, in Fig. 2.1.1b, have larger corrugations that allow them

to compress more and tolerate pipe misalignment. They usually have a multi-ply construction and are designed to absorb pipe expansion. The total movement capacity of the bellows is proportional to the number of convolutions[8].

Boiler & Pressure Vessel Code of the American Society of Mechanical Engineers (ASME) and Standards of the Expansion Joints Manufacturing Association (EJMA)[8] represent the reference standards for flexible pipes.

In the automotive industry, exhaust flexible pipes usually consist of different parts made of stainless steel, as shown in Fig. 2.1.2.
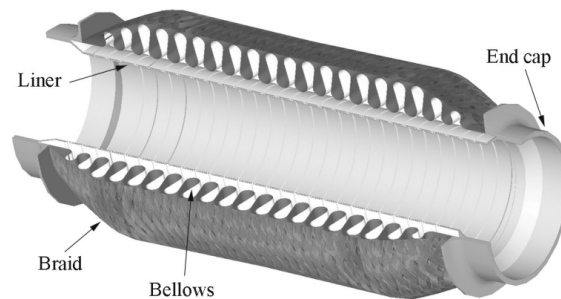
Figure 2.1.2: **Basic design of automobile flexible joint[3].**

The bellow is a single or multi-ply convoluted structure. It can be manufactured by hydraulically forming from thin-walled tubes, as shown in Fig. 2.1.3, or by welding thin-gauge discs serially. In certain pipe assemblies, it must be gas-tight.
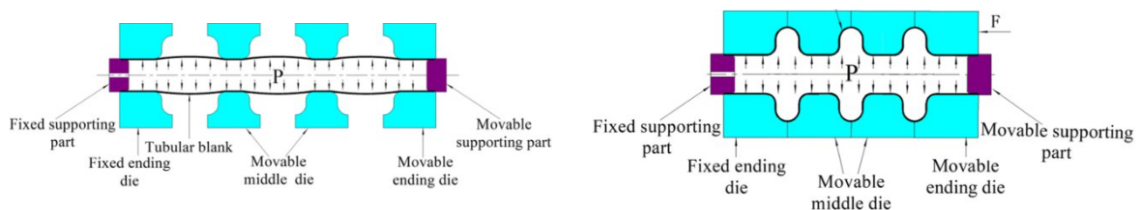
Figure 2.1.3: **Bellows hydroforming process[12].**

The interlock or liner is inside the bellow and is a strip-wound hose produced by helically winding a pre-formed metal strip into a fully interlocked profile, as shown in Fig. 2.1.4. It is connected directly to the end-caps or by the use of inner sleeves. It gets its flexibility and suppleness from the sliding of metal components within the interlock section[11]. Furthermore, it reduces the temperature of the bellows and improves flow conditions.

The braid is around the bellow and is made of wires tightly woven together. It contributes to mechanical protection and limits the possible extension of the pipe. Only

5

non-braided flexible pipes are considered in this work. The three parts are connected with end-caps at the two ends[3].
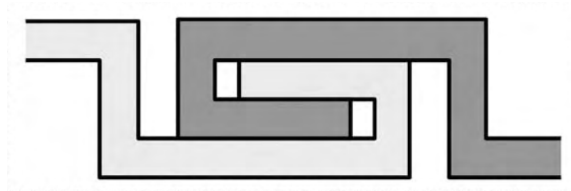
Figure 2.1.4: **Interlocked profile[3].**

2.2 Current state-of-art of modelling exhaust flexible pipes

Previous research about exhaust flexible pipes has applied analytical, numerical, and experimental approaches to investigating design and application.
As regards the study of the dynamic behaviour in heavy truck exhaust systems, not much has been found; however, research about automobile components is considered relevant and exploitable. Literature other than the automotive industry is not taken into account due to considerable differences between components.

Researchers present hand-calculation methods to study one type of vibration at the time for single units of U-shaped bellows (Figs. 2.1.2 and 2.1.3), characterised by specific boundary conditions[13]. The vibrations are mainly in axial and transverse directions, but the torsion case is also discussed.
U-shaped bellows show high flexibility in bending and, at the same time, significant stiffness in radial directions due to their complex geometry[1]. For this reason, the cross-sections remain perpendicular to their axes, while the ovalling and shear deformation phenomena are negligible[14]. The beam approximation representation is thus justified.
The implementation of beam elements needs to include the rotary inertia term, especially for short and large diameter components, in order to reduce errors.
Inertia changes due to fluid flow and convolution distortion are generally significant; however, when studying non-operating components, they are absent. Furthermore, the effects are negligible for the low-density fluids in exhaust systems.

2.2.1 Equivalent thin-walled pipe element method

The desire to simulate the bellows behaviour by standard beam finite element formulation in computation software arises from the difficulty of integrating analytical solutions in the dynamic analysis of larger systems.

The idea of using equivalent thin-walled pipe elements comes from the work of G. Broman, M. Hermann, and A. Jönsson[1]: although shell elements are recognized as the most straightforward formulation, they require an expensive computational effort that makes them less convenient, especially when larger assemblies are evaluated.

According to their method, the convoluted profile is replaced by a beam element, keeping its total mass and stiffness. The stiffness can be computed through finite element calculations on the full-geometry model, experimental measurements on actual bellows, or EJMA formulas[8] and it is used to define the material properties of the equivalent geometry.

In axial and torsion vibrations, the equivalent beam behaves as a uniform rod[15], according to both the governing equations and the computation software formulation. The bending stiffness can be expressed in terms of the axial one and then of the Young's modulus. Bending vibrations are governed by a simplified version of the pipe conveying fluid equation, in which fluid, shear, and pressure terms are neglected[16].

In the numerical model, both two-noded linear or isoparametric three-noded parabolic beam elements are available. The cross-section properties and the mass can be defined in different equivalent ways.

The beam finite element formulation follows the Timoshenko beam theory for bending, but the influence of transverse shear is cancelled by setting the shear area ratio to zero. To simulate both low axial stiffness and high torsion stiffness, the shear modulus must be higher than Young's modulus, and a negative Poisson's ratio follows. The thin-walled pipe analogy generally does not hold entirely.

The possible contribution of the inner liner is briefly discussed: the non-linear behaviour due to friction is high, so it should be modelled separately and connected to the bellows, but this connection to the elements of the bellow is not obvious.

This method includes axial, bending, and torsion vibrations at the same time and makes the integration of the model in larger systems possible.

2.2.2 Expansion of beam approximation method and investigation of non-linear behaviour

The previous research inspired the extended work of J. Wall[3] who investigated the dynamic behaviour of an automobile exhaust system and how it is affected by the presence of a bellows-type flexible joint. The joint in this exhaust system is significantly non-linear due to internal contacts and internal friction in the liner, so a non-linear dynamics analysis is necessary for the complete system. Engine and road irregularities are generally the two sources of excitation.

Initially, the rest of the exhaust system is considered separately, and shell elements are used. Since the ovalling effects of the pipes are negligible, the choice of modelling by beam elements is justified[17], and it is assumed that the exhaust system behaves linearly, but it is excited via the non-linear flexible pipe.
As a second step, the U-shaped bellow flexible joint is considered by adjusting the previous procedure[1] and extending it to multi-ply bellows of a variable mean radius, and including the end caps in the analysis[18].
The plies are assumed to work independently[8], so the stiffness is doubled. The end caps are modelled using lumped mass and mass moments of inertia and connected through rigid elements.

By exciting the system at different amplitudes, the eigenfrequencies shifted, as shown in Fig. 2.2.1a. This can described by the frequency response function (FRF) where the displacement is normalised by the reaction force and plotted versus the frequency. It seems that at levels of excitation below the friction limit, the plies are still stuck together in some parts, so the bending stiffness is high due to the large thickness. When the plies come into contact as a consequence of bending, friction occurs. At higher excitation, they just slip, and the shift no longer occurs.
Since the liner introduces a more significant non-linear phenomenon, the effect of friction between different plies is negligible[18].

The third step involves a model of the combined bellow and liner joint for axial and bending load cases[19]. The liner is affected by Coulomb-type dry friction due to the relative motion between the coils: below the friction limit, it behaves elastically and the coils are stuck; above that, slipping occurs.

Just like the bellow, an equivalent thin-walled pipe formulation is adopted and parameters are chosen to keep the same weight. The connection among them takes place only at the outer nodes of the elements at the ends.
Non-linear characteristics are modelled through ideal elastic-plastic behaviour by assuming symmetrical and independent frequency friction. Since numerical problems

arise when connecting ideal-plastic elements in series, only a short element is used and connected to the rest of the elastic elements.

Since the joint is strongly non-linear, direct time integration using the explicit solver of Abaqus is performed, and the fast Fourier transform computes the corresponding amplitude by considering only the first harmonic.
Responses to excitations higher and lower than the friction limit are compared in Fig. 2.2.1b.
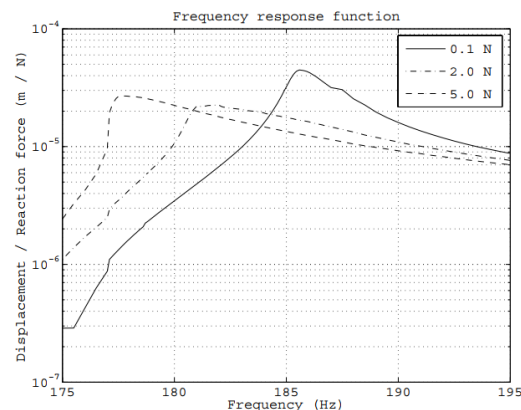
(a) **FRFs at different excitation levels from previous research[18].**
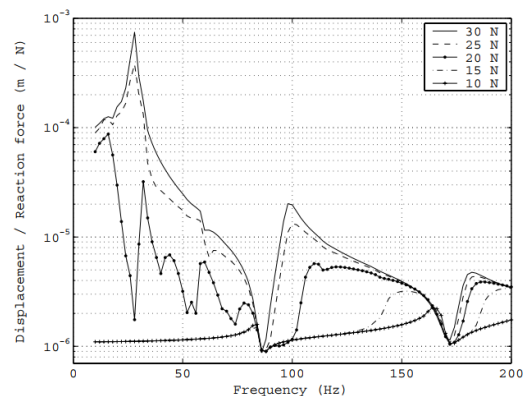
(b) **Simulated axial results for different force levels[19].**

Figure 2.2.1: **Results of the simulation from previous research.**

At low levels of excitation, the normalized response is small, and peaks occur at higher frequencies; indeed, the stiffness of the liner is still high compared to the bellows.
Around the friction limit, both sticking and slipping take place, and large friction-based damping results. The normalized response increases, the peak frequencies are shifted downward and the higher harmonics are significant.
At higher excitation, the liner is mostly slipping and the friction contribution is more negligible; it approaches the behaviour of the bellow and the system becomes more linear. The normalized response increases, but it is lower than in the case of bellow without liner due to the addition of the liner mass.
The research shows the importance of including the liner in the model due to its non-linear behaviour. The dynamic of the flexible joint strongly depends on the excitation level and friction limit.

As a last step, the importance of having a flexible joint is evidenced by comparing the dynamics of the system with and without it, as shown in Fig. 2.2.2a and

9

2.2.2b. Since the response amplitude increases and significant non-linear behaviour is associated with the liner, it is necessary to include it in the model to have reliable simulations[20].
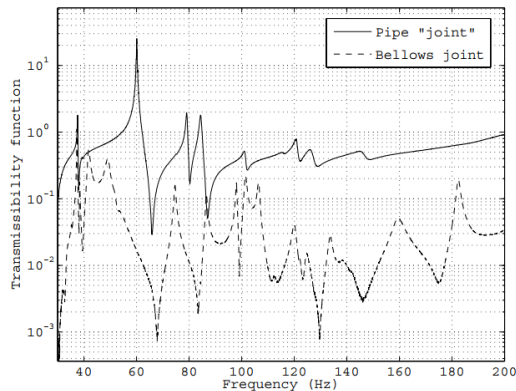
(a) **Comparison of the trasmissibility in an exhaust system with a rigid pipe or the flexible joint[20].**
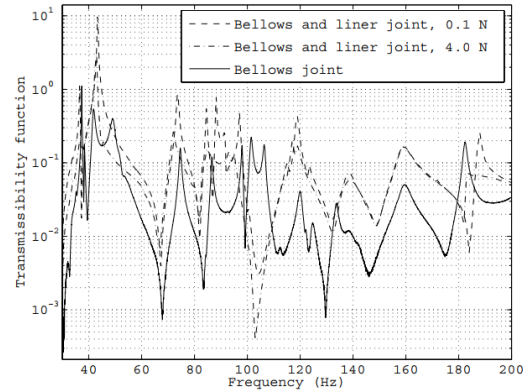
(b) **Comparison of the trasmissibility in an exhaust system with just bellow or bellow-liner joint.**

Figure 2.2.2: **Results of the simulation from previous research[20].**

2.2.3 Alternative formulations

An alternative to the beam representation that consists in the implementation of connector elements in the commercial finite element software Abaqus was explored by R. Wagman[21]. The idea behind this approach is shown in Fig. 2.2.3.
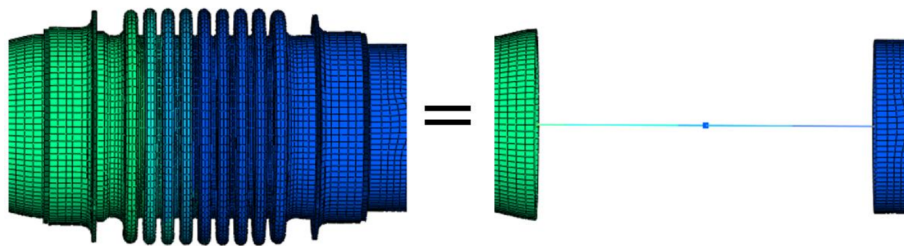
Figure 2.2.3: **Simplified method of modelling bellows by using 1D elements[21].**

Since the inner liner is not trivial to model, this approach does not demand geometrical considerations; it only requires tabular data to describe the nonlinear stiff-

ness characteristics and includes frictional behaviour. The connector type "bushing", the most general one, is adopted, and its Connector Behaviour property is described through the "Connector Elasticity" and "Connector Friction" keywords. "DCOUP3D" elements connect the bellows to the manifold.
A limit of the method consists of the uncoupling between six components of relative motion.

It is also shown how to implement the equivalent thin-walled pipe element method[1] through the "Beam General Section, Section Nonlinear" keyword. The stiffness characteristics are extracted by loading the full FE-model through static analysis. For the remaining pipe section, the actual sizes are modelled by beam elements with linear stiffness parameters.

As regards the flexible hose, the modelling is considered challenging due to the presence of many contact surfaces, as stated in the thesis of N. Björkblad[22]. When detailed studies are required, the actual geometry of the interlocked structure is considered. Shell elements are chosen for the mesh, and, taking advantage of the symmetry axes, the model is reduced to one quarter of three laps of helicoidal cross-section, as shown in Fig.2.2.4.

Figure 2.2.4: **Simplified FE-model of a flexible hose[22].**

In cases where the geometry is missing or there is difficulty modelling it properly, the connector approach can be extended to flexible hoses by using the connector type "cartesian-rotation". This approach is found in the researches of B. Sharifimajd[23] and A. Tchernov[24]. This time, the stiffness is based on strength measurements and has a non-linear behaviour. The "spider" kinematic coupling connects its two ends to other pipes, as shown in Fig. 2.2.5, while the mass is implemented by a point mass at each end. As a drawback, non-diagonal terms of the stiffness matrix are not known, and the influence between different degrees of freedom (DOFs) is not taken into account.

A.I. Ingvason[25] considered the axisimmetry of the component to reduce its struc-

11

ture to a 1D or 2D profile of both the strip-wounded hose and bellow[25], as shown in Fig. 2.2.6a and 2.2.6b.
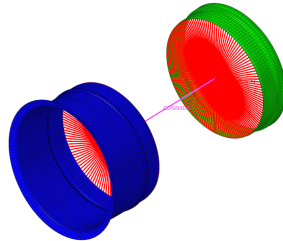
Figure 2.2.5: **Simplified FE-model of a flexible hose[24].**

(a) **Interlock 1D mesh.**

(b) **Bellow mesh.**

(c) **Part of the bellow meshed in shell elements.**
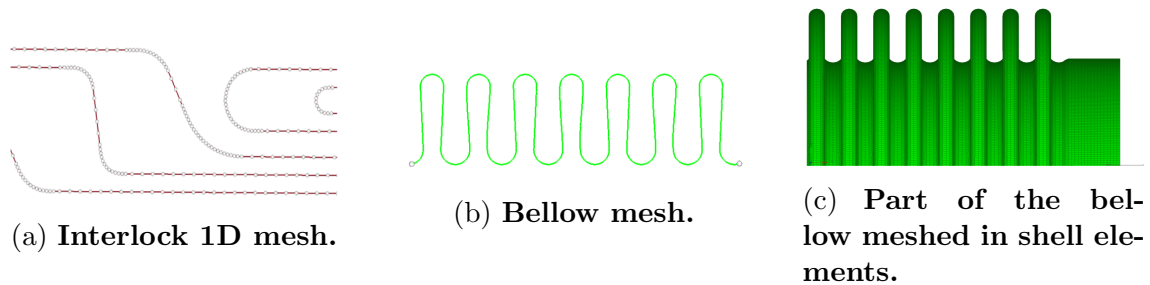
Figure 2.2.6: **Simplified FE-model of a flexible hose[25].**

If the strip-wounded hose is not possible to simulate because of its multiple contact areas and highly curved sections, the bellow is meshed by shell elements, while the inner part is not considered, as shown in Fig. 2.2.6c. It is thus assumed that it does not contribute to the stiffness of the bellow.

2.3 Previous model

2.3.1 Modelling

A previous attempt at simulating a 16-convolutions U-shaped bellow was performed[26]. The results from previous measurements[27] (Sec. 6.2.1) are used as input for tuning a FE-model of the bellow capable of replicating the correct dynamic behaviour. The main goals were the matching of the first eigenfrequencies and full behaviour afterward.

The starting point is the computer-aided design (CAD) model of the flexible pipe, which includes the four parts: bellow, interlock, inner sleeves, and end-caps. A simplified geometry is used for the interlock because its complete profile has a very complex geometry with multiple contact points, so a high number of elements would be needed.
For this reason, only the external surface, which consists of one ply of the U-shaped bellow and end-caps, is considered as attached to two flanges, plates and supports together, used in the measurement to hang the component to the fixtures, as shown in Fig. 2.3.1. The fixtures are not included.

(b) **Complete pipe-assembly.**

(a) **Single bellow.**
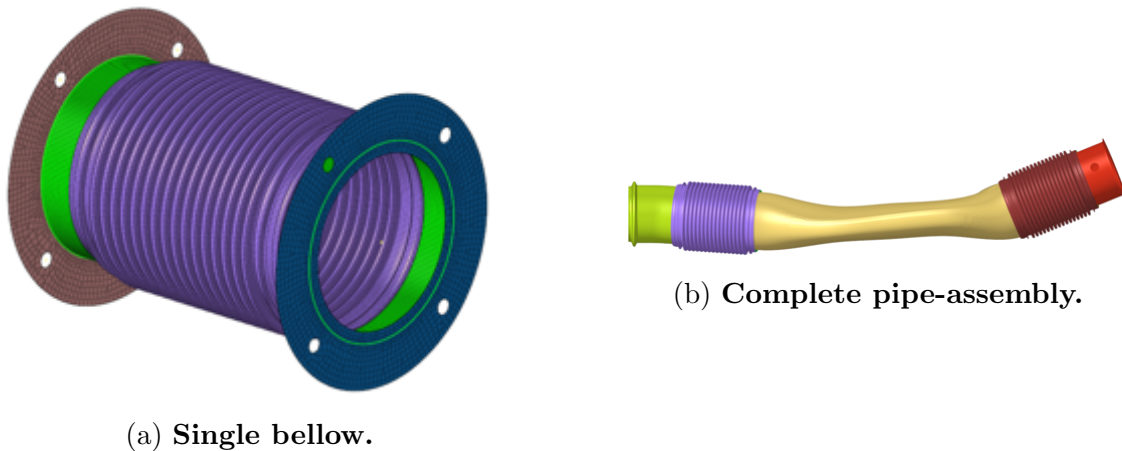
Figure 2.3.1: **FE-models from the previous attempt[26].**

Since some elements are neglected, the mass of the model no longer corresponds to the actual one, so the shell thickness and the geometry are adjusted to reach that value.
The geometry is meshed by using only one layer of shell elements. For the single bellow, all nodes on the edge of the holes, shown in Fig. 2.3.2a, are fixed in all DOFs

to replicate the fastening by bolts.

Note that in the experimental measurement, an older bellow with more convolutions was installed, rather than the standard outlet bellow. In the simulation, a standard bellow was considered, as shown in Fig. 2.3.1b. Moreover, neither the CAD model nor drawings were found for the older bellow used in the pipe-assembly at the time of the simulation.
Two identical models are used. They are connected to the other pipes, and all nodes at the outer edges of outer pipes are fixed in all DOFs to constrain the installation, as shown in Fig. 2.3.2b.

(b) **Boundary conditions in complete pipe-assembly.**
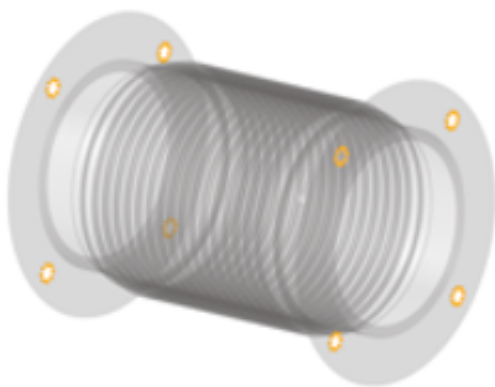
(a) **Boundary conditions in single bellow.**

Figure 2.3.2: **Boundary conditions from the previous attempt[26].**

The stiffness of this model depends on the material and geometry properties of the material assigned.

The simulation is performed in two steps in Abaqus. Firstly, the eigenfrequencies and corresponding mode shapes below 1000 Hz are extracted by using Lanczos eigensolver, and the eigenvectors are scaled with respect to the structure's mass matrix. Subsequently, the measurement is simulated by applying a base motion for an eigenmode-based procedure in the axial and transverse directions separately and running a frequency sweep in the range $0 - 1500$ Hz; its linearized direct steady-state response is then computed.
For all frequencies, the damping is defined as 1%. For each node and element, displacement and stress outputs are computed, respectively. The base motion has an amplitude of 1 m/s^2 in order to get the response as transmissibility.

14

As it was initially built, the model resulted in a too stiff and light structure. The actual mass is then reached by varying the density and shell thickness for the bellow and end caps.

As regards the first natural frequencies, they are rather higher than experimental values. Since high first natural frequencies are typical of stiff structures, and the stiffness of the model depends on the material and geometry properties of the material assigned to the different parts, a manual optimization procedure was then performed by adjusting only the Young's modulus until the first eigenfrequency was fitted.

2.3.2   Results

The different iterations of Young's modulus and the corresponding first eigenfrequencies for both the single pipe and the pipe-assembly are reported in Tab. 2.1.

Iterations	1	2	3	Target
Young's modulus [GPa]	1	7	10	-
Single bellow's first eigenfrequency [Hz]	51	132	156	138
Complete pipe-assembly's first eigenfrequency [Hz]	16	41	48	30

Table 2.1: **Eigenfrequencies for different Young's modulus[26].**

Although the model could be calibrated further, it came close to matching the first eigenfrequency. For the single bellow, the eigenmode directions correspond to the measured ones.

The conclusion was that a more advanced model was required, and it was suggested, as a possible improvement, to add more layers of shells since the bellow is characterised by two plies.

Chapter 3

Theory

3.1 Vibration mechanics

The branch of vibration mechanics deals with oscillating mechanical systems about equilibrium positions. These phenomena are connected to the operating conditions or external sources of excitation and may seriously affect the correct behaviour of the components by introducing noise, dissipation of energy, and decrease of their lifetime. These reasons make it important to take them into account.

3.1.1 SDOFs and MDOFs systems

Even the most complex vibrating system can be studied as a linear combination of SDOFs independent systems[28]. A single degree of freedom (SDOF) system consists of three elements: a rigid mass m, a spring characterised by a certain stiffness k, and a damper that dissipates energy with a damping coefficient c, as shown in Fig. 3.1.1a.

(a) **SDOF system.**
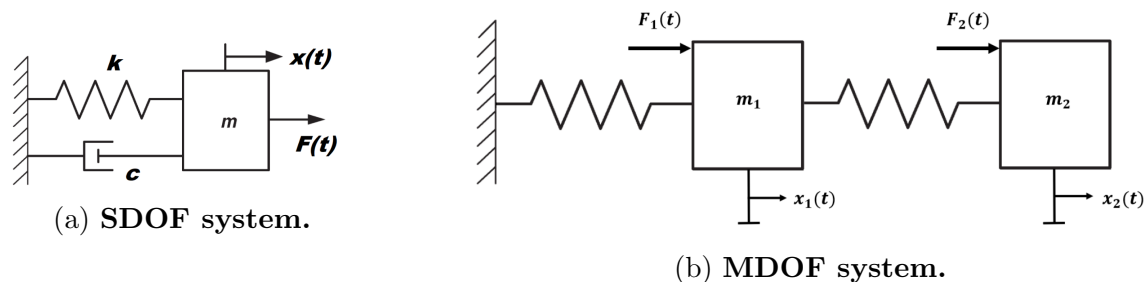
(b) **MDOF system.**

Figure 3.1.1: **Schematic representation of SDOF and MDOF systems[29].**

The properties of the system affect its free response, that is, how the mass moves starting from the initial condition, and forced response, if the mass is excited by an external force.

The system equilibrium is described by the following Equation of Motion:

$$m\ddot{x}(t) + c\dot{x}(t) + kx(t) = F(t). \tag{3.1}$$

The Eq. 3.1 can be expressed in its canonical form as follows:

$$\ddot{x}(t) + 2\xi\omega_n\ddot{x}(t) + \omega_n^2 x(t) = \frac{F(t)}{m} \tag{3.2}$$

where ω_n is the natural frequency and ξ is the damping ratio.

In a linear system where the superposition principle is valid, the steady-state response to an harmonic excitation $F(t)) = F_0 e^{i\Omega t}$ is expressed as:

$$x(t) = A_0 e^{i\Omega t} \tag{3.3}$$

where

$$A_0 = \frac{\frac{F_0}{k}}{1 + 2i\xi\frac{\Omega}{\omega_n} - \frac{\Omega^2}{\omega_n^2}}. \tag{3.4}$$

The ratio between response and excitation depends on the excitation frequency, and it is known as FRF $H(\Omega)$. It can be expressed as transmissibility, the ratio between two commensurable entities that represent, as follows:

$$H(\Omega) = \frac{A_0}{F_0/k}. \tag{3.5}$$

A multiple degree of freedom (MDOF) system can be modelled as multiple SDOF systems coupled among themselves, as shown in Fig. 3.1.1b. The Equations of Motion are generally expressed in matrix form as:

$$\mathbf{M}\{\ddot{x}\} + \mathbf{C}\{\dot{x}\} + \mathbf{K}\{x\} = \{F(t)\}. \tag{3.6}$$

3.1.2   -3dB method

The FRFs are often plotted on a logarithmic scale, such as the dB scale, according to the following equation:

$$A(\Omega)_{dB} = 20log_{10}(|A(\Omega)_{dB}|). \tag{3.7}$$

17

Starting from the peak and going down of 3 dB, two points on the curve with amplitude $A = \frac{A_{max}}{10^{3/20}} = \frac{A_{max}}{\sqrt{2}}$ are obtained, as shown in Fig. 3.1.2.

Since the energy associated with a certain signal in the time domain is proportional to the squared amplitude, these points are characterised by half the power compared to the peak. By assuming a very small damping factor $\xi \ll 1$ and symmetry of the curve around the peak, it is obtained that:

$$\xi = \frac{\Omega_{max} - \Omega_{min}}{2\omega_n}. \tag{3.8}$$
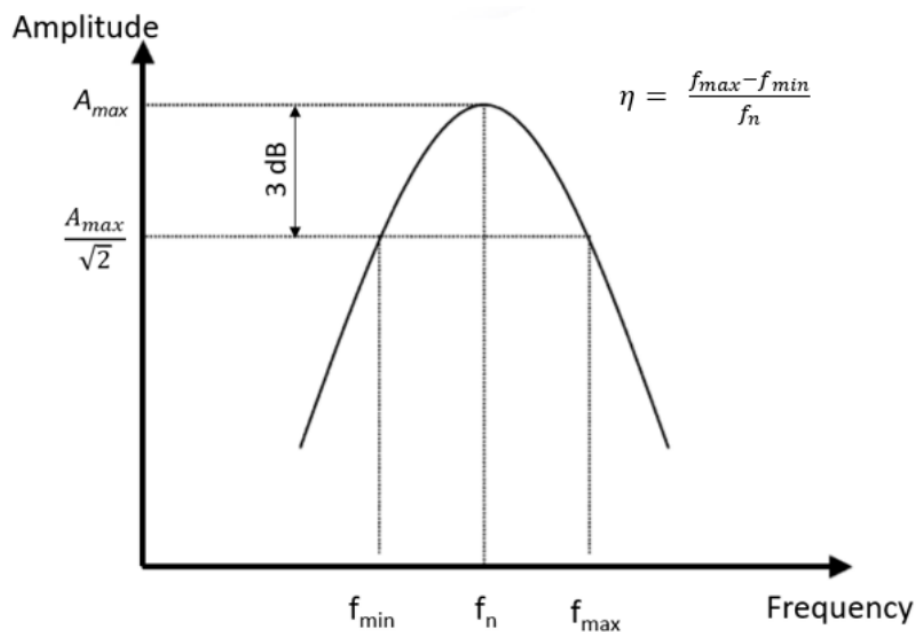
Figure 3.1.2: -3 dB **or half-power bandwidth method[30].**

3.1.3   Modal analysis

The determination of the natural frequencies or eigenfrequencies of a system and their corresponding modes of vibration is called modal analysis. They are the frequencies at which the system reaches the highest vibration amplitudes.

By considering an undamped system and assuming that the solution can be expressed

in the form $\{x(t)\} = \phi\{\eta(t)\}$, the corresponding eigenvalue problem is obtained starting from Eq. 3.6:

$$(\mathbf{K} - \omega_i^2 \mathbf{M})\phi_i = 0, \tag{3.9}$$

where $\omega_i = 2\pi f_i$ and $\{\phi_i\}$ are the angular eigenfrequencies and eigenmodes of the system, respectively. They are collected in the respective eigenvalue and modal matrix:

$$\Lambda = \begin{bmatrix} \omega_1^2 & 0 & \cdots & 0 \\ 0 & \omega_2^2 & \cdots & 0 \\ \vdots & \vdots & \ddots & \vdots \\ 0 & 0 & \cdots & \omega_i^2 \end{bmatrix} \quad \phi = \begin{bmatrix} \phi_{1,1} & 0 & \cdots & \phi_{1,n} \\ \phi_{2,1} & \phi_{2,2} & \cdots & \phi_{2,n} \\ \vdots & \vdots & \ddots & \vdots \\ \phi_{n,1} & \phi_{n,2} & \cdots & \phi_{3,3} \end{bmatrix} \tag{3.10}$$

According to the principle of the modal superposition, it is possible to decompose the original MDOF system into n SDOF systems expressed as:

$$m_i\ddot{\eta}_i(t) + c_i\dot{\eta}_i(t) + k_i\eta_i(t) = F_i(t), \tag{3.11}$$

and the response is given by the sum of all the individual modal contributions:

$$x(t) = \sum_{i=1}^{n} \phi_i\eta_i(t). \tag{3.12}$$

3.1.4 Signal analysis

Every periodic function can be expressed by a Fourier series, which is a sum of harmonic functions:

$$f(t) = a_0 + \sum_{k=1}^{\infty}(a_k cos(k\Omega_0 t) + b_k cos(k\Omega_0 t)). \tag{3.13}$$

It can also be written in exponential form as:

$$f(t) = a_0 + \sum_{k=1}^{\infty}(\frac{a_k - ib_k}{2}e^{ik\Omega_0 t} + \frac{a_k + ib_k}{2}e^{-ik\Omega_0 t}). \tag{3.14}$$

Although the response of a system is measured in the time-domain as the amplitude of displacement, velocity, or acceleration signal that represents a waveform, the associated harmonic functions $c_k sin(w_k t + \phi_k)$ allow to represent its spectrum, the collection of the spectral lines (ω_k, c_k), in the frequency-domain.

As regards non-periodic functions, they can be assumed to be periodic over an infinite period of time, so the corresponding waveform can be written as a linear combination

19

of harmonic functions. It is obtained by using the Fourier transform.
The Direct Fourier transform is computed as follows:

$$F(\omega) = \int_{-\infty}^{\infty} f(t)e^{-i\omega t}dt, \tag{3.15}$$

while the inverse Fourier transform is defined by:

$$F(\omega) = \frac{1}{2\pi} \int_{-\infty}^{\infty} F(\omega)e^{i\omega t}d\omega. \tag{3.16}$$

The FRFs are computed by applying harmonic excitation at constant amplitude and measuring the response at different frequencies.

3.1.5 Random process

During measurements, similarities in the signals are investigated. A stationary process is characterized by a constant average value and auto-correlation, which is how much a signal can be predicted from past observations, along the time axis. They are computed as follows:

$$\mu_x(t) = lim_{N\to\infty}\frac{1}{N}\sum_{n=1}^{N} x_n(t). \tag{3.17}$$

$$R_{xx}(\tau) = lim_{N\to\infty}\frac{1}{N}\sum_{n=1}^{N} x_n(t)x_n(t+\tau). \tag{3.18}$$

If it also happens in different sample functions, it is called ergodic. If two different signals $x_n(t)$ and $y_n(t+\tau)$ are compared, the cross-correlation function is computed. In the presence of stationary random processes, the Fourier transform allows for the computation of the corresponding spectral functions. The Auto-Power Spectral Density (PSD) function is defined as the Fourier transform of the autocorrelation function $R(\tau)$,

$$S_{xx}(\omega) = \int_{-\infty}^{\infty} R_{xx}(\tau)e^{-i\omega\tau}d\tau, \tag{3.19}$$

while the Cross-Power Spectral Density (CPSD) function is defined as:

$$S_{yx}(\omega) = \int_{-\infty}^{\infty} R_{yx}(\tau)e^{-i\omega\tau}d\tau. \tag{3.20}$$

An estimation of the accuracy of a measurement is indicated by the linearity between input and output functions. It is given the coherence function computed by:

$$\gamma_{yx}(\omega) = \frac{|S_{yx}(\omega)|^2}{S_{xx}(\omega)S_{yy}(\omega)}. \tag{3.21}$$

20

3.1.6   Non-linear vibrations

The linear approximation stated in Sec. 3.1 allows to deal with simplified problems in which the superposition principle can be applied, both the FRF and the modal parameters are invariant from the excitation amplitude, and the solution is unique. This approximation is no longer valid in the presence of large oscillations and friction, and non-linear behaviour must be taken into account. Harmonic distortions represent a warning of the non-linear behaviour: both harmonics and sub-harmonics of the excitation frequency, not directly excited by the input, may be present in the response, as shown in Fig. 3.1.3.
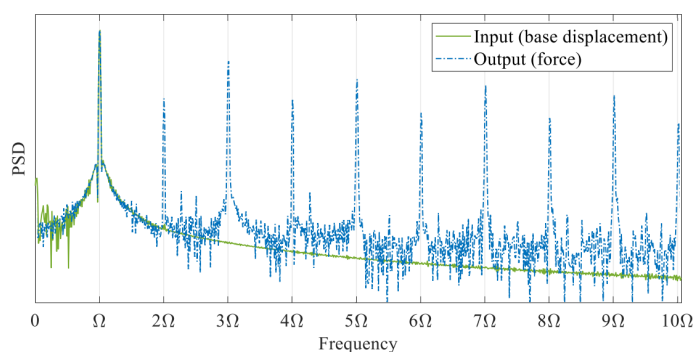
Figure 3.1.3: **Example of harmonic distortion[31].**
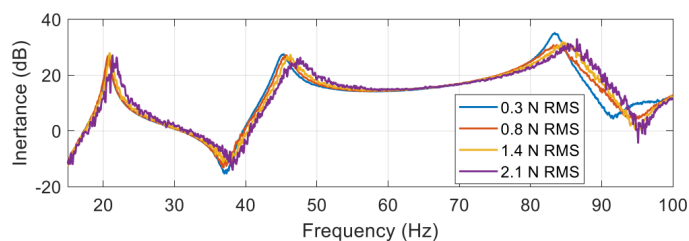
Figure 3.1.4: **Example of FRF distortions[31].**

Differently from linear systems, they are characterised by multiple solutions that are stable only for small perturbations. Furthermore, the response may be significantly affected by a change in the initial conditions, just as chaotic systems. The level of excitation entails a softening or hardening non-linear behaviour and the FRFs change, as shown in Fig. 3.1.4.

It is important to verify the presence of these phenomena by using sine sweeps, random vibrations, or hammer tests at different amplitudes.

3.2   Finite Element Method

The Finite Element Method (FEM) is a numerical technique for solving partial differential equations in boundary value problems. Finite elements defined by a set of nodes are used to discretize the problem domain[32].
Each finite element is characterised by a set of governing equations which are then assembled into a global system of equations, associated with the entire problem.
The use of such a principle guarantees the best, but approximated, solution of the governing system equation under certain conditions.

This method is implemented in many computational software programs. The choice of the element types depends on the application: the use of solid and shell elements can provide more information, but it makes the model more computationally expensive, so 1D elements can be preferred and are easier to employ.

3.2.1   Shell elements

Shell elements are 2D elements applied to structures with one dimension significantly smaller than the others and in which the stresses in the thickness direction are negligible, such as plates and tubes.
They are formulated starting from a 2D solid element superimposed onto a plate element: the first one handles the membrane or in-plane effects, while the second one deals with bending or off-plane effects[32]. So these elements undergo bending and twisting, as well as in-plane deformation.
In Abaqus[33], plane sections perpendicular to the shell mid-surface are assumed to remain plane. In this case, four nodes shell with 6 DOFs per node are used, as shown in Fig. 3.2.1.
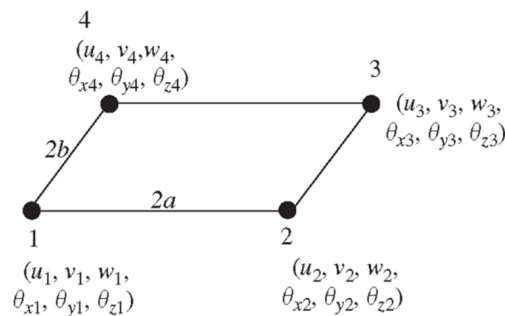
Figure 3.2.1: **4 nodes shell element[29].**

3.2.2 Beam elements

Beam elements are 1D elements that connect two points, and they are less expensive than shell elements. In beam theory, a one dimensional approximation is based on the assumption that the cross-section dimensions are quite smaller compared to the one along the axis of the beam.

In Abaqus[33], it is considered a solid beam with 6 DOFs per node, as shown in Fig. 3.2.2, that can deform along the beam axis in bending and torsion. The deformation of the beams is influenced by variables that change only with the position along the beam axis.
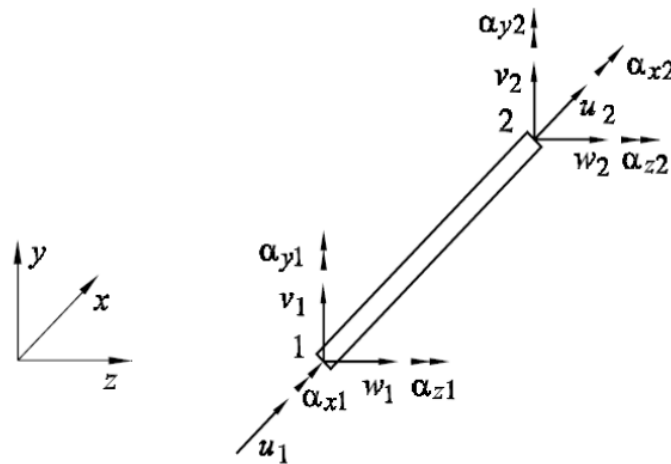
Figure 3.2.2: **3D beam element.**

These elements also have additional flexibility associated with transverse shear deformation between the beam's axis and its cross-section directions. Shear deformation is neglected in cubic elements, so they cannot be used to model short beams, while the quadratic ones are Timoshenko beams, so they are shear deformable.

A cross-section is assigned to the element, and it cannot deform in its own plane. Different shapes are available, and its orientation must be specified. As regard the dynamic behaviour, the rotary inertia of a beam cross-section is considered for thick beams, while it is negligible for slender beams.

Two different beam sections can be used: Beam Section is characterised by the integration of the beam section during the analysis, while it is not required by using Beam General Section. The two approaches turn out to be equivalent for the purposes of this work.

3.2.3 Connector elements

Connector elements are point-to-point connections defined between two nodes. The connection-type library in Abaqus[33] contains translational and rotational basic connection components that affect translational and rotational degrees of freedom at both nodes on the connector element. Assembled connectors are combinations of translational and rotational degrees of freedom.

The Cartesian and Rotation types are chosen for this application, as shown in Fig. 3.2.3a and 3.2.3b.

(a) **Connection type cartesian.**

(b) **Connection type rotation.**
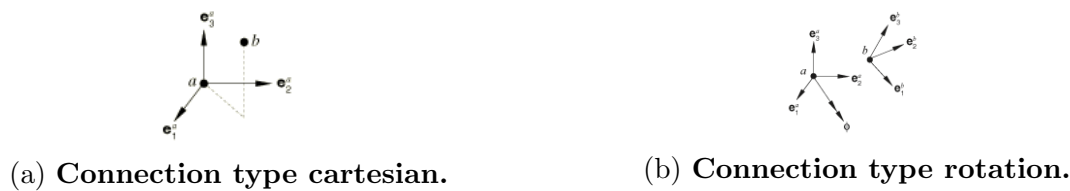
Figure 3.2.3: **Cartesian-rotation connector type[33].**

There are different ways of assigning mechanical behaviour to the elements. Spring-like elastic characteristics can be specified for each available component of relative motion independently, and the behavior can be linear or non-linear.

It is not possible to specify the density or mass of the elements, but additional lumped mass elements can be added manually. For these elements, it is also necessary to specify the orientation of the local coordinate system to consider the stiffness characteristics.

Different definitions of stiffness are available, for example, the entire stiffness matrix, including the non-diagonal parameters, can be defined, but further coupled tests would be necessary.

3.2.4 Kinematic coupling

The kinematic coupling, also known as "spider" and shown in Fig. 3.2.4, allows to constrain a large number of nodes to the rigid body motion of a single node in certain DOFs. It provides coupling between different types of elements, such as shells and beams or connectors.
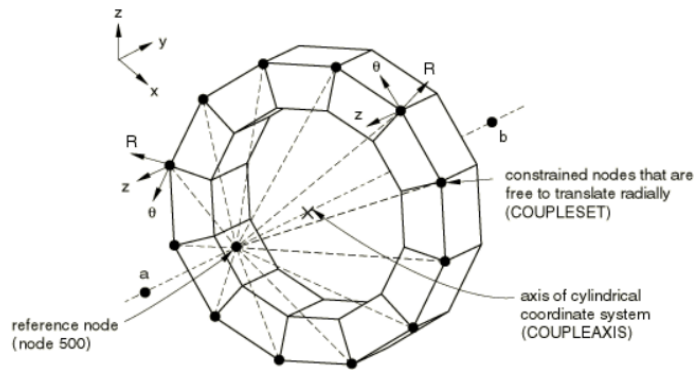
Figure 3.2.4: **Kinematic coupling[33].**

3.3 Timoshenko beam element

In the presence of a beam with symmetric cross-section to the y-axis and symmetric loads to the x-y plane, only the axial force N_x, bending moment M_z and shear force V_y are not negligible, as shown in Fig. 3.3.1. This is the in-plane beam model, in which the displacements of the axis remain in the x-y plane and the cross-sections do not rotate about the axis. The material behaviour is assumed to be linear elastic.
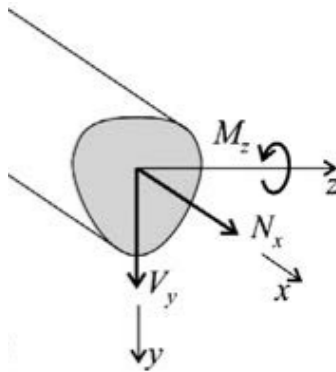
Figure 3.3.1: **Stress resultants for a symmetric beam subjected to in-plane loads[34].**

If distributed loads in the direction of the axis or perpendicular to it and distributed

moment loads are present, the following equilibrium equations are formulated:

$$\begin{cases} \frac{\mathrm{d}N_x}{\mathrm{d}x} + q_x = 0 \\ \frac{\mathrm{d}V_y}{\mathrm{d}x} + q_y = 0 \\ V_y = \frac{\mathrm{d}M_z}{\mathrm{d}x} - m = 0 \end{cases} \tag{3.22}$$

In Euler-Bernoulli beam theory, shear deformations are neglected. Two equilibrium equations are then obtained:

$$\begin{cases} \frac{\mathrm{d}N_x}{\mathrm{d}x} + q_x = 0 \\ \frac{\mathrm{d}^2 M_z}{\mathrm{d}x^2} + q_y = 0 \end{cases} \tag{3.23}$$

In the presence of a homogeneous cross-section, and then a uniform Young's modulus E, the centroid of the beam results in the centre of gravity, and its tensile EA and bending stiffness EI_z are so defined.

According to the Bernoulli-Navier assumption, cross sections perpendicular to the axis of the beam, after the development of the deformations, remain plane and perpendicular to the curved axis.

In Timoshenko beam theory, the shear deformations are taken into account, as shown in Fig. 3.3.2.
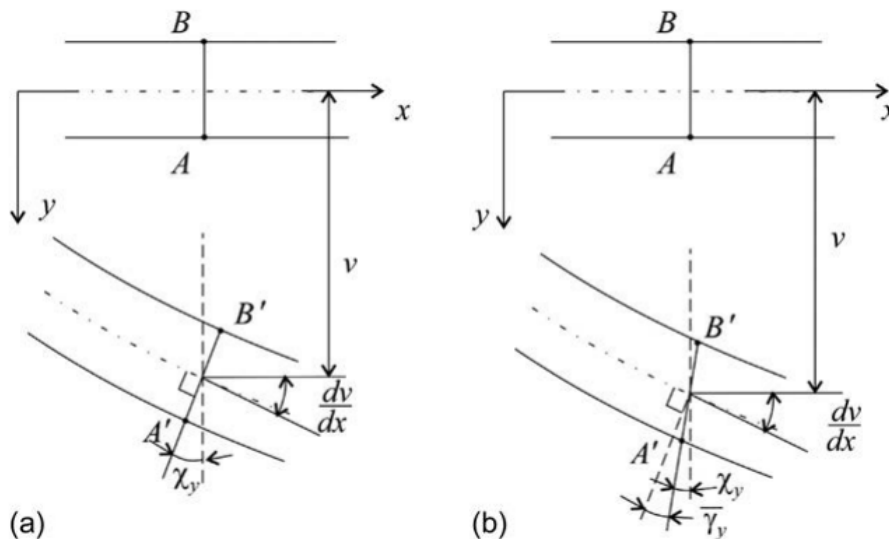
Figure 3.3.2: **Deformation of a beam when the shear deformation are neglected (a) and when they are taken into account (b)[34].**

In case (a), the cross section is perpendicular to the axis of the beam, and for small displacements $\frac{\mathrm{d}w}{\mathrm{d}x} \ll 1$, it is true that:

$$\begin{cases} \chi_y = \frac{\mathrm{d}w}{\mathrm{d}x} \\ \kappa_z = -\frac{\mathrm{d}^2 w}{\mathrm{d}x^2} \end{cases} \tag{3.24}$$

where χ_y is the rotation of the plane cross-section when the plane cross-section approximation holds.

The material equation of the Euler-Bernoulli beam theory is computed as:

$$M_z = EI_z \kappa_z \tag{3.25}$$

According to the Timoshenko beam theory, the cross-section plane is no longer normal to the beam axis. The rotation of the beam axis is due to both the bending and shear deformation:

$$\frac{\mathrm{d}w}{\mathrm{d}x} = \chi_y + \bar{\gamma}_y \tag{3.26}$$

Looking at Fig. 3.3.3, the equilibrium equations from Eq. 3.22 can be rewritten as follows:

$$\begin{cases} V_y = \frac{\mathrm{d}M_z}{\mathrm{d}x} \\ q_y + \frac{\mathrm{d}V_y}{\mathrm{d}x} + N_x \frac{\mathrm{d}^2 w}{\mathrm{d}x^2} = 0 \end{cases} \tag{3.27}$$

After further calculations, Timoshenko's beam equation can be written as:

$$EI_z \frac{\mathrm{d}^4 w}{\mathrm{d}x^4} = \left(1 - \frac{EI_z}{S}\frac{\mathrm{d}^4}{\mathrm{d}x^4}\right)\left(N_x \frac{\mathrm{d}^2 w}{\mathrm{d}x^2} + q_y\right). \tag{3.28}$$

In order to consider the dynamic equilibrium, the inertia forces are introduced. The
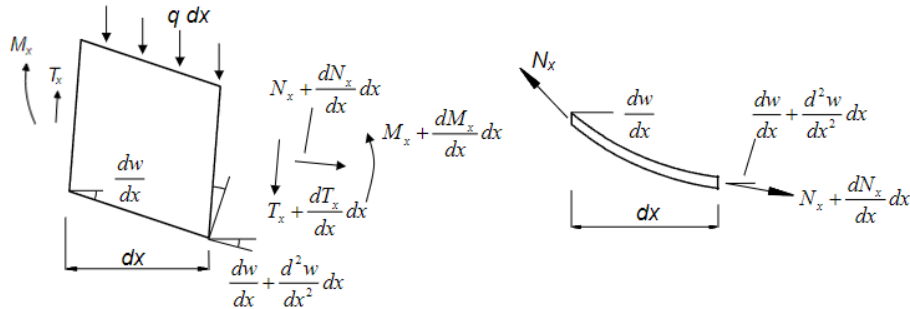
Figure 3.3.3: **Distorted beam element[35].**

rotary inertia term opposes the cross-section rotation due to bending. For a homogeneous cross-section, mass and rotary inertia are computed as:

$$\begin{cases} m = \rho A \\ R = \rho I_z \end{cases} \tag{3.29}$$

The equilibrium equations are given by:

$$\begin{cases} \frac{\partial V_y}{\partial x} + q_y + N_x \frac{\partial^2 w}{\partial x^2} - m \frac{\partial^2 w}{\partial t^2} = 0 \\ -V_y + R \frac{\partial^3 w_b}{\partial x \partial t^2} + \frac{\partial M_x}{\partial x} = 0. \end{cases} \tag{3.30}$$

that allows us to write the equation:

$$EI_z \frac{\partial^4 w}{\partial x^4} + \left(\frac{EI_z}{kGA} \frac{\partial^2}{\partial x^2} - 1 - \frac{R}{kGA} \frac{\partial^2}{\partial t^2} \right) \left[q_y + N_x \frac{\partial^2 w}{\partial x^2} - m \frac{\partial^2 w}{\partial t^2} \right] - R \frac{\partial^4 w}{\partial x^2 \partial t^2} = 0. \tag{3.31}$$

With q_y and N_x equal to zero, it is obtained that:

$$EI_z \frac{\partial^4 w}{\partial x^4} + m \frac{\partial^2 w}{\partial t^2} - \frac{m}{S} \left(EI_z \frac{\partial^4 w}{\partial x^2 \partial t^2} - R \frac{\partial^4 w}{\partial t^4} \right) - R \frac{\partial^4 w}{\partial x^2 \partial t^2} = 0 \tag{3.32}$$

which describes the dynamic behaviour of a Timoshenko's beam.

3.4 Vibrations governing equations for flexible pipes

As already stated, the bellows can be modelled as pipe elements whose dynamic behaviour can be described by using partial differential equations.

In the presence of axial vibrations, the pipe elements behave like a uniform rod[15], as shown in Fig. 3.4.1a and the governing equation is given by:

$$\frac{\partial^2 u}{\partial t^2} - \frac{E}{\rho} \frac{\partial^2 u}{\partial x^2} = 0. \tag{3.33}$$

Since the beam formulation is justified[14], the bending stiffness can be expressed in terms of the Young's modulus. For the bending vibrations in Fig. 3.4.1b, the differential equation for a pipe conveying fluid is considered[16]. Since the pipe is in non-operating conditions, the terms related to fluid flow and pressure are neglected, and Eq. 3.32 is obtained. The shear deformations are negligible due to the high stiffness in the radial direction, so the final equation is written as:

$$EI_z \frac{\partial^4 w}{\partial x^4} + m \frac{\partial^2 w}{\partial t^2} - R \frac{\partial^4 w}{\partial x^2 \partial t^2} = 0. \tag{3.34}$$

28

As regards the torsion vibrations, the pipe elements follow again the behaviour of a uniform rod[15], as shown in Fig. 3.4.1c. The governing equation is expressed as:

$$\frac{\partial^2 \theta}{\partial t^2} - \frac{G}{\rho} \frac{\partial^2 \theta}{\partial x^2} = 0. \tag{3.35}$$

(a) **Displacements of a uniform rod in axial vibration[1].**

(b) **Displacement of a beam in bending vibration[1].**

(c) **Displacement of a uniform rod in torsion vibration[1].**
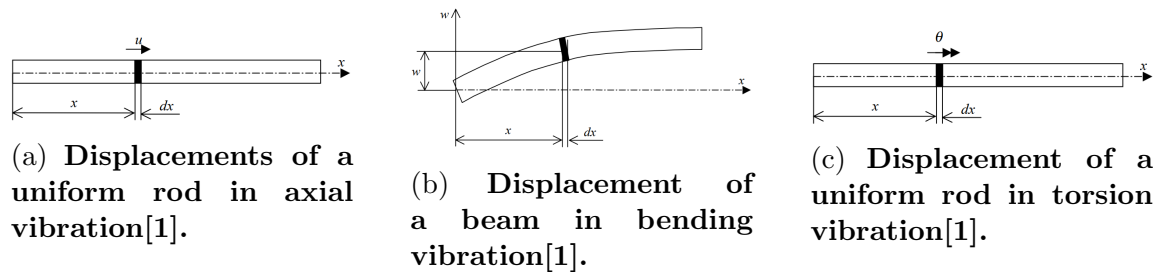
Figure 3.4.1: **Theoretical model of the equivalent thin-walled pipe element in axial, bending and torsion vibration.**

3.5 Optimization

In this work, an optimization process is performed in Heeds MDO[36] software with the aim of fitting the model in relation to the actual behaviour of the component.
The Simultaneous Hybrid Exploration that is Robust, Progressive, and Adaptive (SHERPA) algorithm is adopted: it employs multiple search strategies at once and adapts to the problem as it learns about the design space.

The optimization study consists of the investigation of different design conditions obtained by changing design parameters and has as its final purpose the achievement of certain goals. In particular, one or more objective functions must be minimized or matched.
The investigation includes an iterative procedure in which a new design is set and the defined response is computed by specified formulas or as a difference between two curves. At the end of each iteration, the objective function is computed and it is checked that the solution is feasible and the variation from the previous guess is still higher than the tolerance. Otherwise, the study continues until a maximum number of evaluations is reached.
The problem is constrained if upper or lower limits are defined for the parameters or responses. In that case, not all the solutions are feasible. Constrained problems are generally more difficult to solve.

Chapter 4

Case studies

4.1 Components

In trucks, according to current design solutions for exhaust systems, flexible pipes are part of different pipe-assemblies placed before or between the after-treatment system components.

The after-treatment system deals with the collection of the exhaust gases, cleaning them to ensure the engines meet emission regulations, reducing the level of noise caused by the exhaust gases, and finally discharging them out of the vehicle. The exhaust pipes harness gases into the system and through different components, before discharging them through the tailpipe into the environment.

Since working conditions, as well as requirements, change along the after-treatment system, different flexible pipes are chosen for each pipe-assembly.

Three components belonging to single and dual flexible pipe assemblies are considered in this work.

The dual bellow pipe-assembly is characterised by two identical bellows located between two outer pipes and the central one. This installation is mounted under the frame, between the main and secondary silencers. Hydroformed U-shaped bellows with an interlock are used. Two alternative versions are introduced in Figs. 4.1.1a and 4.1.1b. They differ in geometrical dimensions, especially in the number of convolutions and length. In the first one, the interlock hangs on a pair of inner sleeves inserted in the end caps.

The purpose of these bellows is to allow movement and flexibility of the exhaust pipe with movements of the chassis. Since the load in the chassis is mainly road induced, excitation arises at low frequencies, and these bellows are generally developed with respect to the displacement in the chassis[27].

In the single flexible pipe assembly, a flexible hose is implemented. In this case, the assembly line connects the engine to the main silencer. This configuration adopts the welded U-shaped bellow in Fig. 4.1.1c. Due to its closeness to the engine, its working conditions are more critical. Exhaust gases are at higher temperatures and in more untreated exhausts, entailing the need for gas-tight bellows. In addition to road induced vibrations, excitation can also arise at higher frequencies related to engine rotational speed.

Since premature and unpredictable failures have been experienced, strip-wounded hoses have been analyzed several times, and wear has been identified as a major failure mechanism[22], and stiffening phenomena associated to high temperatures have been detected[37].

(a) **Flexible pipe A1: 16 convolutions U-shaped bellow.**

(b) **Flexible pipe A2: 27 convolutions U-shaped bellow.**

(c) **Flexible pipe B: Gas tight hose (GTH).**

Figure 4.1.1: **Components from exhaust dual (left,centre) and single (right) flexible pipe installations.**

4.2   Design information

The information about mass, geometry, material properties, and static stiffness values of the three flexible pipes is reported in the following Tabs. 4.1 and 4.2.

The bellow is made of a different material with respect to the interlock and end caps in order to be gas-tight; despite that, the material properties, density, and Young's modulus are the same.

The geometry is provided by design engineers through technical drawings from suppliers or CAD models; otherwise, it can be obtained by taking physical measurements

of the components themselves. The masses are measured by weighing the components on digital scales.

As regards the flexible pipes A1 and B, the values of static stiffness are available from previous testing of different samples, and the average values are taken.

For the bellow A1, the axial static stiffness is computed by the test rig in Sec. 6.3.2. The torsional one instead is assumed.

Property	Bellow A1	Bellow A2	Bellow B
m [kg]	1.7168	1.7096	2.7873
n	16	27	62
L [m]	0.182	0.182	0.286
D [m]	0.1374	0.130	0.140
E [GPa]	193	193	193
ρ [kg/m^3]	8000	8000	8000

Table 4.1: **Mass, geometrical dimensions and material properties of the three flexible pipes.**

Property	Bellow A1	Bellow A2	Bellow B
k_T [N/m]	42100	54363	5725
t_T [N/m]	58900	-	2673
b_T [Nm/rad]	264	-	-
c_T [Nm/rad]	55900	60000	17380

Table 4.2: **Static stiffness values of the three flexible pipes.**

Chapter 5

Methodology

As already stated, this work aims to select a new method for modelling the dynamic behaviour of flexible pipes used in exhaust piping systems. Three different components and one pipe-assembly line are involved. The study is carried out by following several steps, as shown in the flow chart diagram below.

The results from shaker testing represent the starting point for the investigation. The possible uncertainties from physical testing related to the FRFs are not considered, and the results are retained as reliable.
For two of the three flexible pipes, they are already available from previous measurements, while a new test on the third component is designed and performed within this project. The objective is the evaluation of the response in different directions by frequency sweep and the identification of the first eigenfrequencies and eigenmodes. They are used in the fitting of the model for the single flexible pipe.

The state of the art review identifies a few methods already implemented by other researchers and provides evidence of their relative pros and cons. After a first selection, the nominated methods are applied to the bellow A1 (Fig. 4.1.1a).
A model for each approach is built starting from the CAD model, known geometry, and previous testing results.
Through a numerical modal analysis, the first eigenfrequencies and, in general, the FRFs are evaluated through a linear perturbation. The results are then compared with the experimental ones, and, if they are not captured with enough accuracy, an optimization process is performed by varying the chosen parameters until the match or the maximum number of iterations is reached.
If the match with the experimental results is not satisfactory, a new method is considered; otherwise, it is identified as the final method and it is used in the following models.

One or more methods able to capture the dynamic behaviour of the flexible pipe are selected, and the most efficient one is implemented in other case-studies as validation. In particular, it is applied to the bellow A2 (Fig. 4.1.1b), and then the model for the single bellow is substituted in the dual bellow assembly to simulate the global behaviour of the entire installation.

The results are then compared with the experimental ones. If the selected method is not successful, one of the alternatives is tried.

The same procedure is followed for the flexible hose B (Fig. 4.1.1c).

The models are developed by using Hypermesh and Abaqus Keywords in parallel. The analysis, performed in Abaqus, consists of an eigenfrequency extraction and a direct steady state analysis, as shown in Sec. B. The FRFs are computed at the nodes corresponding to the locations of accelerometers on the components during the measurements. In the simulations of complete pipe-assembly, the nodes associated with the accelerometers in the middle and at the inner ends of the bellows are considered.

Heeds optimization software is used subsequently to adjust the model to the results by using the Sherpa method. In each iteration, the computed and experimental first two eigenfrequencies are compared, and the model is adjusted in order to match the experimental values, as shown in Fig. 5.0.1a.

The structure of the optimization process is shown in Fig. 5.0.1b.

Optimization Statement

Objective: Match w1 to 138
                    Match w2 to 166

(a) **Objectives of the optimization.**

(b) **Different analysis in the optimization procedure.**
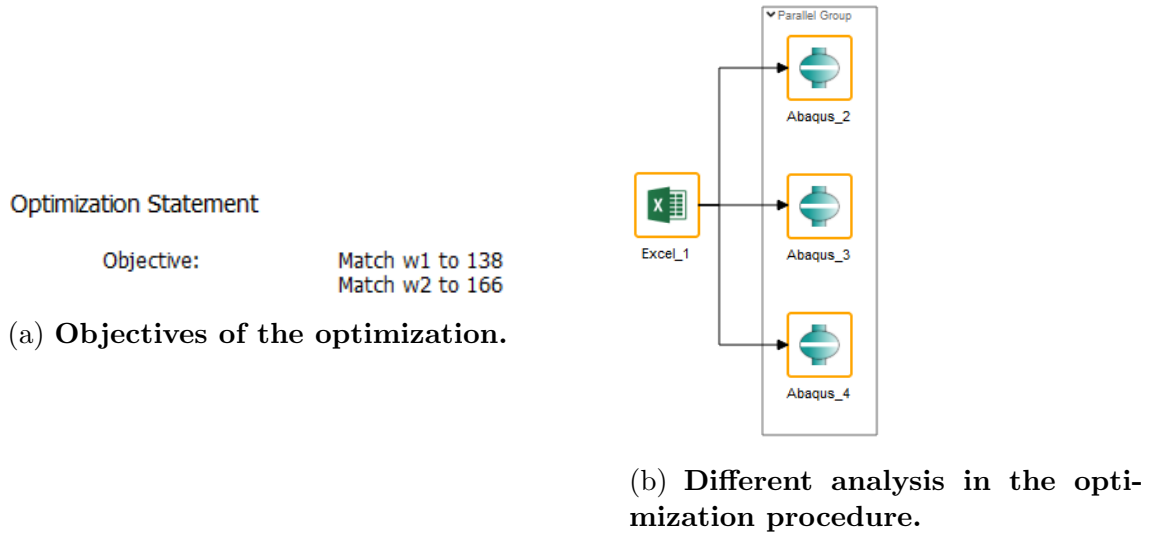
Figure 5.0.1: **Structure of the optimization process in Heeds[36].**

At the beginning of each iteration, a new set of parameters is proposed. Depend-

ing on the model, these parameters are directly provided to "Abaqus 2" in order to perform the numerical modal analysis, or they are first substituted in an Excel sheet[38] that computes the actual parameters through the formulas associated with a theoretical model and substitutes them in Abaqus afterwards.

"Abaqus 3" and "Abaqus 4" analyses are performed in parallel to compute the axial and torsion stiffness values in the models composed of different parts, with the aim of comparing those with results from static tests. The model is fixed at the node at one end, and an axial force and a torque are applied one at a time at the other end. An attempt at using curve-fitting in Heeds has been performed, and the guidelines are provided in the attached presentation[39].

The optimization procedures provide information about the influence of different parameters on the dynamic behaviour (Sec. C), so that it can be considered in the design process.
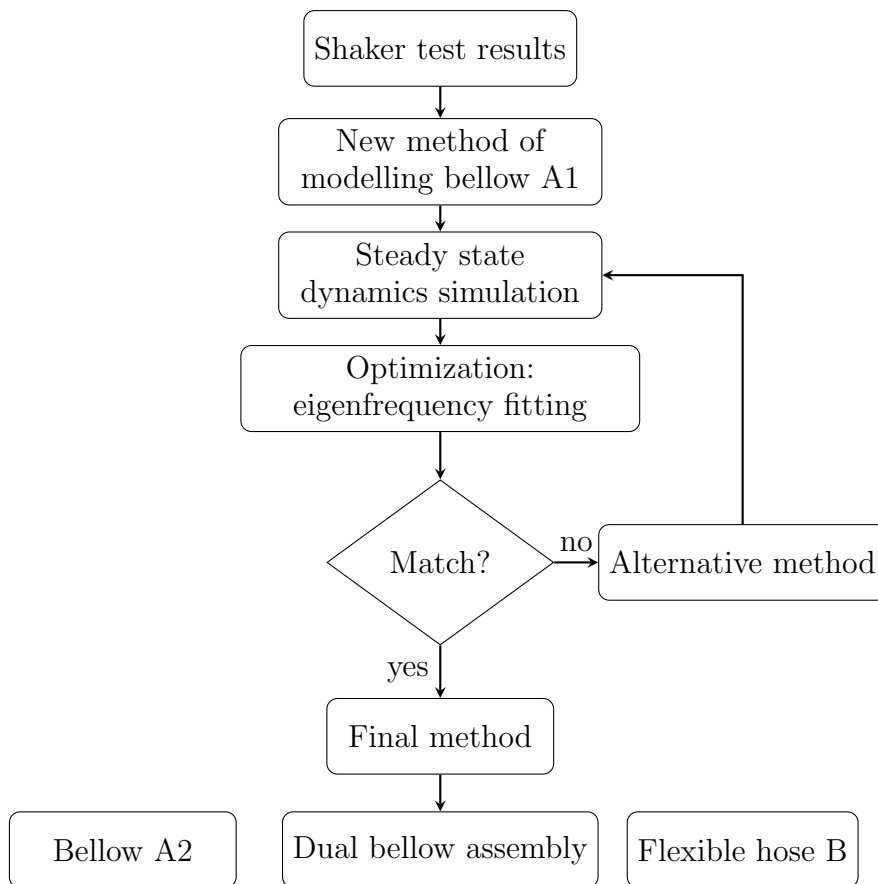
Chapter 6

Testing

6.1 Experimental modal analysis

In the study of physical dynamics, experimental tests play an important role in understanding the characteristics of the system and providing information to compare with analytical and numerical approaches, especially when they are not accurate enough due to the complexity of the system.

Experimental modal analysis is performed with the aim of measuring the FRFs as magnitude, mainly acceleration, or transmissibility, given by the ratio between response and excitation.
The common measuring chain requires the presence of different tools[28]. First of all, a signal generator establishes the type of excitation, usually of low amplitude, and sends it to an amplifier. The structure is then excited by a shaker, an electromagnetic exciter, connected by a stinger, which causes the oscillation. Depending on the number of signal channels available, a certain number of accelerometers, that are, transducers able to measure acceleration, is attached to the structure to record the response. The data are finally sent to an analyzer that computes and stores the FRF.

Damping is introduced in the oscillations to reduce the amplitude of the peaks and avoid damaging the component. It usually varies with the excitation frequency.
The structure can be constrained or in free-free conditions. This choice must be taken carefully with the aim of replicating the operating conditions because it affects the results significantly.

Since the human eye is not able to directly observe the response of a system due to the small and quick motions that characterize it, a stroboscope is used. It is shown

in Fig. 6.1.1. This instrument provides intermittent illumination of a rotating or vibrating object, and when its frequency is either the same or a sub-multiple of the system one, it produces an optical illusion of stopped or slowed motion.
This direct observation allows us to verify the response of the system, especially the presence of resonances at certain frequencies. It turns out to be useful when there are doubts about the accuracy of the measurement setup and the independence of the results from that.

Figure 6.1.1: **Stroboscope from manufacturing company[40].**

In this work, experimental modal analysis is performed through frequency sweeps on a shaker table.
As regards the experimental damping, it is computed according to the -3 dB or half-power bandwidth method (Sec. 3.1.2).

Depending on the type of signal, different vibration tests can be run. The characteristics of the system and the purpose of the analysis influence on this choice.
A sine test provides a general understanding of the dynamic behaviour of a system. A harmonic excitation at a given frequency and constant amplitude is applied until steady-state conditions are reached and the peak sinusoidal value of the response is recorded. The frequency is then swept in a certain range to study the responses to different harmonics applied at a time.
This type of excitation is far from being a real-life vibration, so it does not provide information related to actual responses in applications because the same amount of energy is used in exciting the system at each frequency.

Differently from the sine test, random vibration testing involves a broad spectrum of vibration frequencies and tries to simulate real working conditions.
Random vibrations represent a physical phenomenon that cannot be described by meaningful mathematical expression. The signal is characterised by a series of different frequencies that overlap.

The Power Spectral Density (PSD) provides information about the shape of random signal that indicates the distribution of the signal over frequency range. Not all the frequencies have the same importance in the excitation. Estimation of the response and durability of the system can be performed.

6.2 Previous measurements

6.2.1 Shaker test

Test setup

The dual bellow assembly has been the object of previous measurements with the purpose of understanding the dynamics of the bellows[27]. Two different test setups were used, one with a complete exhaust pipe assembly and one with only a single bellow. One at a time, they were mounted on the shaker table.
The pipe-assembly in Fig. 6.2.1 used the bellow A2 (Fig. 4.1.1b). It was fixed to the fixtures with V-band clamps, which in turn were attached to the shaker table. Five tri-axial accelerometers were located along the pipe, and two additional ones were placed on the fixtures.
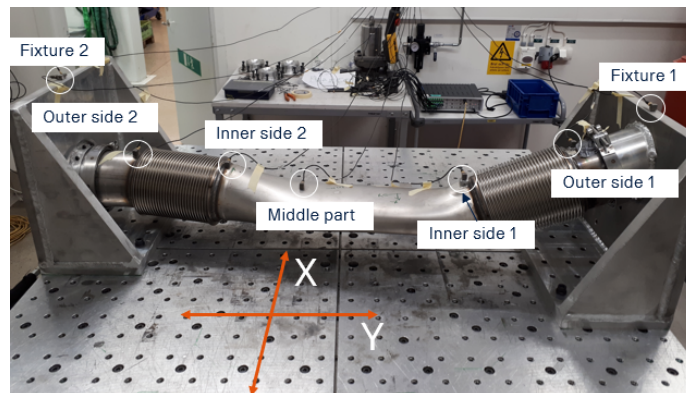
Figure 6.2.1: **The test setup with the complete exhaust pipe assembly, mounted on the shaker table[27].**

In the second setup, both bellow A1 (Fig. 4.1.1a) and A2 (Fig. 4.1.1b) were considered, as shown in Figs. 6.2.2a and 6.2.2b. They were welded to two flanges, which in turn were attached to the fixtures. A tri-axial accelerometer was attached to one of the convolutions, and the directions of measurement coincided with the local coordinate system.

Tests were performed by both running frequency sweeps and using random vibrations along and transverse the component, in the Y and X directions, respectively, according to local coordinate systems.
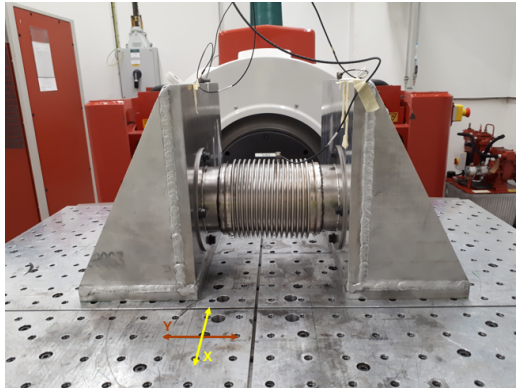
(a) **Bellow A1.**
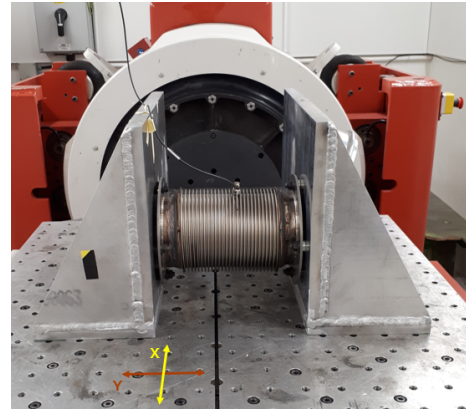
(b) **Bellow A2.**

Figure 6.2.2: **The test setup with the single bellow[27].**

The frequency was swept from 10 Hz to 1500 Hz for both complete assembly and single bellow, while the amplitude of the shaker table was held constant at 20 m/s^2 in the first case and at 10 m/s^2 in the second one. For the random vibrations, the test setups were excited by Scania's specific test spectrum for chassis components. Since the fixtures were characterised by distinct resonances at frequencies at around 400 Hz, as shown in Fig. 6.2.3, and, from Fig. 6.2.4, it appeared to influence the response in the pipe assembly, the analysis was focused on frequencies up to 300 Hz.
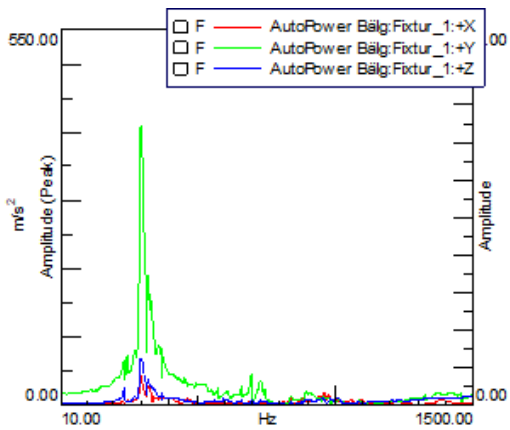
(a) **Right hand side fixture, frequency sweep in Y-direction.**
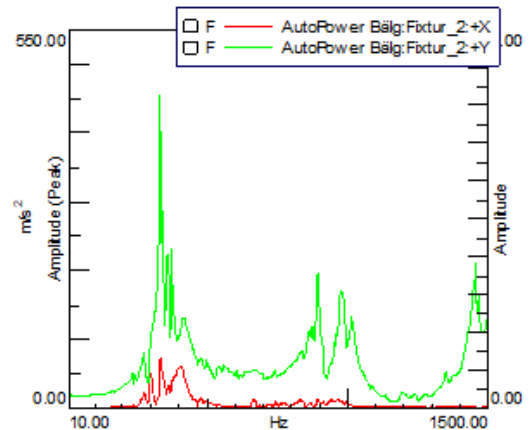
(b) **Left hand side fixture, frequency sweep in Y-direction.**
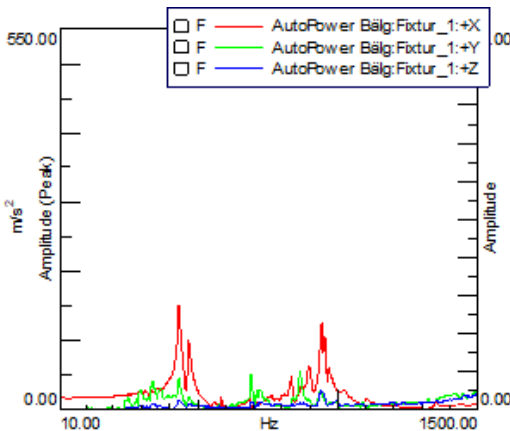
(c) **Right hand side fixture, frequency sweep in X-direction.**
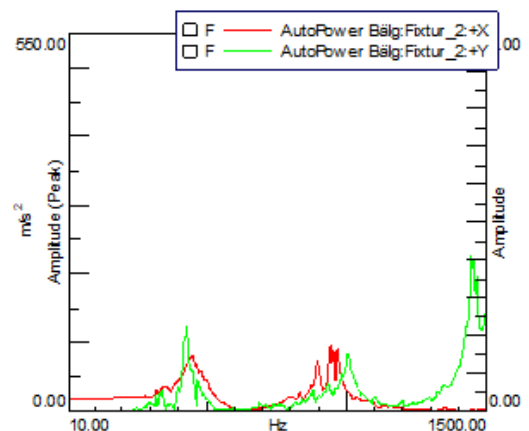
(d) **Left hand side fixture, frequency sweep in X-direction.**

Figure 6.2.3: **Response in acceleration in individual directions for accelerometers at the fixtures (in Fig. 6.2.1) from frequency sweep in Y and X test direction[27].**
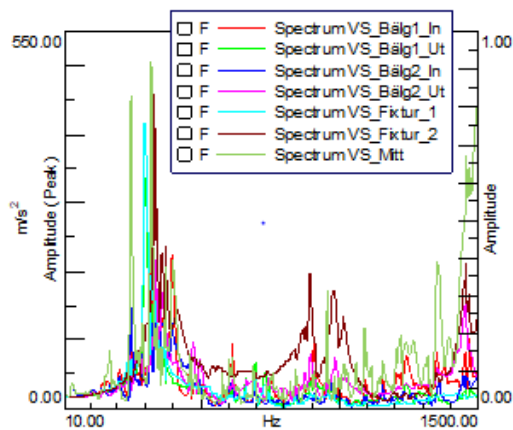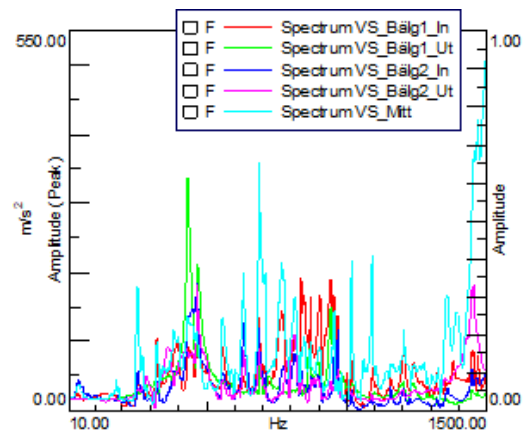
(a) **Frequency sweep in Y-direction.**   (b) **Frequency sweep in X-direction.**

Figure 6.2.4: **Response in acceleration as vectorial sum for all the accelerometers along pipe-assembly from frequency sweep in Y and X test direction[27].**

Test results

Pipe-assembly   For complete pipe-assembly, the main response arises in the middle part (Fig. 6.2.1) in vertical direction. Looking at Fig. 6.2.5, two evident peaks are identified at around 170 Hz and 250 Hz.

Another peak at around 30 Hz becomes clear by comparing the response in velocity to the shaker table one in Fig. 6.2.6.

The respective mode shapes were determined with a simplified modal analysis. At 30 Hz, the middle part moves mainly along the pipe, alternately compressing and decompressing the bellows.

At higher frequencies, the middle part mainly moves more in the vertical direction, and the bellows compress or decompress as a reaction to that.

The random vibration test highlights in the middle part the same peaks of the frequency sweep, as shown in Fig. 6.2.7. Furthermore, an additional peak at around 130 Hz, not noticed previously, is obtained in the responses in the Y direction by accelerometers at the inner sides of bellows.
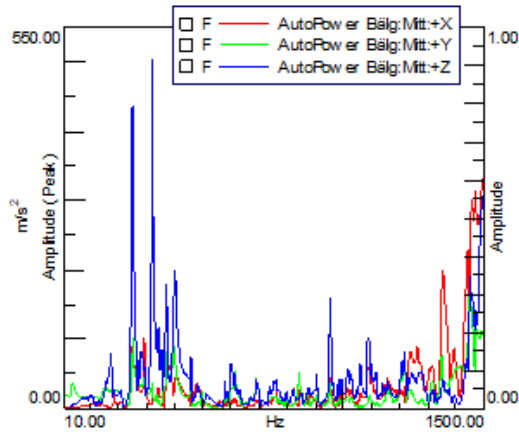
(a) **Frequency sweep in Y-direction.**
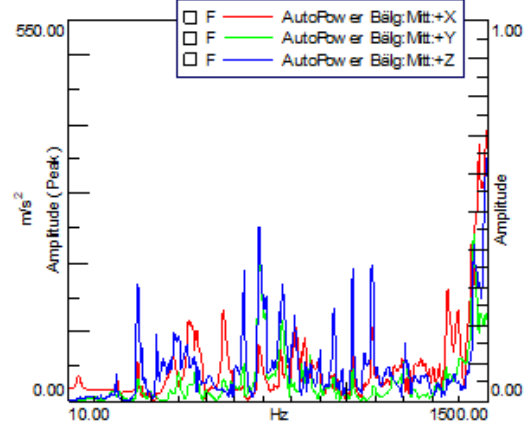
(b) **Frequency sweep in X-direction.**

Figure 6.2.5: **Response in acceleration as vectorial sum for all the accelerometers along pipe-assembly from frequency sweep in Y and X test direction[27].**
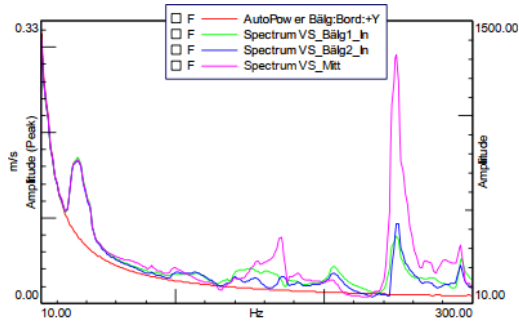
(a) **Frequency sweep in Y-direction.**
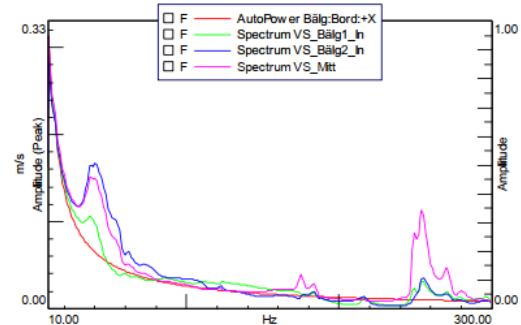
(b) **Frequency sweep in X-direction.**

Figure 6.2.6: **Response in velocity as vectorial sum for the accelerometers at the middle part, inner sides of the bellows, and for the shaker table (pipe-assembly setup), from frequency sweep in Y and X test direction[27].**
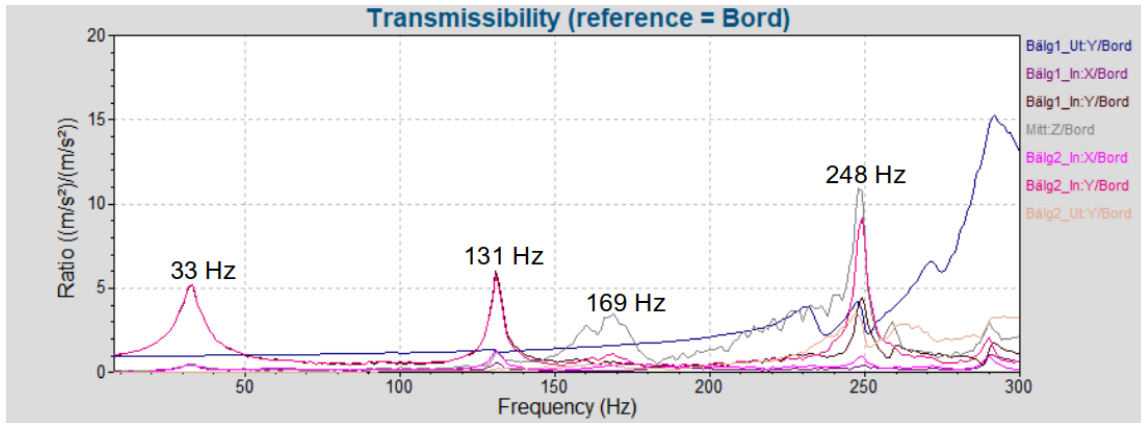
(a) **Random vibration in Y-direction.**
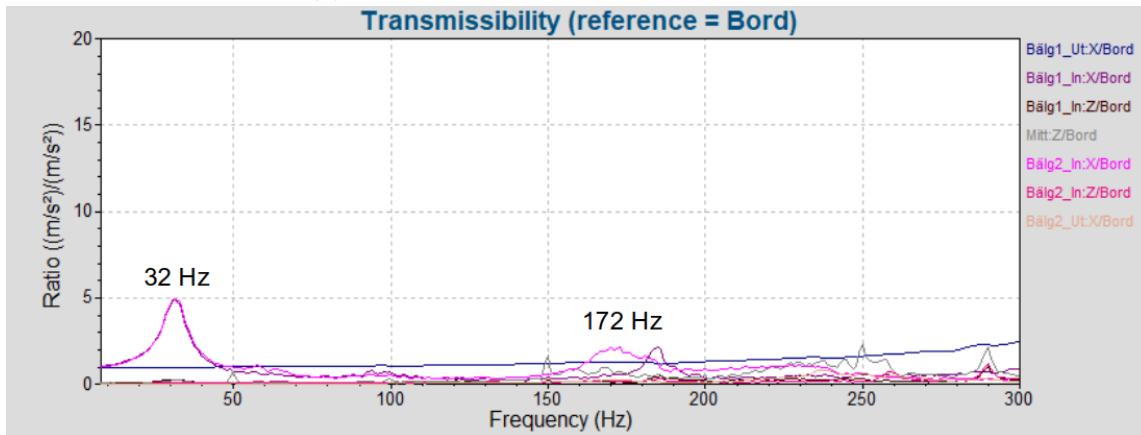
(b) **Random vibration in X-direction.**

Figure 6.2.7: **Response in transmissibility in individual directions for the accelerometers along the pipe-assembly, from random vibration in Y and X test direction[27].**

The result of measurements on complete pipe-assembly is summarised in Tab. 6.1.

43

Mode	Eig. [Hz]	Damp. [%]	Reference accelerometer	Mode shape
1	30	15(Y)-36(X)	Middle part, inner side of bellows	Test direction
2	130	-	Inner side of bellows	Test direction
3	170	-	Middle part	Vertical direction
4	250	-	Middle part	Vertical direction

Table 6.1: **Eigenfrequencies and eigenmodes of complete pipe-assembly[27].**

Single bellows For single bellows, the main response arises in the axial direction in both bellows A1 and A2, as shown in Figs. 6.2.8, 6.2.9, and 6.2.10.
The bellow A1 shows the first peaks at around 138 Hz and 166 Hz, while for the bellow A2, they are located at 116 Hz and 178 Hz.
The same result is obtained by random vibration, as shown in Figs. 6.2.11 and 6.2.12, with the exception of the first peak of bellow A1 from the frequency sweep in the X-direction: the peak at 166 Hz in the vertical direction is not recorded; instead, it is at 218 Hz in the transverse direction.

Thanks to a close-up in Fig. 6.2.11b, it is possible to see that a peak at around 160 Hz in the vertical Z-direction is also captured by using random vibrations, but it results in a lower response in the X-direction and excitation table, as shown in Fig. 6.2.13, and for this reason it is considered.
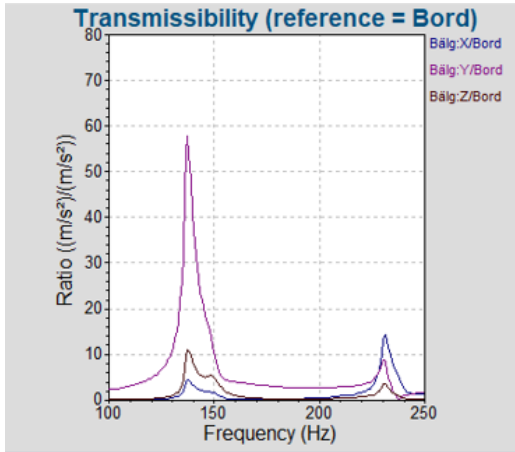
(a) **Frequency sweep in Y-direction.**
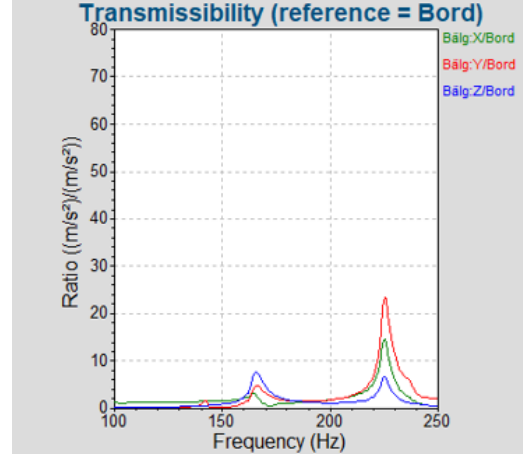
(b) **Frequency sweep in X-direction.**

Figure 6.2.8: **Close-up at response in transmissibility in individual directions for bellow A1 from frequency sweep in Y and X test direction[27].**
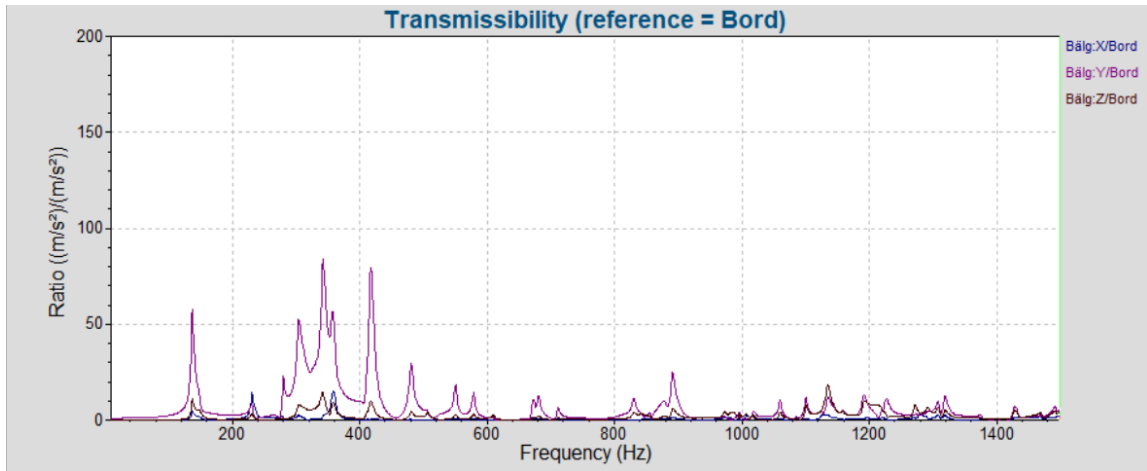
(a) **Frequency sweep in Y-direction.**
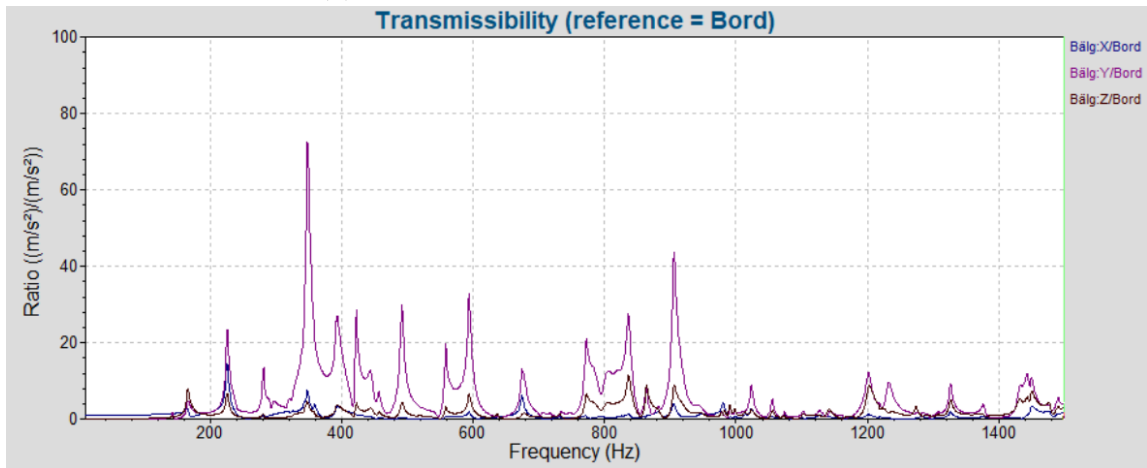
(b) **Frequency sweep in X-direction.**

Figure 6.2.9: **Response in transmissibility in individual directions for bellow A1 from frequency sweep in Y and X test direction[27].**
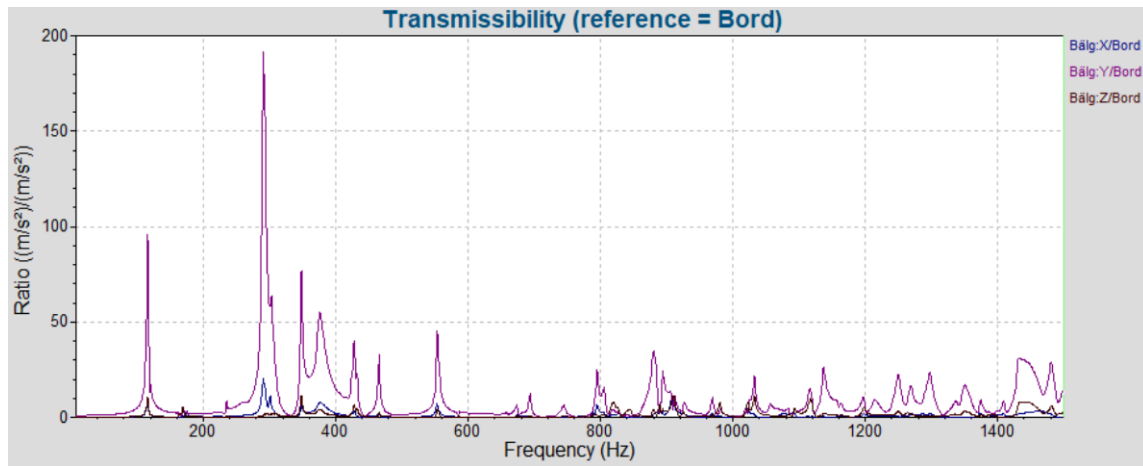
(a) **Frequency sweep in Y-direction.**
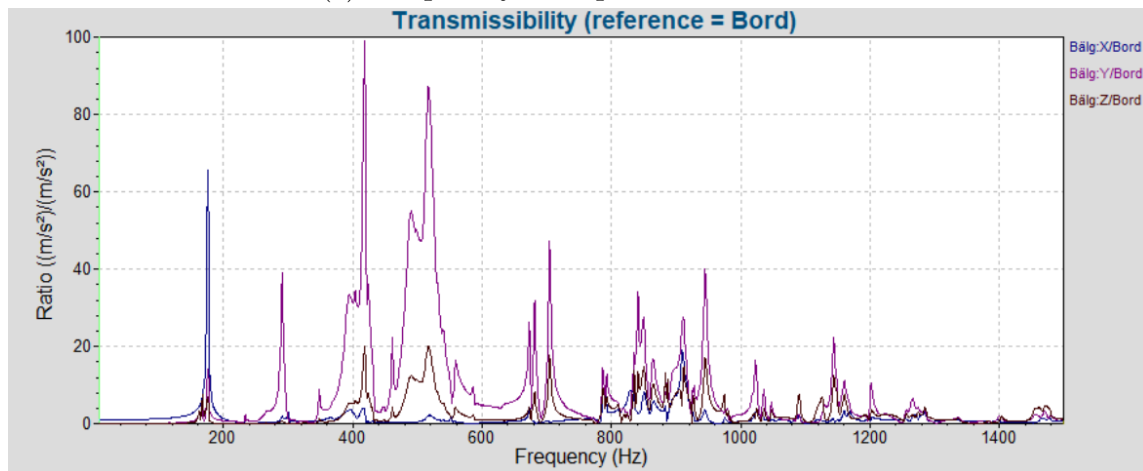
(b) **Frequency sweep in X-direction.**

Figure 6.2.10: **Response in transmissibility in individual directions for bellow A2 from frequency sweep in Y and X test direction[27].**
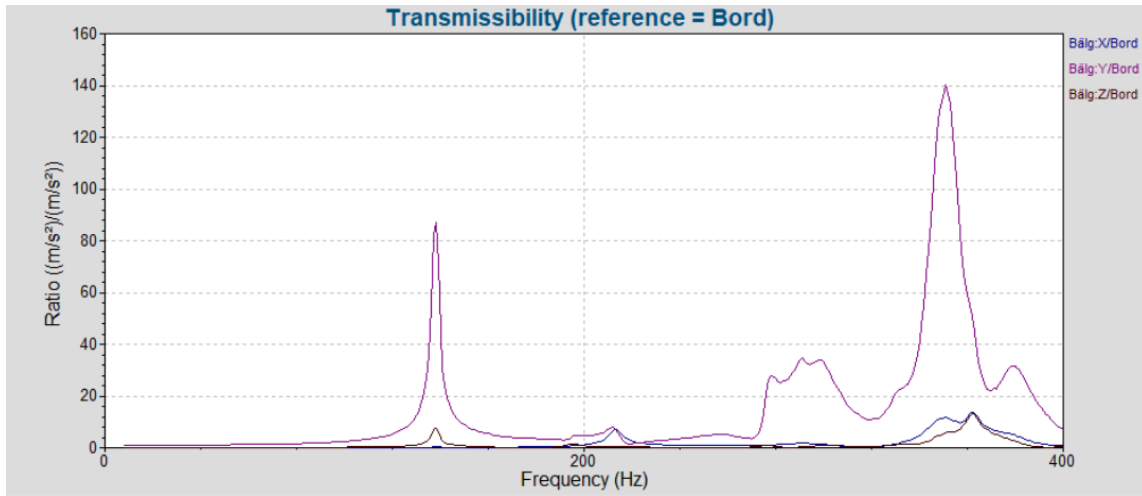
(a) **Random vibration in Y-direction.**
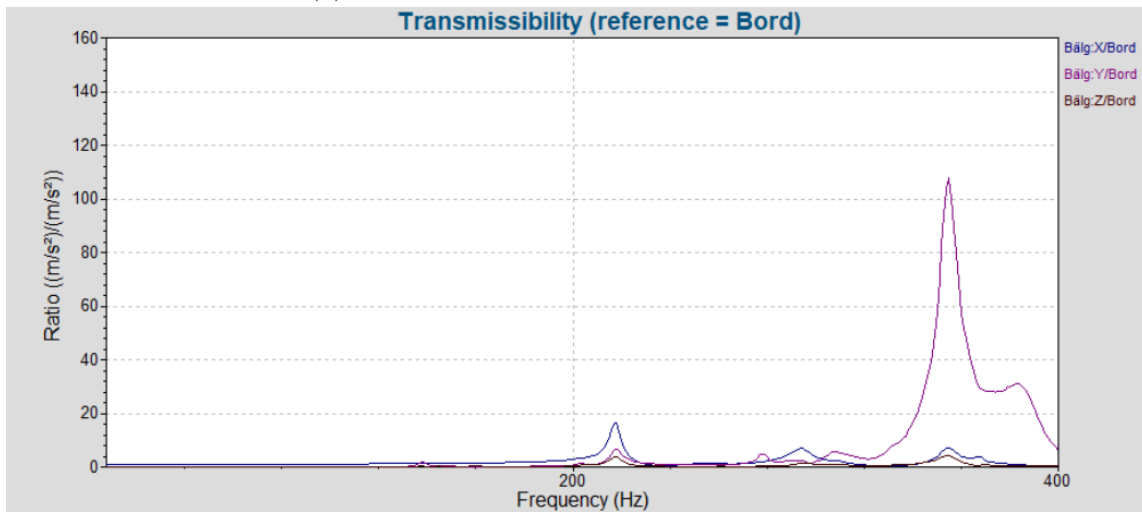
(b) **Random vibration in X-direction.**

Figure 6.2.11: **Response in transmissibility in individual directions for bellow A1 from random vibration in Y and X test direction[27].**
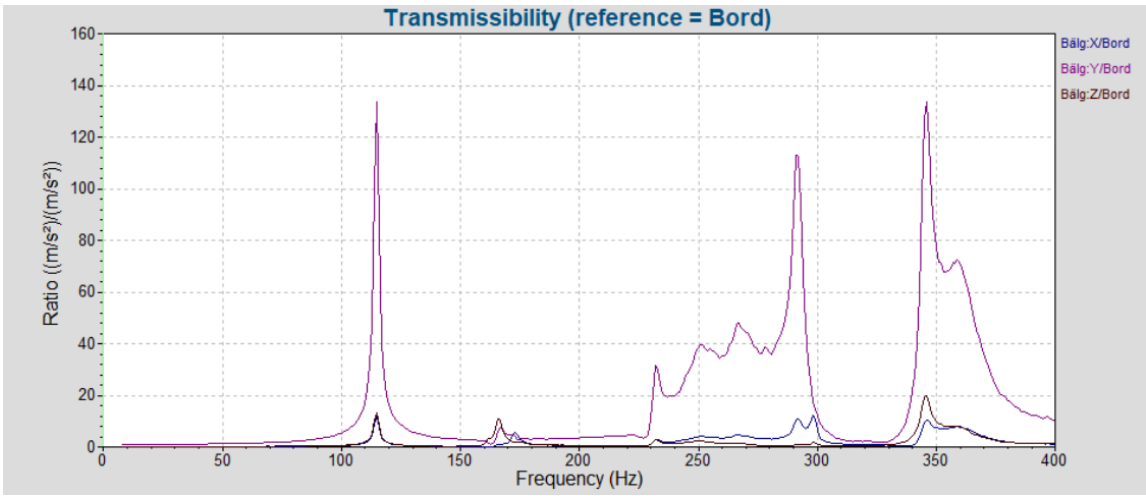
(a) **Random vibration in Y-direction.**
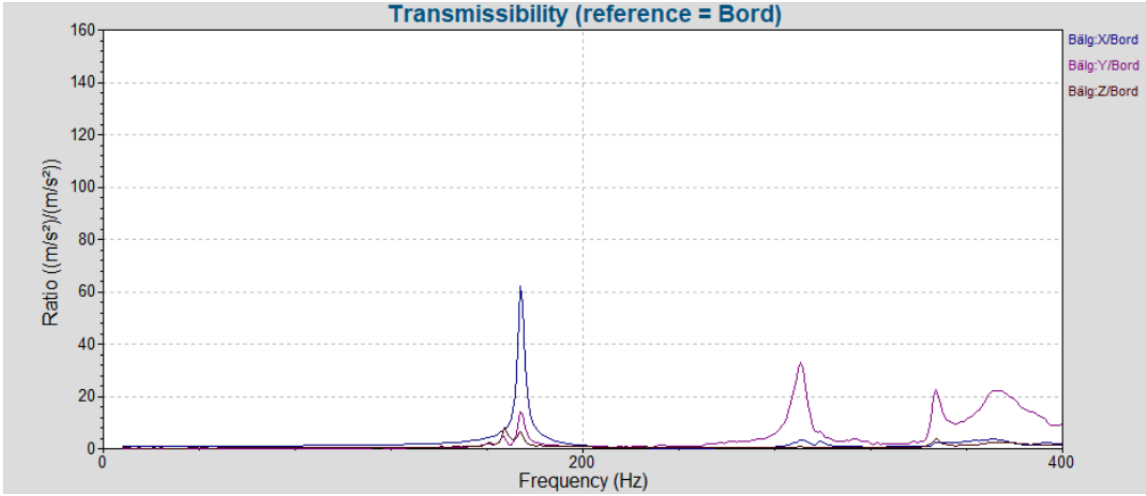
(b) **Random vibration in X-direction.**

Figure 6.2.12: **Response in transmissibility in individual directions for bellow A2 from random vibration in Y and X test direction[27].**
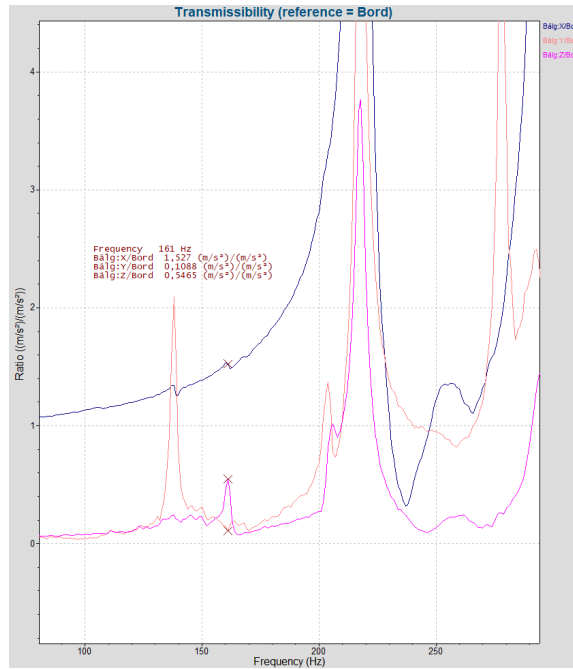
Figure 6.2.13: **Close-up at response in transmissibility in individual directions for bellow A1 from random vibration in X direction.**

The results of measurements on single bellows are summarised in Tabs. 6.2 and 6.3, and the related damping ratios are specified.

Mode	Eigenfrequency [Hz]	Damping ratio [%]	Mode shape	Test direction
1	138	1.48	Axial	Y
2	166	-	Vertical	X

Table 6.2: **Eigenfrequencies and eigenmodes of bellow A1[27].**

Mode	Eigenfrequency [Hz]	Damping ratio [%]	Mode shape	Test direction
1	116	1.11	Axial	Y
2	178	0.63	Transverse	X

Table 6.3: **Eigenfrequencies and eigenmodes of bellow A2[27].**

49

By comparing the random vibration response of the single bellow with the complete pipe-assembly one, as shown in Fig. 6.2.14, the left-hand side bellow in the installation (Fig. 6.2.1) has a first peak at around 121 Hz, slightly higher than the one measured for the single bellow and in the same direction. Its location is the closest to the single bellow test setup.
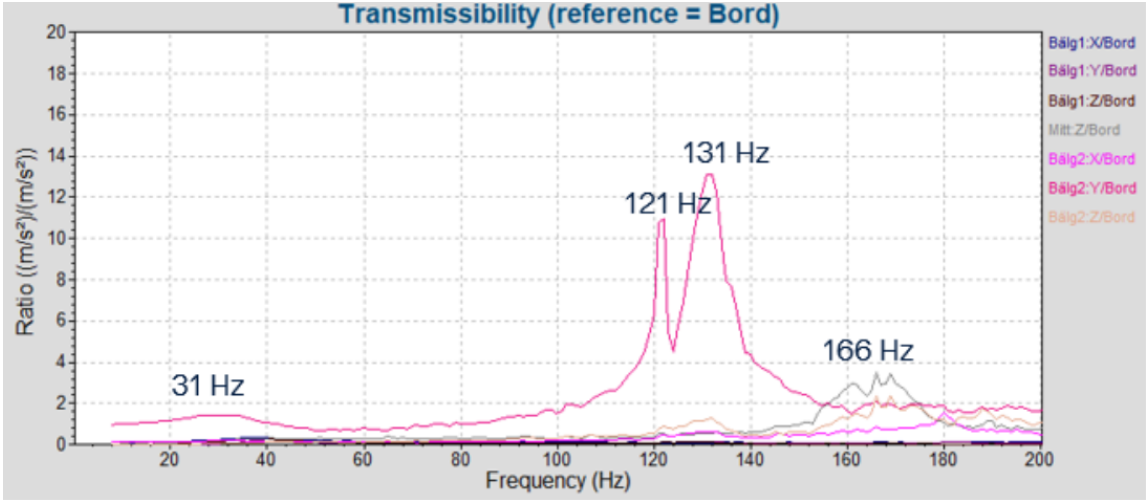
(a) **Random vibration in Y-direction.**
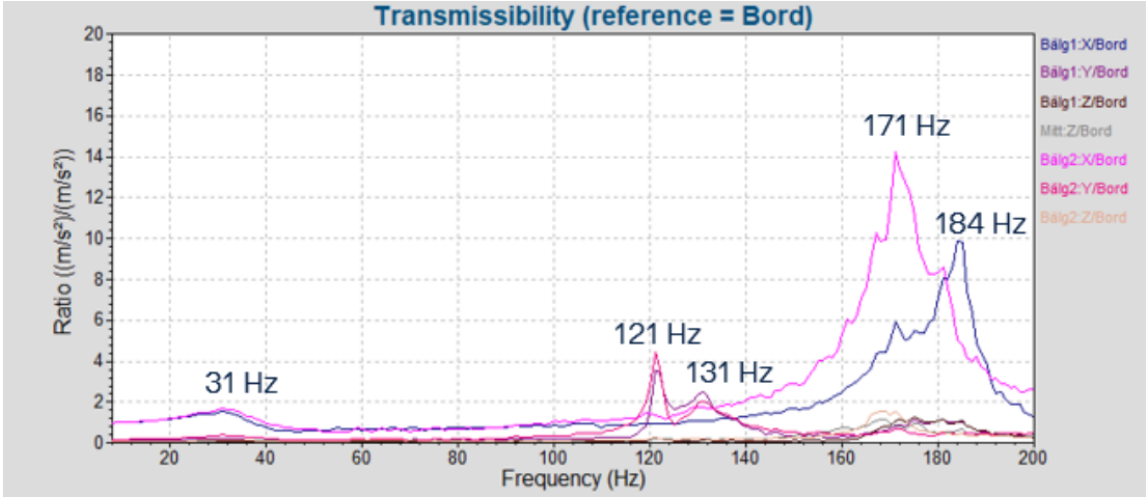
(b) **Random vibration in X-direction.**

Figure 6.2.14: **Response in transmissibility in individual directions for the accelerometers at the bellows in complete pipe-assembly from random vibration in Y and X test direction[27].**

50

6.3   New measurements

6.3.1   Shaker test

Test setup

In order to investigate the dynamic behaviour of the flexible hose B from the single flexible pipe assembly (Fig. 4.1.1c), new measurements are requested at the Scania shaker test lab. The aim is to get the same kind of results as the previous test and investigating the possible amplitude dependence of the responses.
The flexible hose is fixed to two flanges with V-band clamps, which are attached to the fixtures, designed specifically for this test.
The fixtures, in turn, are mounted on the shaker table.

Tests are performed by frequency sweeps along and transverse the component in the Y and X directions, respectively, according to local coordinate systems. Firstly, the frequency is swept from 20 Hz to 1500 Hz with the amplitude of the shaker table, which is held constant at 20 m/s^2. Secondly, the frequency is swept from 20 Hz to 400 Hz at different amplitudes of the shaker table, including between 5 and 50 m/s^2.

In the previous measurements, attaching the tri-axial accelerometer to the flexible pipe was not trivial, but in this case, it is even harder because the convolutions are sharper and thinner. The configuration with the accelerometer attached to one of the convolutions is shown in Figs. 6.3.1a and 6.3.1b.
An alternative setup is also tried out by fixing a hose clamp on two convolutions and glueing the accelerometer on the top, as shown in Fig. 6.3.1c. The accelerometer is moved to the side of the clamp, as shown in Fig. 6.3.1d, in order to get a measurement of the response in the direction of excitation by running a frequency sweep in the Y-direction and compare the influence of two positions on the results.
The frequency sweeps at different amplitudes are performed by using this setup with the addition of a further accelerometer at one end of the flexible hose as a reference, as shown in Fig. 6.3.2a.

Two transducers are located on the fixtures to verify their possible influence on the response. This influence is further examined by testing the fixtures without flexible pipe, as shown in Fig. 6.3.2b. The directions of measurement for accelerometers generally coincide with the local coordinate system.
During the tests, a stroboscope allows for direct observation of the vibrations on the flexible pipe in order to check that the setup does not alter its behaviour.
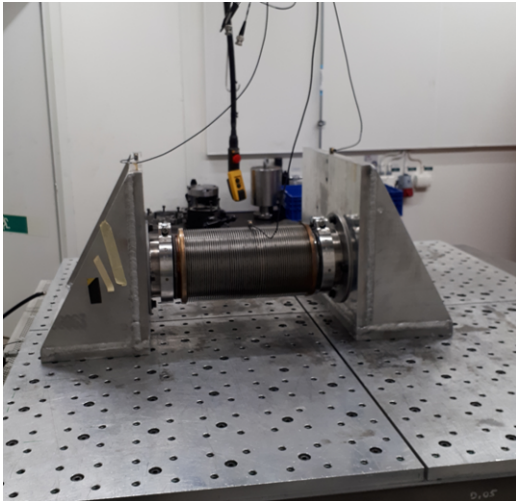
(a) **Setup with accelerometer attached directly to one convolution.**

(b) **Close-up at accelerometer attached directly to one convolution.**
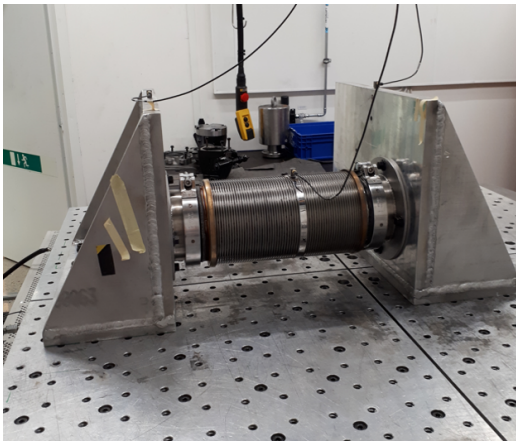
(c) **Setup with accelerometer attached to the top of the hose clamp.**
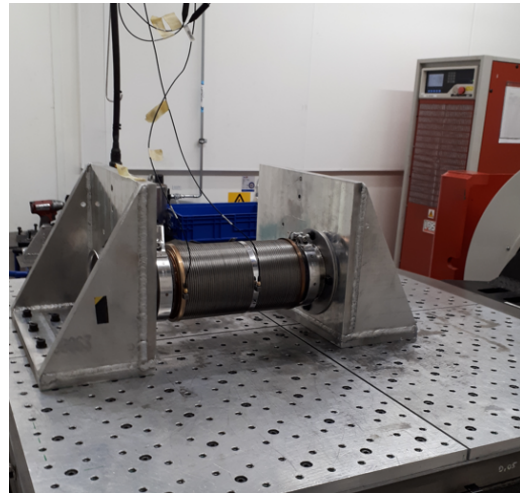
(d) **Setup with accelerometer attached to the side of the hose clamp.**

Figure 6.3.1: **Different setups for the new measurements.**
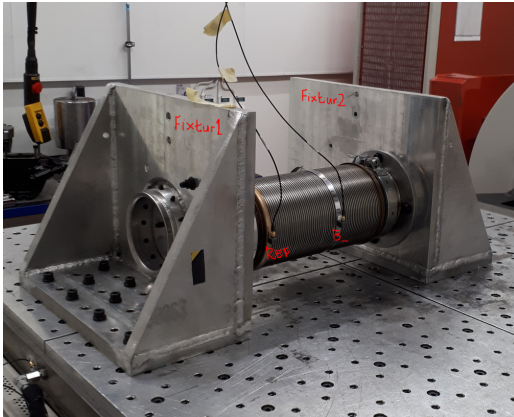
(a) **Setup for frequency sweeps at different amplitudes.**

(b) **Setup with only the fixtures.**

Figure 6.3.2: **Different setups for the new measurements.**

Test results

All setups show the main response in the axial direction, as shown in Figs. 6.3.3 and 6.3.4. The responses in the directions of excitation for different setups are compared in Figs. 6.3.5a and 6.3.5b.

Since the fixtures are characterised by first resonances at around 280 Hz, as shown in Figs. 6.3.6a and 6.3.6b, and it appears to influence the response in the flexible hose starting from 280 Hz, as shown in Figs. 6.3.5a and 6.3.5b, the analysis is focused on lower frequencies.

The first setup (in Fig. 6.3.1a) shows the first peaks at around 163 Hz and 207 Hz, while by using the second one (in Fig. 6.3.1c), they are located at around 131 Hz and 211 Hz. The accelerometer attached to the side of the hose clamp (in Fig. 6.3.1d) records a first peak at around 147 Hz for the excitation in the Y-direction.
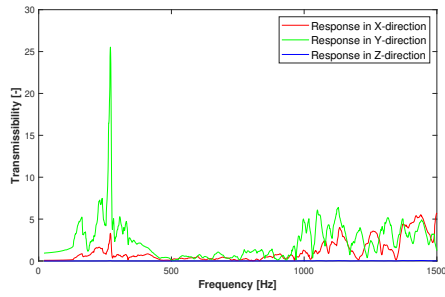
(a) **Frequency sweep in Y-direction.**
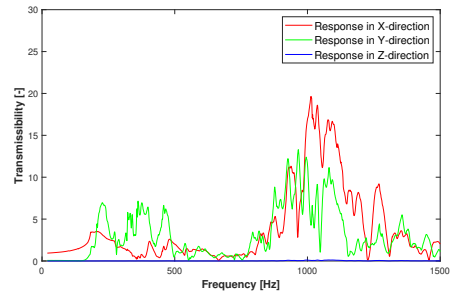
(b) **Frequency sweep in X-direction.**

Figure 6.3.3: **Setup with accelerometer on the convolution: response in transmissibility in the direction of excitation from frequency sweep in Y and X test direction.**
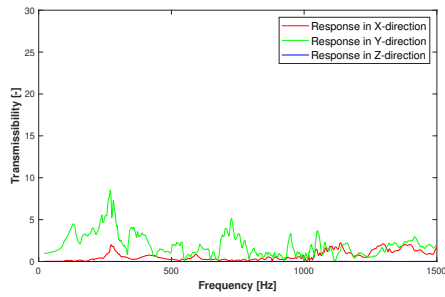
(a) **Frequency sweep in Y-direction.**
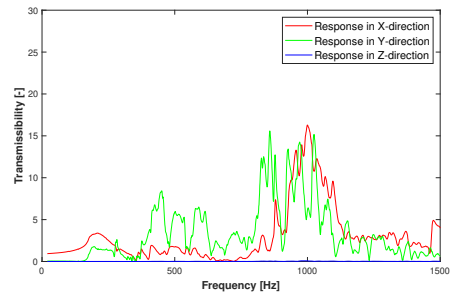
(b) **Frequency sweep in X-direction.**

Figure 6.3.4: **Setup with hose clamp: Response in transmissibility in individual directions from frequency sweep in Y and X test direction.**

54
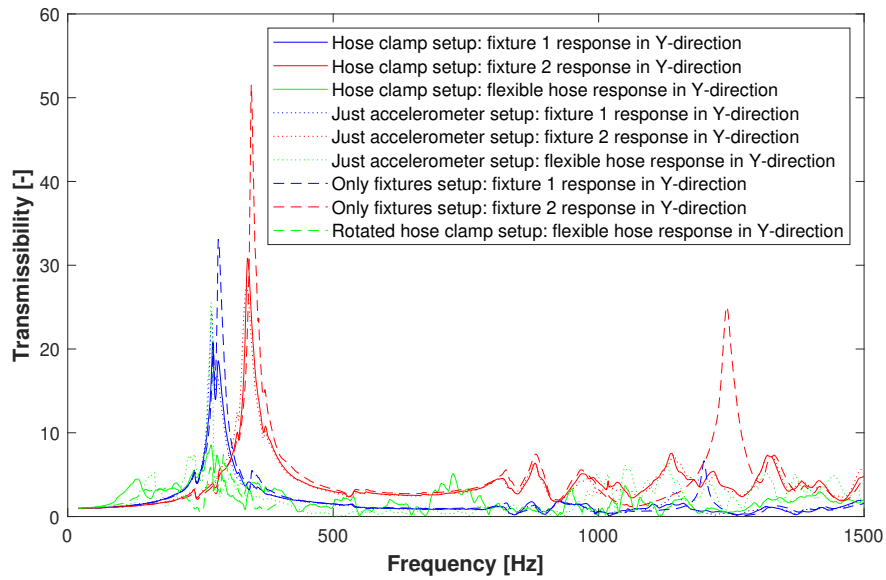
(a) **Frequency sweep in Y-direction.**
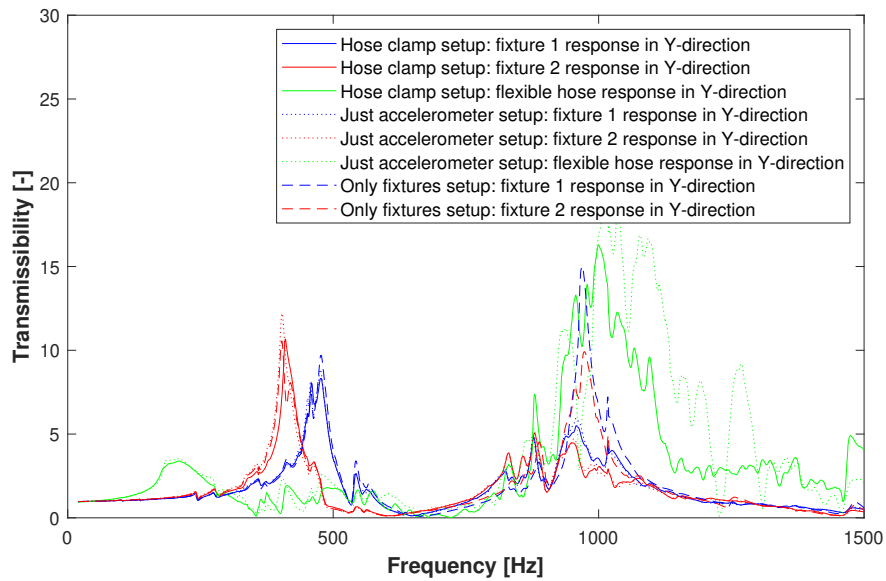
(b) **Frequency sweep in X-direction.**

Figure 6.3.5: **Response in transmissibility in the direction of excitation for different setups from frequency sweep in Y and X test direction.**
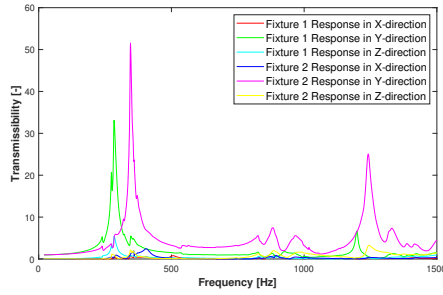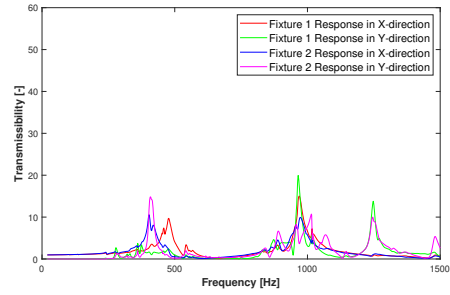
(a) **Frequency sweep in Y-direction.**   (b) **Frequency sweep in X-direction.**

Figure 6.3.6: **Setup with only fixtures: response in transmissibility in the direction of excitation for different setups from frequency sweep in Y and X test direction.**

The results of the first measurements are summarised in Tab. 6.4.

Mode	Eigenfrequency [Hz]	Damping ratio [%]	Mode shape	Test direction
1	131-163	11.87-6.57	Axial	Y
2	207-211	-	Transverse	X

Table 6.4: **Eigenfrequencies and eigenmodes of flexible hose B.**

As regards the second investigation, the responses in different directions for the accelerometer on the hose clamp are obtained at different acceleration amplitudes. The results are reported in App. A, and they are summarised in Tab. 6.5. Acceleration responses related to three different values of acceleration amplitude are compared in Figs. 6.3.7 and 6.3.8.

Acceleration amplitude [m/s^2]	First peak in Y-dir. [Hz]	First peak in X-dir. [Hz]
5	198	227
10	185	224
15	159	194
20	147	176
25	136	165
30	130	152
35	97	140
40	87	126
45	87	120
50	78	108

Table 6.5: **First eigenfrequencies of the flexible hose B at different acceleration amplitudes.**
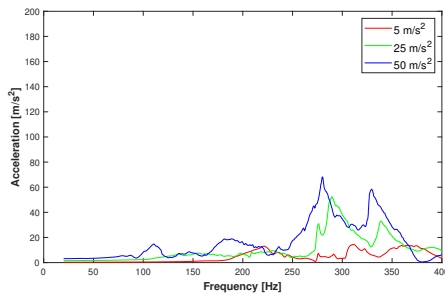
(a) **Acceleration response in X-direction.**
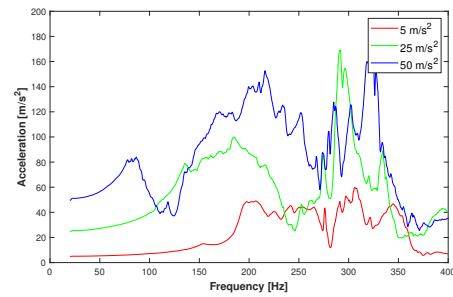
(b) **Acceleration response in Y-direction.**
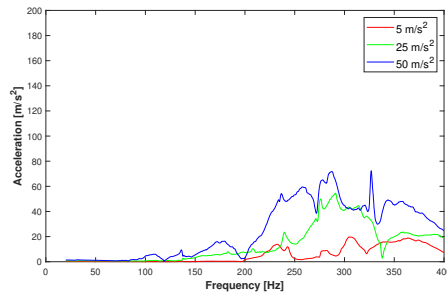
(c) **Acceleration response in Z-direction.**

Figure 6.3.7: **Acceleration responses from frequency sweep in Y-direction at 5** m/s^2, **25** m/s^2 **and 50** m/s^2.
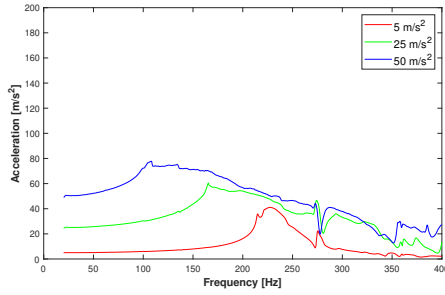
(a) **Acceleration response in X-direction.**
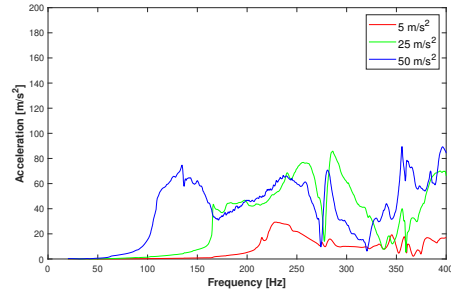
(b) **Acceleration response in Y-direction.**
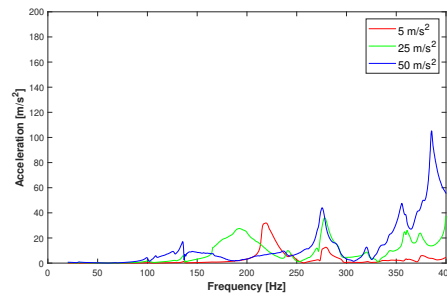
(c) **Acceleration response in Z-direction.**

Figure 6.3.8: **Acceleration responses from frequency sweep in X-direction at 5** m/s^2**, 25** m/s^2 **and 50** m/s^2**.**

Discussion

The measurements turn out to be non trivial at all. As regards the excitation in the Y direction, the first peak is found at three different eigenfrequencies, distributed in a range of 32 Hz, for the different setups. On the other side, the excitation in the X direction evidences the presence of a peak between 207 and 211 Hz with a narrow margin of error.

These differences cause one to think that results are partially affected by the setup itself, not only due to the addition of mass but also by the grip of the hose clamp on the component.

In the first case, in Fig. 6.3.1a, the accelerometer is glued to the tip of the thin convolution, and it adds a small, but not negligible, mass to the system. It can be seen as a lumped mass hung at the end of a slender beam. From this observation, the suspicion that the accelerometer is capturing a response strongly influenced by

58

its own presence arises.

In the second case, in Fig. 6.3.1a, in order to avoid any slipping between the hose clamp and flexible hose, it must be tightened enough, but at the same time, too much tightening can compress the convolutions and alter the actual behaviour of the system. It is also shown that moving the accelerometer on the side (in Fig. 6.3.1d) affects the response in the Y direction.

Furthermore, the use of the stroboscope allows to notice a concentration of the vibrations on one side with respect to the hose clamp; it is another hint about the possible alteration of the responses due to the setup.
Running the measurements with only the fixtures (in Fig. 6.3.2b) allows us to confirm that they are not affected by the behaviour of the flexible pipes, so their first eigenfrequencies are known precisely.

The results in Sec. A and the comparison in Fig. 6.5 evidence that the response is influenced by the acceleration amplitude of the shaker table. In particular, the higher the amplitude, the lower the eigenfrequency of the first peak. The dynamic behaviour then shows an extreme softening at high acceleration amplitudes. As expected, the amplitude of the peak grows as the excitation level increases.
In Fig. 6.5, it can also be seen that other harmonics appear at different amplitudes, and the identified first peak does not always belong to the same one. These are both warnings of the presence of non-linear dynamic behaviour.
Since there were two convolutions of the bellow dent during the measurements, the results in general should not be considered totally accurate. For example, some differences are found in the responses of two measurements at the same amplitude and setup, as shown in Figs. 6.3.4a, A.0.1d, 6.3.4b, and A.0.3d, respectively.

6.3.2   Static test

Test setup

In order to extract the missing static stiffness values for the bellow A2, an axial static test is run on a test rig. Previously, the flexible pipes were tested by suppliers who provided the test data sheets.
As regards the setup, the component is located vertically, with the bottom flange fixed at the base and the top one attached to the cross-head that moves up and down thanks to four screws, as shown in Fig. 6.3.9. At the beginning, the bellow is slightly compressed, and then a cycle of stretching and compressing is run by recording the force and the axial displacement. The procedure is repeated four times at doubling rates, respecting the original value V.

Figure 6.3.9: **Test setup for static test on the test rig.**

The axial static stiffness value is then computed by interpolating the experimental data by using a straight line and considering its slope. The average value is chosen as the axial static stiffness for the component.

Test results

The results for the four measurements are shown in Fig. 6.3.10 and the corresponding static stiffness values from the interpolation are reported in Tab. 6.6.

Measurement	Rate	Axial static stiffness [N/m]
1	V	54640
2	2V	54330
3	4V	55500
4	8V	52990

Table 6.6: **Axial static stiffness from the different measurements on the test rig at doubling rate.**
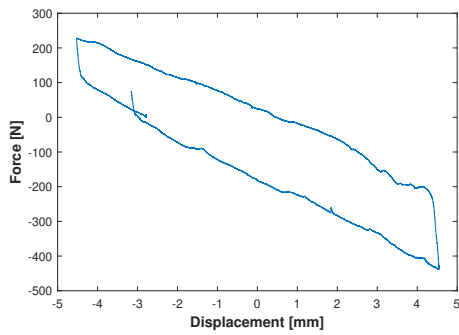
(a) **Test at starting rate** V**.**
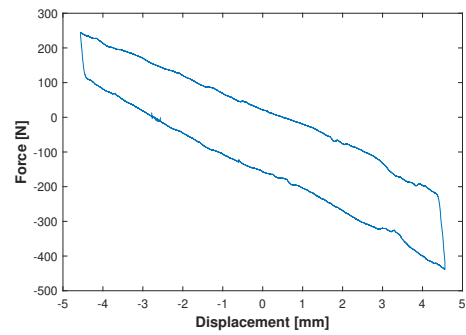
(b) **Test at the rate** $2V$**.**
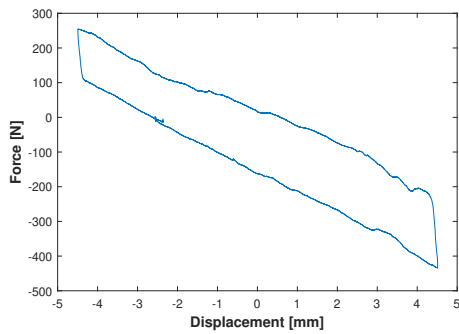
(c) **Test at the rate** $4V$**.**
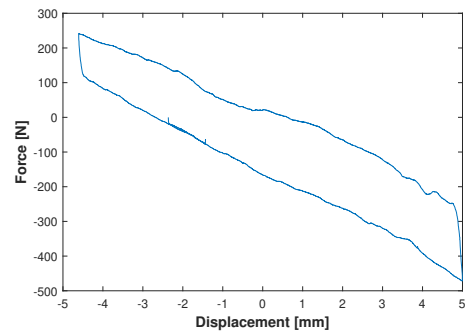
(d) **Test at the rate** $8V$**.**

Figure 6.3.10: **Static tests of the axial stiffness at the doubling rate.**

61

Chapter 7

Modelling

7.1 Proposed models for the bellow A1

As a result of the state of the art review conducted, three different methods were identified.

The idea is to start from the previous model and propose a new one for bellow A1, so that they can also be used for other flexible pipes.

In the different methods, the geometry is characterised by the current model of the flexible pipe attached to the flanges kept from previous models as well as the boundary conditions, as shown in Sec. 2.3.1.

As regards the analysis, some changes are made to be more coherent in relation to the testing. The steady-state analysis is considered between 10 and 500 Hz, and the frequency resolution is increased, while the amplitude for the base motion is changed to 20 m/s^2 for the single bellow and 20 m/s^2 for the complete assembly.

This time, the damping ratio is taken from experimental measurements, and it is approximated to 1% only if it is not known.

The FRFs are now computed at the nodes located in the position where the corresponding accelerometers are placed during the measurements.

7.1.1 Shell elements method

The shell approach is quite similar to the one defined in the previous model; only small adjustments are made with the aim of allowing easier comparison of results with respect to the tests and other methods.

This method requires a CAD model of the flexible pipe whose outer surface is meshed by using shell elements, as shown in Fig. 7.1.1. As already stated, the interlock cannot be considered because its proper structure is not present in the CAD; however,

its complex geometry would require too many elements, and the model would become computationally expensive.
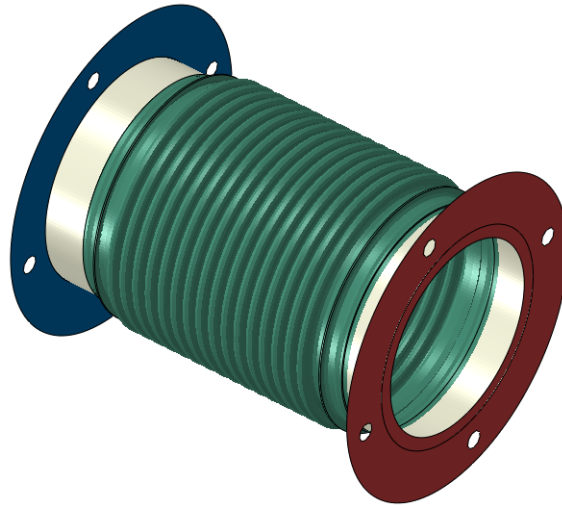
Figure 7.1.1: **Bellow A1 by using shell elements model.**

The mass of the element depends on the density and shell thickness used for the flexible pipe, while the stiffness is determined by material properties and geometry. The Young's modulus can then be varied to change the stiffness and match the first eigenfrequency. It is not suggested to compute the different iterations by using an optimization software because the time required will be much higher than in other cases.

7.1.2 Connector elements method

In the absence of a CAD model or when the geometry of the component is unknown or even more complex, the connector approach is suitable. The model is shown in Fig. 7.1.2.
It only requires as input the stiffness characteristics in the directions of 6 DOFs, which are the results of the measurements obtained by axial, transverse, bending, and torsion static tests.
These elements include all the different parts of the flexible pipe, so no information about their single mass or stiffness is required.

The definition of the mass or density of the element is not available, but it must be included in a different way to get reliable results, especially in a dynamic simulation. A possible solution is to add lumped mass elements at the two ends of the connector.

A better approach sees the use of more connectors in series, one attached to the other, and with mass elements located in each intermediate node. They are connected to the flanges by "spiders". The complete model is sketched in Fig. 7.1.3.
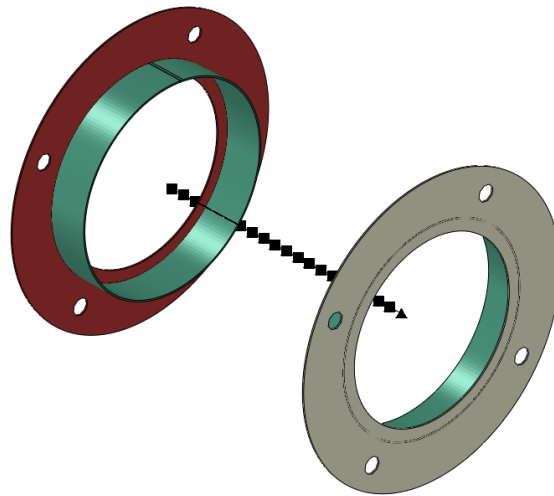
Figure 7.1.2: **Bellow A1 by using connector elements model.**

Figure 7.1.3: **Simplified representation of the parts of Bellow A1 by using thin-walled pipe elements model.**

Since they are characterised by spring-like stiffness characteristics for each DOF, each element has its own contribution to the total stiffness of the component.
In particular, they behave like springs in series subjected to the same force or moment and the single element is characterised by stiffness values computed as follows:

$$\begin{cases} k_c = n_c k_T \\ t_c = n_c t_T \\ b_c = n_c b_T \\ c_c = n_c c_T \end{cases} \tag{7.1}$$

for all the axial, transverse, bending and torsion directions. As regards the mass, a single lumped element is characterised by:

$$m_c = \frac{m}{n_c + 1}, \tag{7.2}$$

64

This model is easy to implement by assuming that the mass and stiffness are equally distributed along the axis of flexible pipe. It is certainly not true, but, at the same time, their distributions are unknown.

If the match of the first eigenfrequency is not achieved at the first attempt, it is possible to set an optimization process to fit the model by using the optimization software Heeds[36]. In this case, the parameters related to the stiffness assigned to the single elements and single masses can be changed.
Since the use of a large number of parameters makes the optimization more difficult with a lower probability of success, the elements and lumped masses are assumed to be the same for each element.
Later, the attempt to consider two different values for the elements at the ends and the ones in the middle of flexible pipe, taking into account the heavier and stiffer characteristics of the ends, is investigated.

7.1.3   Equivalent thin-walled pipe elements method

The following method is applicable if the geometry of the component as well as its axial and torsion stiffness are known. It becomes more and more precise if information about the dimensions, mass, and stiffness values of the single parts of flexible pipes is available.
Differently from the shell elements method, it does not consider the actual geometry of the component but tries to build an equivalent one. If the connector approach includes all the parts in the same element, in this case, there is an attempt to model them separately.
For describing the equivalent pipe elements with linear static behaviour in Abaqus[33], two geometrical dimensions, mean radius and wall thickness, and three material properties, density, Young's modulus, and Poisson's ratio, are required.
The procedure for computing these parameters is described below. The total mass is kept the same with respect to the original geometry, while the total stiffness varies and is verified later.

Equivalent bellow model

A simplified representation of the profile of one U-shape convolution is shown in Fig. 7.1.4a. The lateral surface is assumed to be perfectly straight and vertical. By assuming that $s \ll R_r$, R_c, and $h \ll R_m$, the length of the convoluted part is given by:

$$L = 2(R_r + R_c)n. \tag{7.3}$$

65

The bellow is then equivalent to an equivalent thin-walled pipe of length L and with a pipe section characterised by radius $R_m = \frac{D+h}{2}$ and wall thickness s_p, as shown in Fig. 7.1.4b.

(a) **U-shaped convolution geometry[1].**

(b) **Thin-walled pipe analogy of bellows[1].**
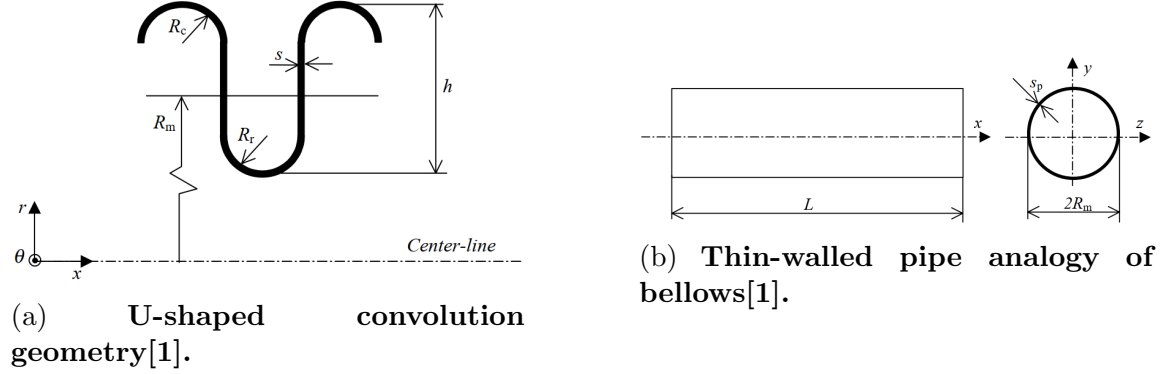
Figure 7.1.4: **Basics of the equivalent thin-walled pipe element model.**

The mass per unit of length is not constant due to the convoluted profile. Since the mass of the only U-shaped part is unknown, it is computed starting from the geometry as follows:

$$m = \frac{\rho 2\pi R_m [\pi(R_r + R_c) + 2(h - R_r - R_c)]s}{2(R_r + R_c)}. \tag{7.4}$$

All the mass is assumed to be located at the mean radius of the bellows, as described by the thin-walled pipe analogy. In the presence of bending or torsion rotations, the rotary inertias of the cross-section per unit length are expressed as:

$$\begin{cases} J = J_{yy} = J_{zz} = \frac{mR_m^2}{2} \\ J_{xx} = mR_m^2 \end{cases} \tag{7.5}$$

The definition of the pipe density and wall thickness are connected: since the mass per unit length and mean radius are defined, one of the parameters is assumed, and the other one is computed as a consequence by meeting the requirement:

$$s_p\rho_p = \frac{m}{2\pi R_m}. \tag{7.6}$$

The density is assumed to be the same as that of the bellow material.
As regards the geometrical characteristics, the area, area moment of inertia, and polar

66

area moment of inertia of the equivalent pipe cross-section are computed according to the equations:

$$\begin{cases} A_p = 2\pi R_m s_p \\ I_p = \pi R_m^3 s_p \\ K_p = 2\pi R_m^3 s_p. \end{cases} \tag{7.7}$$

As already stated, the total axial stiffness of the convoluted part depends on the characteristics of the convolute as follows:

$$k_p = \frac{k}{2n}. \tag{7.8}$$

Since it depends on Young's modulus, the last one can be computed as:

$$E_p = \frac{k_T L}{A_p}. \tag{7.9}$$

Following the same reasoning, the total torsion stiffness of the convoluted part is given by:

$$c_p = \frac{c}{2n}, \tag{7.10}$$

and the associated shear modulus is computed as:

$$G_p = \frac{c_T L}{K_p}. \tag{7.11}$$

By considering the Young's and shear moduli, the corresponding Poisson's ratio should be:

$$\nu_p = \frac{E_p}{2G_p} - 1. \tag{7.12}$$

Based on the computed equivalent geometry and material properties, the equivalent Poisson's ratio can be negative.

The transverse shear stiffness and rotary inertia are computed internally, starting from the shear stiffness, area, and moment area of inertia of the cross-section.

Equivalent models of the other parts

As regards the non-convoluted section of the bellow, it can be modelled by simple pipe elements. The diameter and thickness are taken from the original geometry. The material properties are the same as those of the bellow material.

The end caps are represented by lumped masses located in the middle of the straight pipe ends.

The interlock is the most difficult part to model because, apart from its diameter, its geometry, mass, and stiffness values are not known.

The inner sleeves have a known structure that consists of cylindrical and conical pipe sections in series, but the mass and stiffness are not known, so it is not convenient to model them separately, introducing new parameters to consider.

The inner structure, including both interlock and inner sleeves, is then modelled together by using other pipe section elements.

Equivalent flexible pipe model

The inner and outer structures are considered in parallel, but all the nodes are in common since they are supposed to move in a synchronous way due to the inner contact. The two ends are connected to the flanges by "spiders". The complete model is sketched in Fig. 7.1.5.

Figure 7.1.5: **Simplified representation of the parts of Bellow A1 by using thin-walled pipe elements model.**

As already stated, the actual values of the geometric and material parameters of single parts are not known.

For the convoluted part of the bellow, theoretical[8] and numerical[1] approaches can be followed with the aim of estimating the axial and torsion static stiffness values starting from the corresponding characteristics of half convolution, but the related attempts resulted in excessively rigid structures.

The optimization process is then needed. Initial guesses of the material properties of convoluted and inner parts are estimated by their stiffness characteristics in order to meet the stiffness of the entire component.

The interlock geometry and end-cap masses are defined so that the total mass is met. This condition is maintained by varying the end-cap masses and computing the interlock one as a difference.

Since the bellow geometry is known for both the convolutions and end caps, the only uncertain parameters are used in the optimization in order to keep the number of design variables low. They are the stiffness of convolutions and interlock, interlock geometry, and end cap mass. In this case, the characteristics to assign to pipe

elements, lumped masses, and rotary inertia terms are computed automatically in an Excel sheet[38]. The parameter values already known are reported in Tab. 7.1. The final model is represented in Fig. 7.1.6a, while the beam profiles are rendered

Property	Parameter value
ρ_p [kg/m^3]	8000
R_m [m]	0.068
s_p [m]	0.0012
ρ_s [kg/m^3]	8000
$R_{m,s}$ [m]	0.053
s_s [m]	0.0005

Table 7.1: **Known parameters design of the beam element model for bellow A1.**

in Fig. 7.1.6b to show the corresponding geometry.

(a) **Standard representation.**

(b) **Representation with rendered beam profiles.**
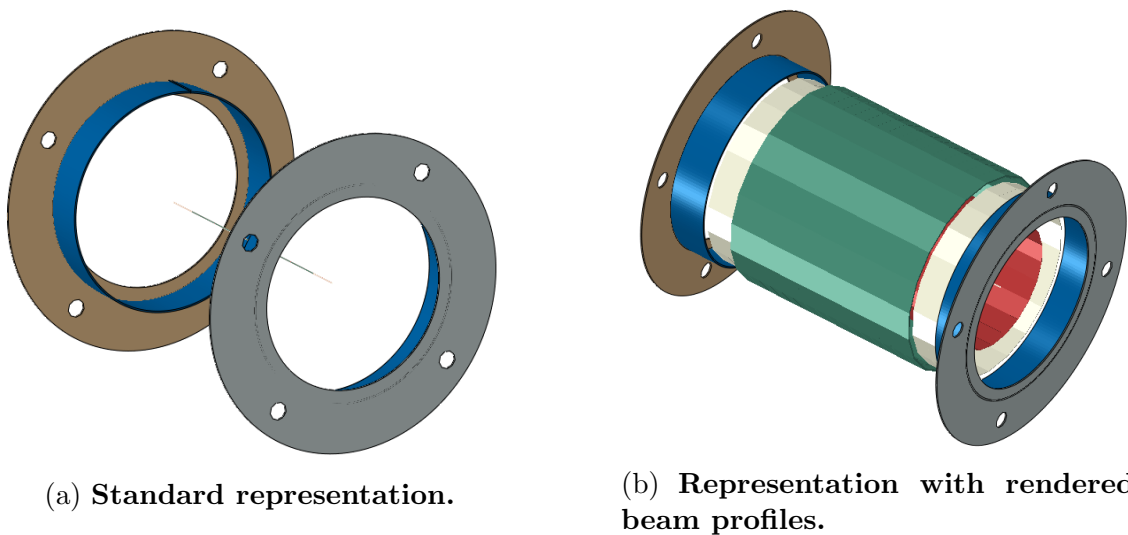
Figure 7.1.6: **Bellow A1 by using thin-walled pipe elements model.**

7.2   Proposed models for the other case-studies

The equivalent thin-walled pipe element method has been chosen to continue the investigation for the other case-studies.

69

7.2.1 Bellow A2

In this case, the same method used for the bellow A1 is applied. Some geometrical dimensions are known with less accuracy because they are measured directly on the component, and the torsion stiffness is assumed. The parameter values already known are reported in Tab. 7.2.

Property	Parameter value
ρ_p [kg/m^3]	8000
R_m [m]	0.069
s_p [m]	0.0015
ρ_s [kg/m^3]	8000
$R_{m,s}$ [m]	0.065
s_s [m]	0.0005

Table 7.2: **Known parameters design of the beam element model for bellow A2.**

Since the bellow was slightly shorter, nuts were used in the measurements to fill the space between the flanges and the supports, as shown in Fig. 6.2.2b. However, this difference is negligible, and the two bellows are assumed to have the same length. Also, the boundary conditions are the same.
The corresponding model is shown in Fig. 7.2.1.
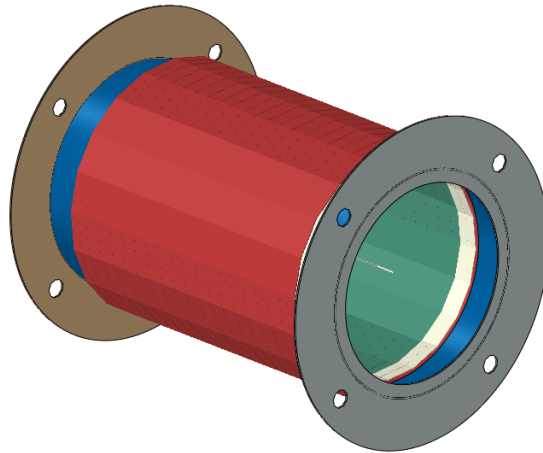
Figure 7.2.1: **Bellow A2 by using thin-walled pipe elements model.**

7.2.2 Dual bellow assembly

The models of bellow A1, obtained by using shell elements, and bellow A2, obtained by using thin-walled pipe elements, are used to represent the two bellows in the pipe assembly.

The same boundary conditions of the previous model, presented in Fig. 2.3.2b, are adopted. The models made by using shell and thin-walled pipe elements are shown in Figs. 7.2.2 and 7.2.3, respectively.

Figure 7.2.2: **Dual bellow assembly by using shell elements model.**

(a) **Standard representation.**

(b) **Representation with rendered beam profiles.**
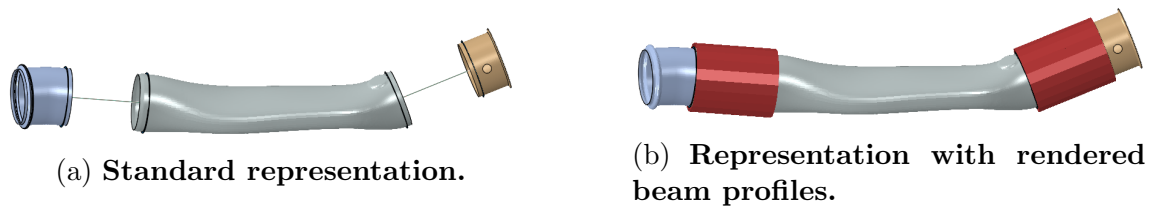
Figure 7.2.3: **Dual bellow assembly by using thin-walled pipe elements model.**

7.2.3 Flexible hose B

In this case, the convolutions are welded, so their profile is more difficult to interpret, but the same approach is followed. The parameter values already known are reported in Tab. 7.3.

The distance between the flanges is increased since the length of flexible hose is greater, while the boundary conditions do not change.

The corresponding model is shown in Fig. 7.2.4.

Property	Parameter value
ρ_p [kg/m^3]	8000
R_m [m]	0.073
s_p [m]	0.0011
ρ_s [kg/m^3]	8000
$R_{m,s}$ [m]	0.07
s_s [m]	0.0003

Table 7.3: **Known parameters design of the beam element model for bellow B.**
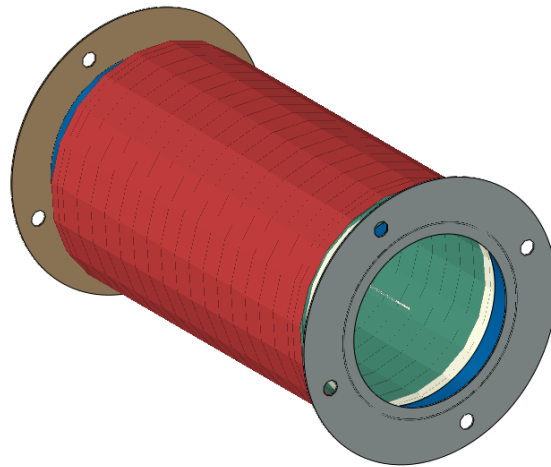
Figure 7.2.4: **Flexible hose B by using thin-walled pipe elements model.**

Chapter 8

Results

The results from numerical simulations are reported in the following sections, in which they are compared among themselves and in relation to experimental measurements. The comparison focuses on the response in the frequency range of $10 - 300$ Hz because, at higher frequencies, the influence of fixtures during measurements becomes not negligible due to the presence of their first eigenfrequency. For the last test on flexible hose B, it occurs at 280 Hz, so the range is reduced to $10 - 240$ Hz.

8.1 Bellow A1

First of all, the results obtained by different methods for bellow A1 (Fig.4.1.1a) are reported together with respective experimental references.

8.1.1 Shell elements method

The results related to the shell method (Fig. 7.1.1), adopted in the previous study[26], are adjusted to make them coherent and comparable with other approaches and reported in Fig. 8.1.1.
The corresponding first two mode shapes are shown in Fig. 8.1.2.
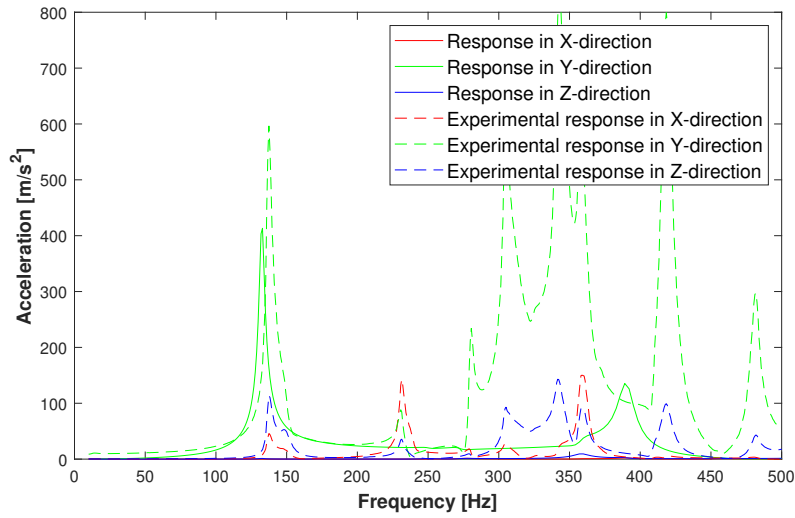
(a) **Frequency sweep in Y direction.**
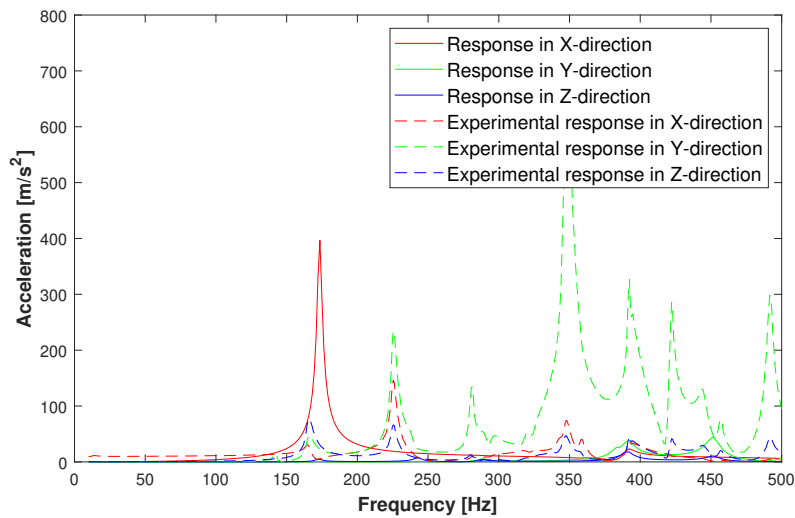
(b) **Frequency sweep in X direction.**

Figure 8.1.1: **Comparison between shell elements model and experimental measurements of the response in acceleration in individual directions for bellow A1 from frequency sweep in Y and X direction.**

74

(a) **First mode shape.**   (b) **Second mode shape.**
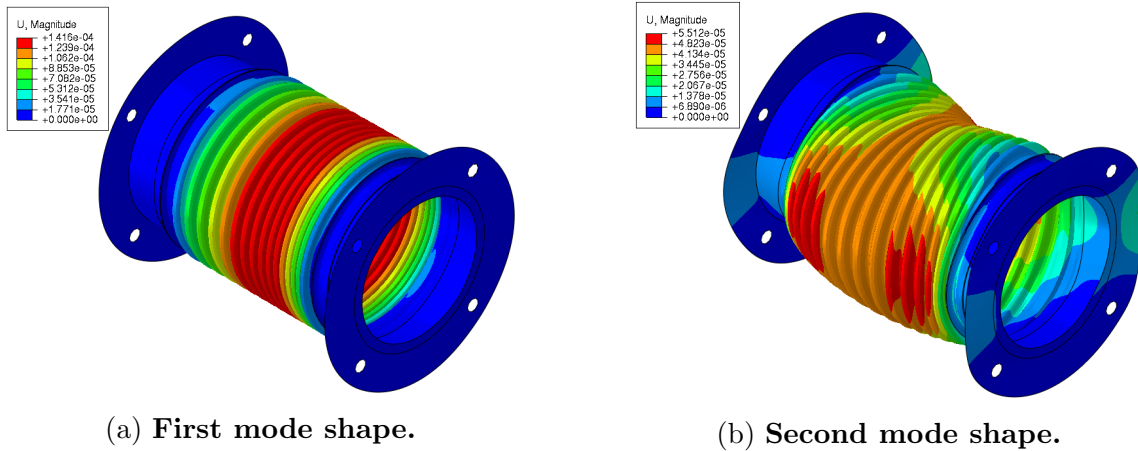
Figure 8.1.2: **First two mode shapes captured for bellow A1 by shell elements model.**

The results of the simulations on the bellow A1 by using the shell elements model are summarised in Tab. 8.1.

Mode	Simulated eig. [Hz]	Experimental eig. [Hz]	Damp. [%]	Mode shape	Test direction
1	133	138	1.48	Axial	Y
2	174	166	1	Transverse	X

Table 8.1: **Eigenfrequencies and eigenmodes of bellow A1 by using shell elements model.**

8.1.2 Connector elements method

The connector elements approach (Fig. 7.1.2) is first applied by considering the static stiffness characteristics provided by the supplier. The results are shown in Fig. 8.1.3.
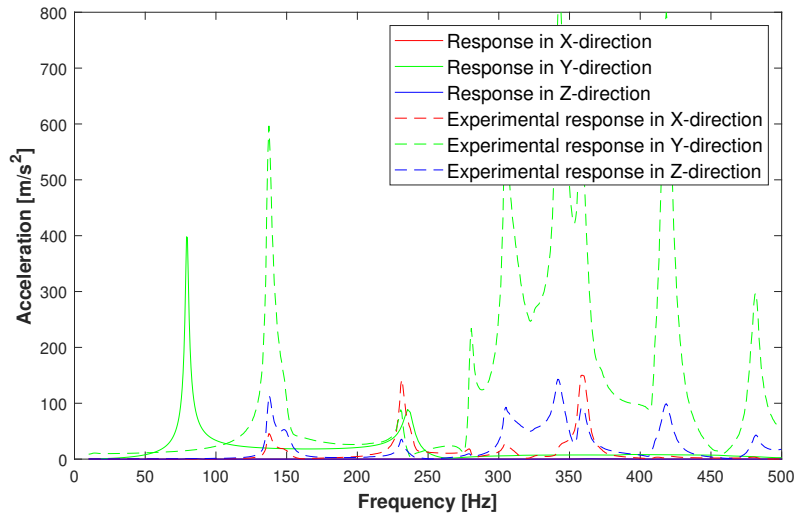
(a) **Frequency sweep in Y direction.**
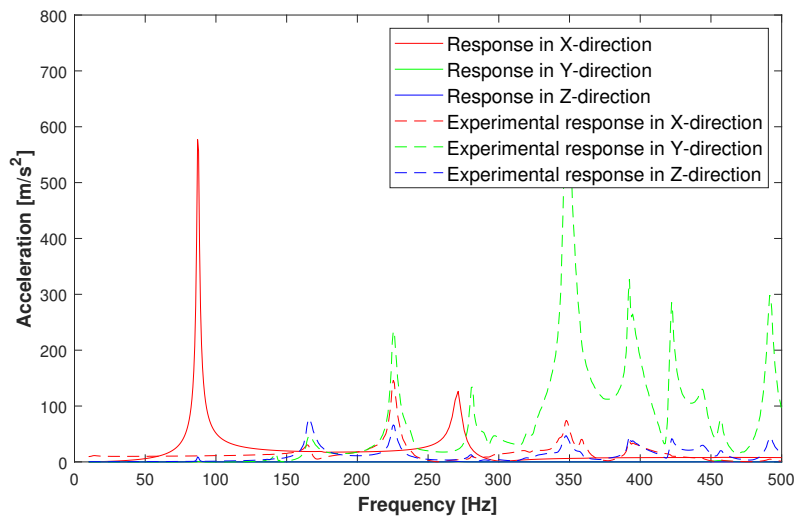
(b) **Frequency sweep in X direction.**

Figure 8.1.3: **Comparison between connector elements model and experimental measurements of the response in acceleration in individual directions for bellow A1 from frequency sweep in Y and X direction.**

The parametric optimization process allows for fitting the model by varying the stiffness parameter values. The best design is reported in Tab. 8.2.

Property	Optimal parameter value	Change [%]
k_T [N/m]	2674000	217
t_T [N/m]	3664000	211
b_T [Nm/rad]	9800020	185156
c_T [Nm/rad]	2080000	86

Table 8.2: **Best design obtained by parametric study on the connector element model for bellow A1.**

The results obtained by using the optimized model and associated mode shapes are shown in Figs. 8.1.4 and 8.1.5.
The results of the simulations on the bellow A1 by using the connector elements model are summarised in Tab. 8.3.

Mode	Simulated eig. [Hz]	Experimental eig. [Hz]	Damp. [%]	Mode shape	Test direction
1	139	138	1.48	Axial	Y
2	167	166	1	Transverse	X

Table 8.3: **Eigenfrequencies and eigenmodes of bellow A1 by using connector elements model with optimized parameters values.**

(a) **First mode shape.**

(b) **Second mode shape.**
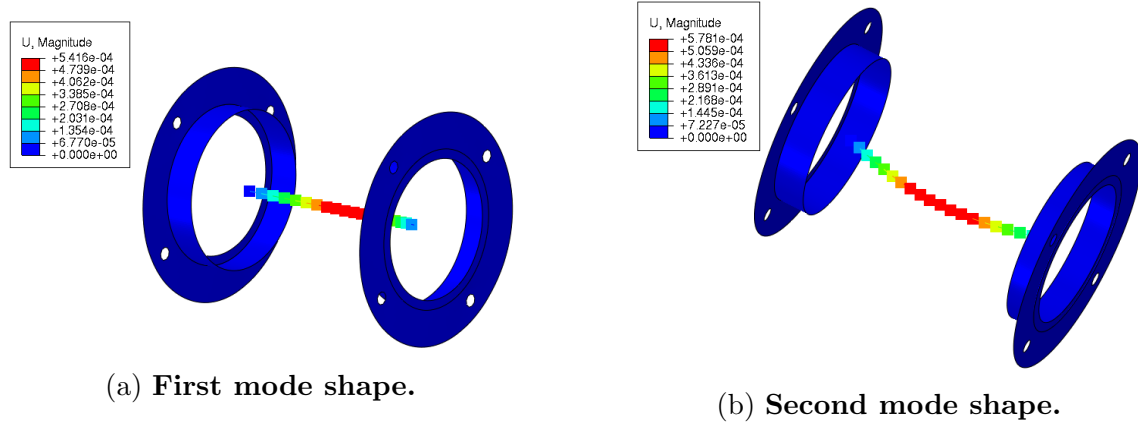
Figure 8.1.4: **First two mode shapes captured for bellow A1 by connector elements model with optimized parameters values.**
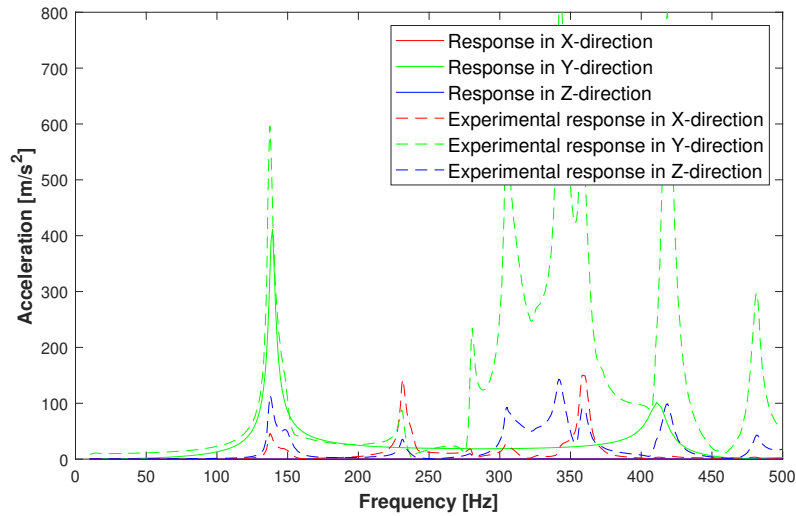
(a) **Frequency sweep in Y direction.**
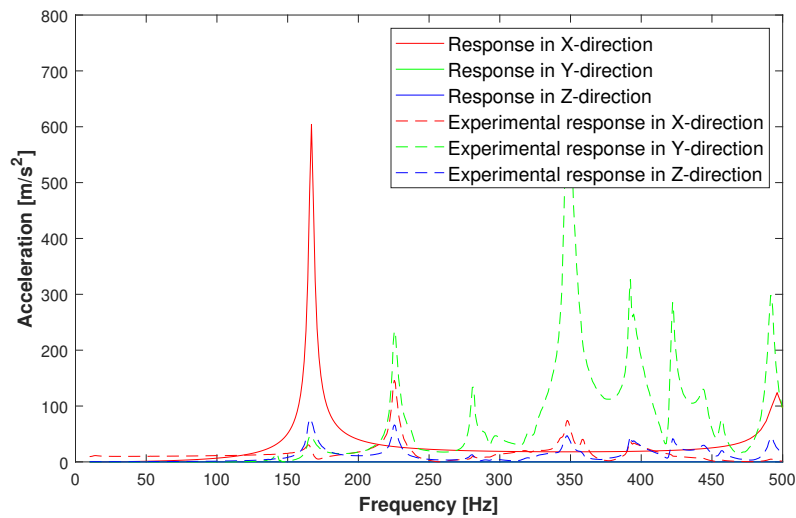
(b) **Frequency sweep in X direction.**

Figure 8.1.5: **Comparison between connector elements model with optimized parameters values and experimental measurements of the response in acceleration in individual directions for bellow A1 from frequency sweep in Y and X direction.**

8.1.3 Equivalent thin-walled pipe elements method

As regards the method by using equivalent thin-walled pipe elements (Fig. 7.1.6), at the end of the parametric study, the optimal values for bellow stiffness, interlock variables, and end-caps mass are found, as shown in Tab. 8.4. The corresponding results and mode shapes can be seen in Figs. 8.1.6 and 8.1.7.

Property	Optimal parameter value
k_b [N/m]	15040
c_b [Nm/rad]	90000
ρ_i [kg/m^3]	7495
$R_{m,i}$ [m]	0.044
k_i [m]	29117
c_i [m]	55310
m_e [kg]	0.3

Table 8.4: **Best design obtained by parametric study on the beam element model for bellow A1.**

By applying static loads, the static stiffness values in Tab. 8.5 are obtained for the model.

Property	Computed	Experimental	Error [%]
k_T [N/m]	53087	42100	26
c_T [Nm/rad]	147357	55900	164

Table 8.5: **Static stiffness values of bellow A1 model obtained by static simulations.**

The results of the simulations on the bellow A1 by using thin-walled pipe elements models are summarised in Tab. 8.6.

Mode	Simulated eig. [Hz]	Experimental eig. [Hz]	Damp. [%]	Mode shape	Test direction
1	141	138	1.48	Axial	Y
2	167	166	-	Transverse	X

Table 8.6: **Eigenfrequencies and eigenmodes of bellow A1 by using thin-walled pipe elements model.**
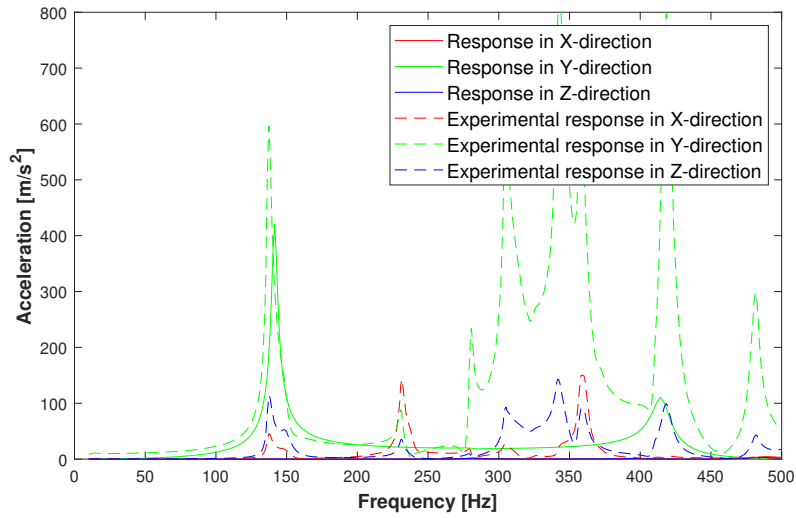
(a) **Frequency sweep in Y direction.**
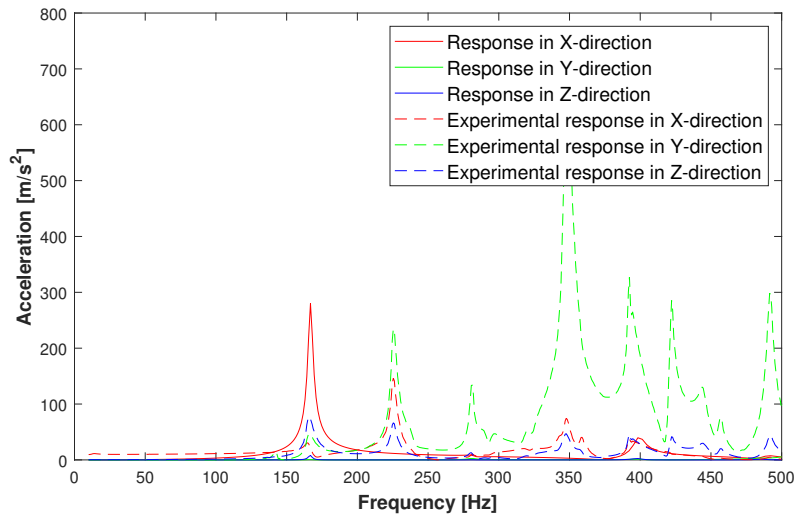
(b) **Frequency sweep in X direction.**

Figure 8.1.6: **Comparison between thin-walled pipe elements model and experimental measurements of the response in acceleration in individual directions for bellow A1 from frequency sweep in Y and X direction.**

(a) **First mode shape.**   (b) **Second mode shape.**
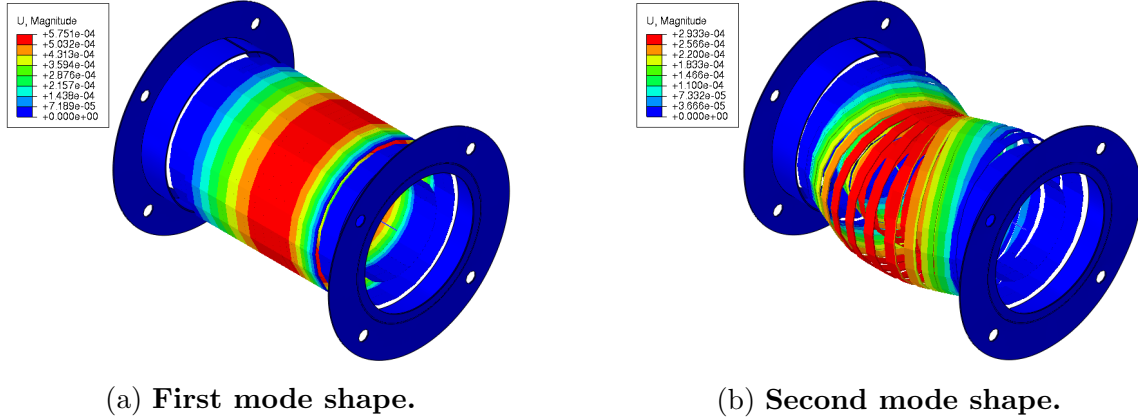
Figure 8.1.7: **First two mode shapes captured for bellow A1 by thin-walled pipe elements model.**

8.2 Bellow A2

For the bellow A2 (Fig. 4.1.1b), only the equivalent thin-walled pipe elements (Fig. 7.2.1) have been used. The parameter values of the optimal design obtained from the parametric study and corresponding static stiffness are reported in Tab. 8.7.

Property	Optimal parameter value
k_b [N/m]	6073
c_b [Nm/rad]	50500
ρ_i [kg/m^3]	6900
$R_{m,i}$ [m]	0.076
k_i [m]	48295
c_i [m]	48934
m_e [kg]	0.206

Table 8.7: **Best design obtained by parametric study on the beam element model for bellow A2.**

The corresponding results and mode shapes can be seen in Figs. 8.2.1 and 8.2.2.
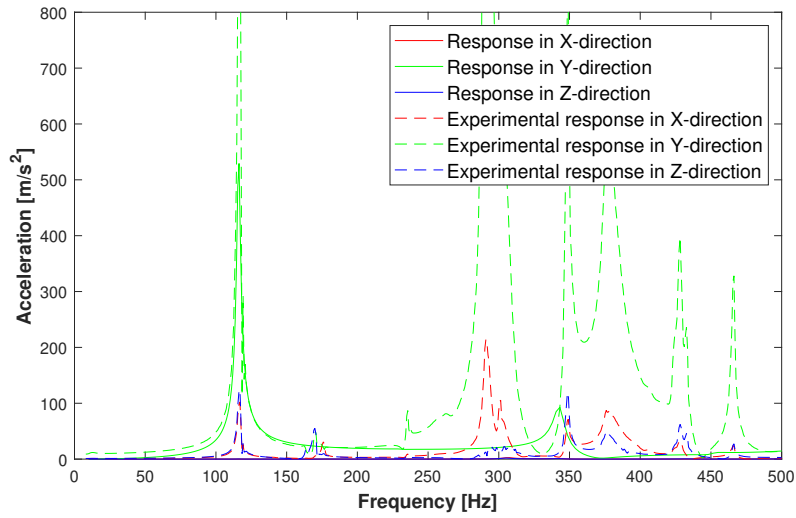
(a) **Frequency sweep in Y direction.**
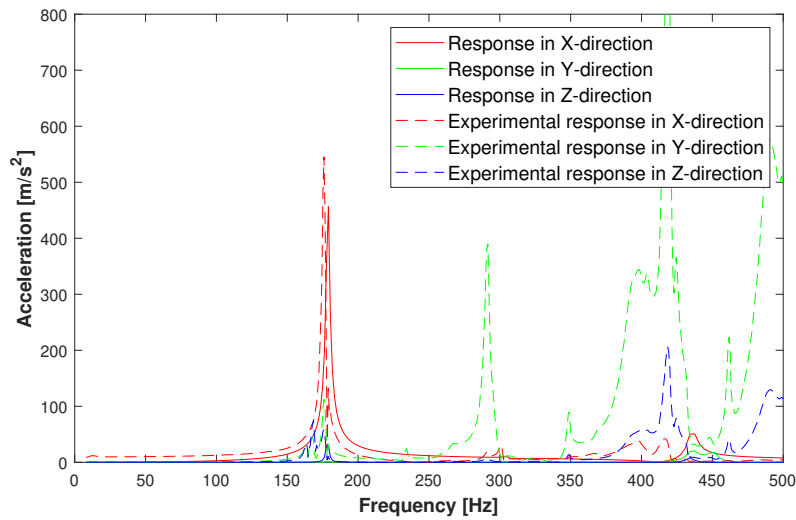
(b) **Frequency sweep in X direction.**

Figure 8.2.1: **Comparison between thin-walled pipe elements model and experimental measurements of the response in acceleration in individual directions for bellow A2 from frequency sweep in Y and X direction.**

(a) **First mode shape.**

(b) **Second mode shape.**
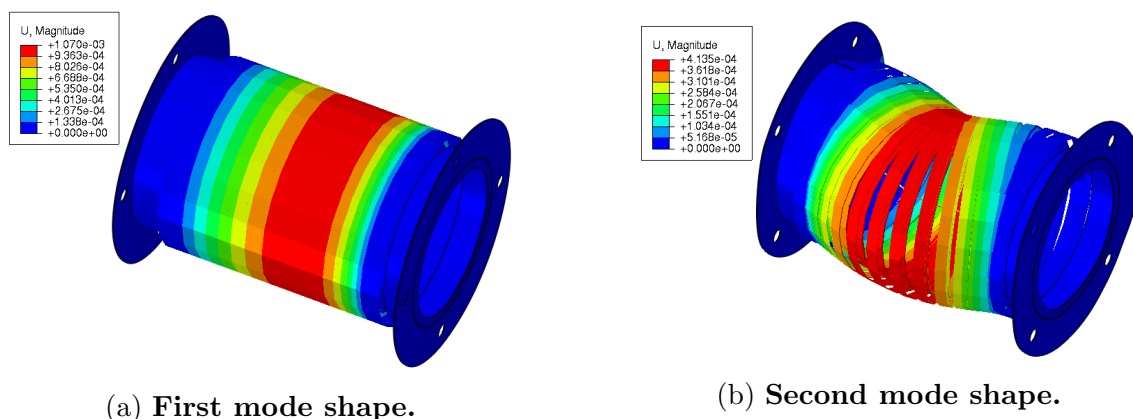
Figure 8.2.2: **First two mode shapes captured for bellow A2 by thin-walled pipe elements model with optimized parameters values.**

By applying static loads, the static stiffness values in Tab. 8.8 are obtained for the model.

Property	Computed	Experimental	Error [%]
k_T [N/m]	62074	54363	14
c_T [Nm/rad]	103622	60000	73

Table 8.8: **Static stiffness values of bellow A2 model obtained by static simulations.**

The results of the simulations on the bellow A2 by using the thin-walled pipe elements model are summarised in Tab. 8.9.

Mode	Simulated eig. [Hz]	Experimental eig. [Hz]	Damping ratio [%]	Mode shape	Test direction
1	116	116	1.11	Axial	Y
2	179	178	0.63	Transverse	X

Table 8.9: **Eigenfrequencies and eigenmodes of bellow A2 by using thin-walled pipe elements model.**

83

8.3   Pipe-assembly

Starting from bellow A2 model, the results related to the complete pipe-assembly
(Fig. 6.2.1) are reported together with respective experimental references.

8.3.1   Shell elements method

In the previous study[26], it was only possible to substitute the bellow A1 model in
the pipe-assembly (Fig. 7.2.2). Although it is not actually comparable, the associated results are reported to show the potentiality of the method.
The responses corresponding to the accelerometers located in the middle of the central pipe and at the inner sides of the bellows are adjusted to make them coherent
and comparable with other approaches, and compared with experimental measurements in Figs. 8.3.1, 8.3.2, and 8.3.3.
The associated mode shapes are shown in Figs. 8.3.4, 8.3.5, 8.3.6 and 8.3.7.
The results for pipe-assembly using the shell elements model are summarised in Tab.
8.10.

Mode	Simulated eig. [Hz]	Experimental eig. [Hz]	Damp. [%]	Reference accelerometer	Mode shape
1	43	30	15(Y) 36(X)	Middle part, Inner side of bellows	Test direction
2	152	130	-	Middle part, Inner side of bellows	Test direction
3	176	170	-	Middle part	Vertical direction
4	195	250	-	Middle part	Vertical direction

Table 8.10: **Eigenfrequencies and eigenmodes of complete pipe-assembly by
using shell elements model.**
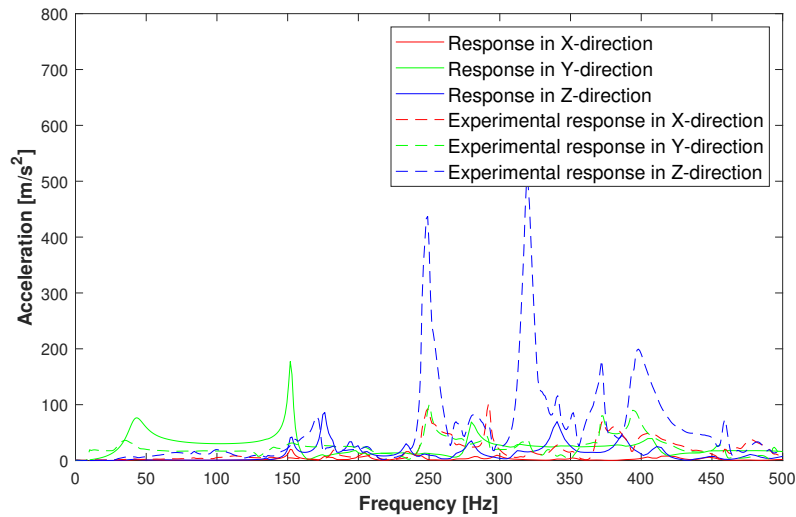
(a) **Frequency sweep in Y direction.**
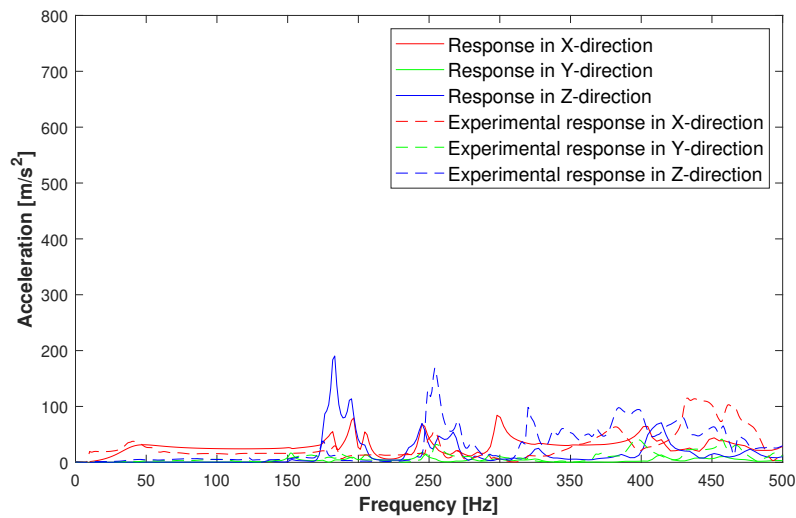
(b) **Frequency sweep in X direction.**

Figure 8.3.1: **Comparison between shell elements model and experimental measurements of the response in acceleration in individual directions for the accelerometer in the middle of the complete pipe assembly from frequency sweep in Y and X direction.**

85
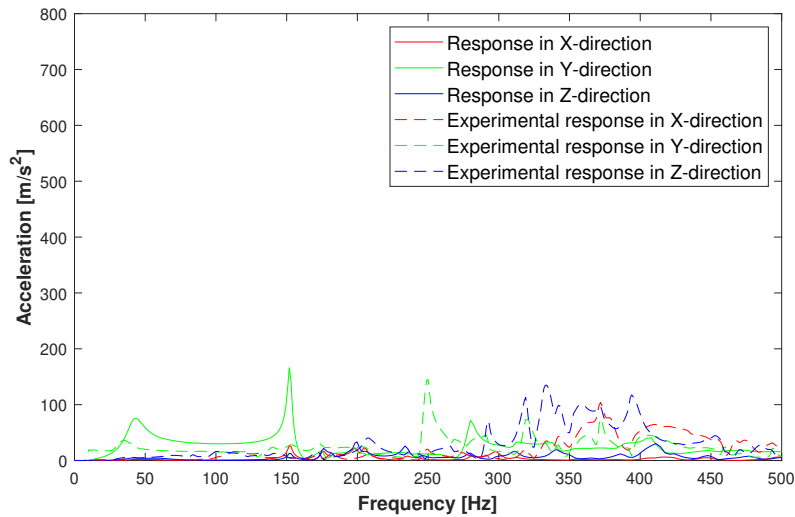
(a) **Frequency sweep in Y direction.**
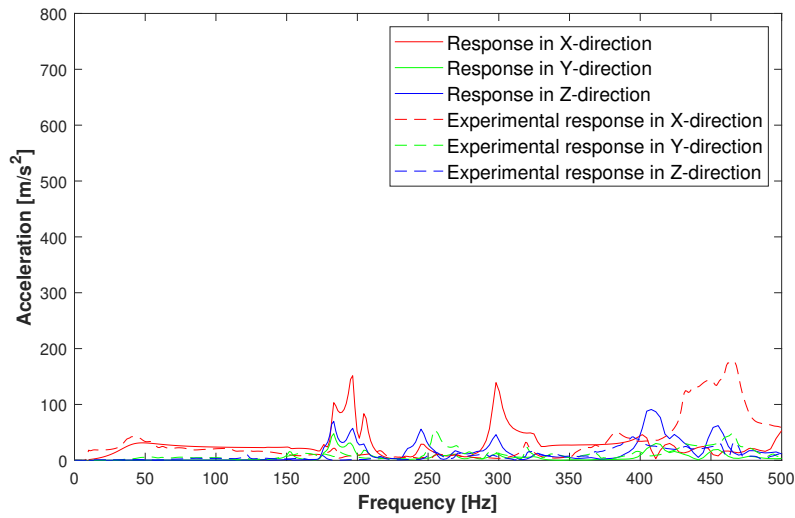
(b) **Frequency sweep in X direction.**

Figure 8.3.2: **Comparison between shell elements model and experimental measurements of the response in acceleration in individual directions for the accelerometer at the inner side of the left hand bellow in the complete pipe assembly from frequency sweep in Y and X direction.**
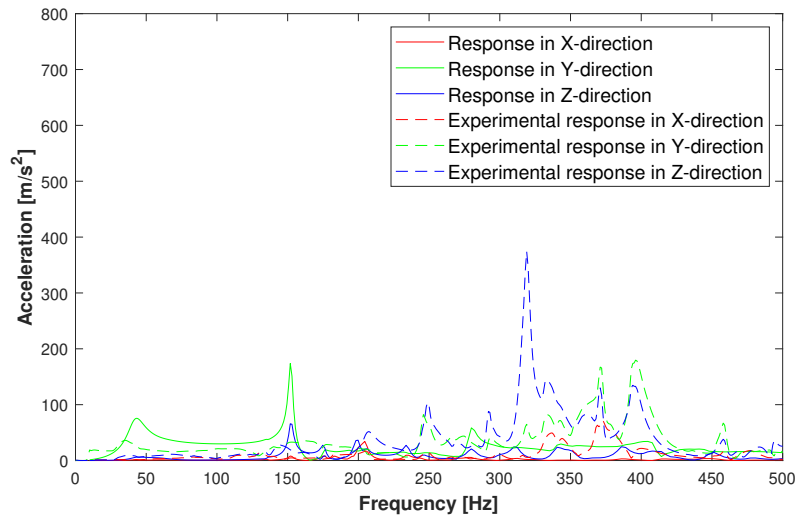
(a) **Frequency sweep in Y direction.**
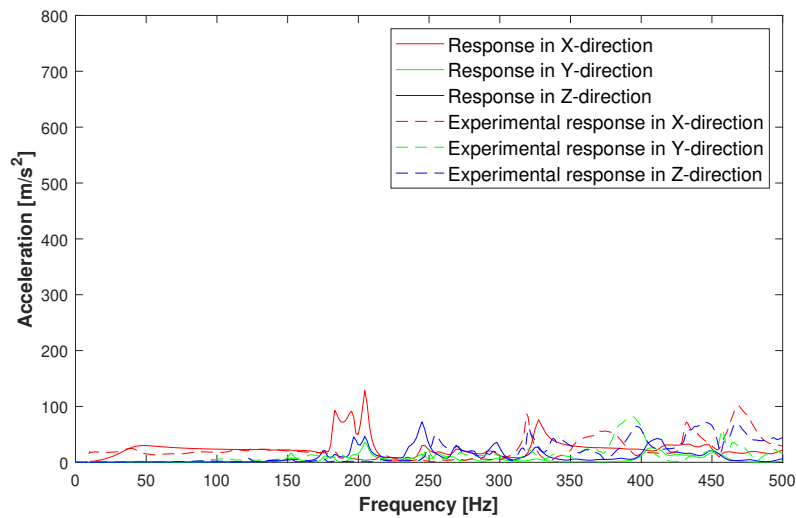
(b) **Frequency sweep in X direction.**

Figure 8.3.3: **Comparison between shell elements model and experimental measurements of the response in acceleration in individual directions for the accelerometer at the inner side of right hand bellow in complete pipe assembly from frequency sweep in Y and X direction.**

87
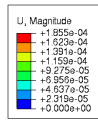
(a) **First mode shape with excitation in Y-direction.**
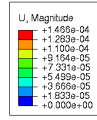
(b) **First mode shape with excitation in X-direction.**

Figure 8.3.4: **First mode shapes captured for complete pipe-assembly by shell elements model.**
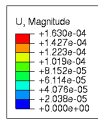
(a) **Second mode shape with excitation in Y-direction.**
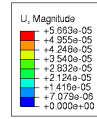
(b) **Second mode shape with excitation in X-direction.**

Figure 8.3.5: **Second mode shapes captured for complete pipe-assembly by shell elements model.**
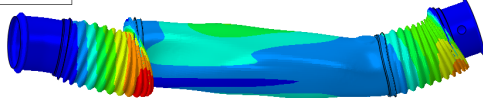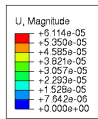
(a) **Third mode shape with excitation in Y-direction.**
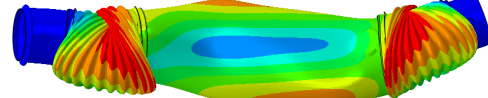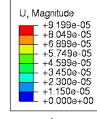
(b) **Third mode shape with excitation in X-direction.**

Figure 8.3.6: **Third mode shapes captured for complete pipe-assembly by shell elements model.**

(a) **Fourth mode shape with excitation in Y-direction.**

(b) **Fourth mode shape with excitation in X-direction.**
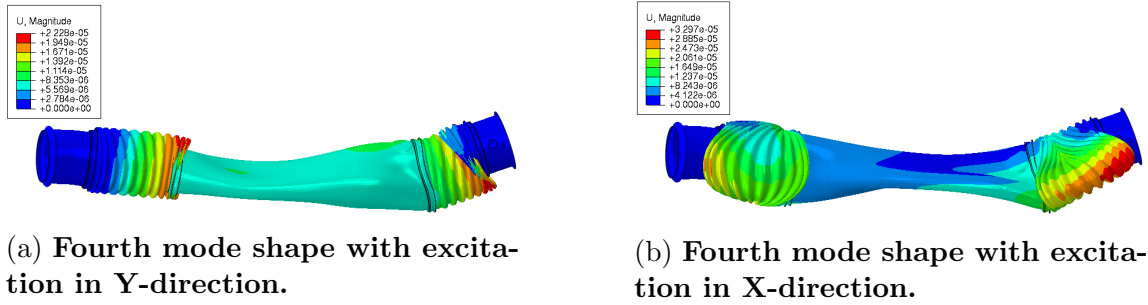
Figure 8.3.7: **Fourth mode shapes captured for complete pipe-assembly by shell elements model.**

8.3.2 Equivalent thin-walled pipe elements method

As regards the equivalent thin-walled pipe elements method, starting from bellow A2 model obtained in Fig. 8.2, the results related to the complete pipe-assembly (Fig. 7.2.3) are obtained. They are compared to experimental measurements in Figs. 8.3.8, 8.3.9, and 8.3.10.

The associated mode shapes are shown in Figs. 8.3.11, 8.3.12, 8.3.13 and 8.3.14, respectively.

The results of the simulations on the pipe-assembly by using the shell elements model are summarised in Tab. 8.11.

Mode	Simulated eig. [Hz]	Experimental eig. [Hz]	Damp. [%]	Reference accelerometer	Mode shape
1	32	30	15(Y) 36(X)	Middle part, Inner side of bellows	Test direction
2	127	130	-	Inner side of bellows	Test direction
3	186	170	-	Middle part	Test, vertical directions
4	239	250	-	Middle part	Test direction

Table 8.11: **Eigenfrequencies and eigenmodes of complete pipe-assembly by using thin-walled pipe elements model.**
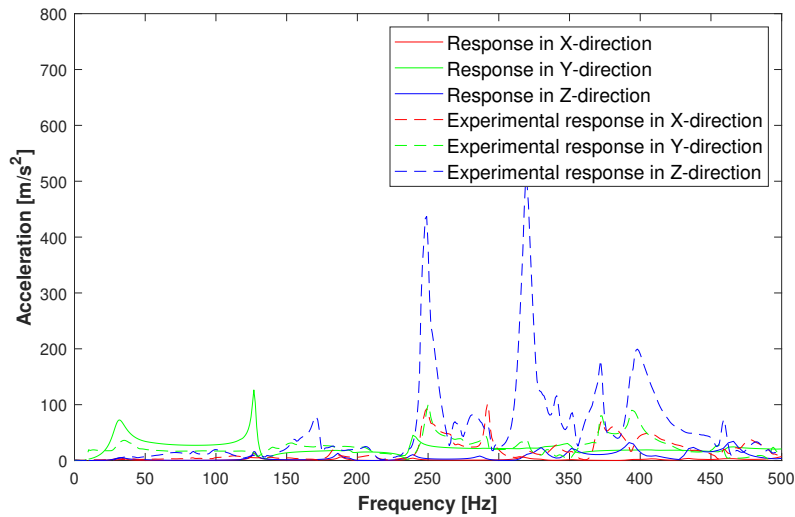
(a) **Frequency sweep in Y direction.**
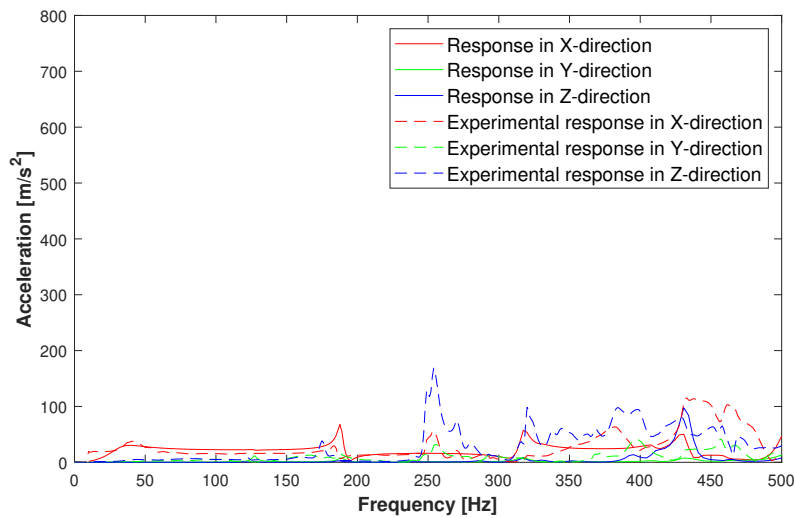
(b) **Frequency sweep in X direction.**

Figure 8.3.8: **Comparison between thin-walled pipe elements model and experimental measurements of the response in acceleration in individual directions for the accelerometer in the middle of the complete pipe assembly from frequency sweep in Y and X direction.**
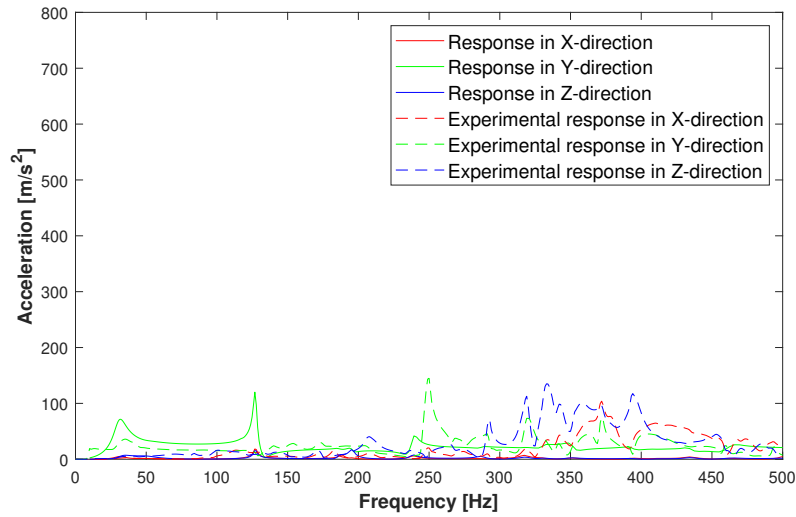
(a) **Frequency sweep in Y direction.**
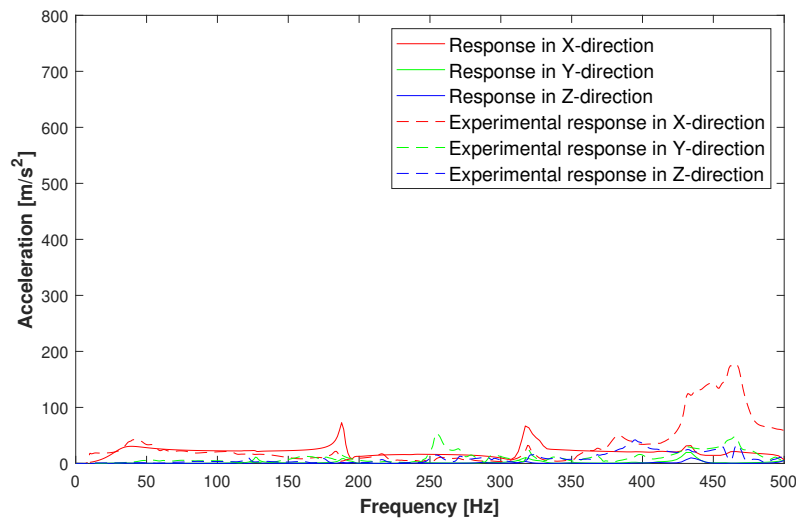
(b) **Frequency sweep in X direction.**

Figure 8.3.9: **Comparison between thin-walled pipe elements model and experimental measurements of the response in acceleration in individual directions for the accelerometer at the inner side of the left hand bellow in the complete pipe assembly from frequency sweep in Y and X direction.**
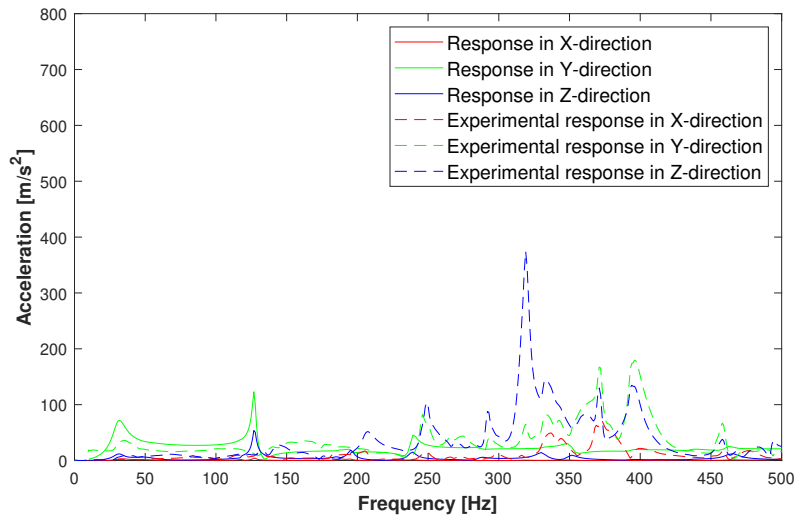
(a) **Frequency sweep in Y direction.**
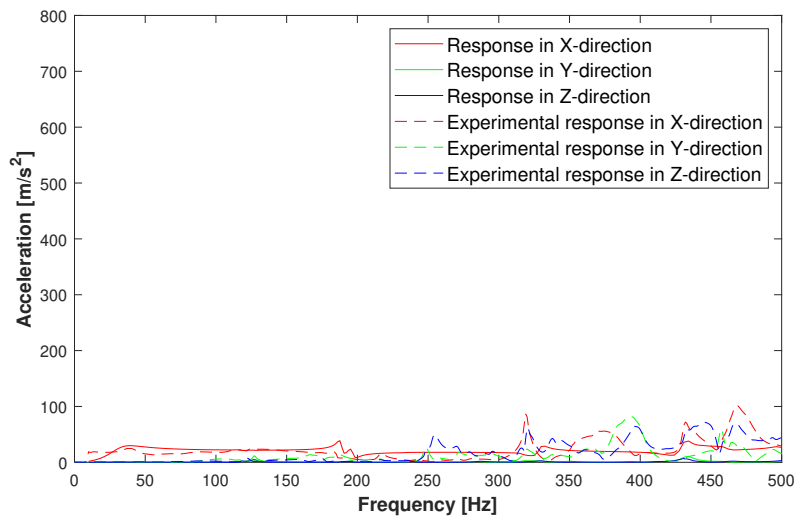
(b) **Frequency sweep in X direction.**

Figure 8.3.10: **Comparison between thin-walled pipe elements model and experimental measurements of the response in acceleration in individual directions for the accelerometer at the inner side of right hand bellow in complete pipe assembly from frequency sweep in Y and X direction.**
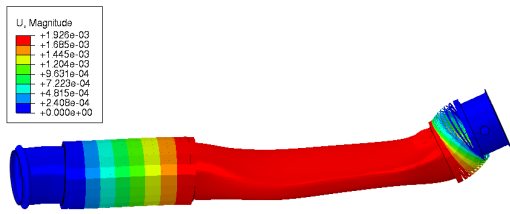
(a) **First mode shape with excitation in Y-direction.**
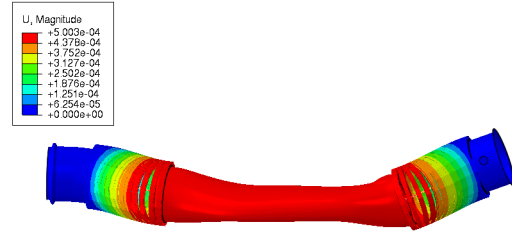
(b) **First mode shape with excitation in X-direction.**

Figure 8.3.11: **First mode shapes captured for complete pipe-assembly by thin-walled elements model.**
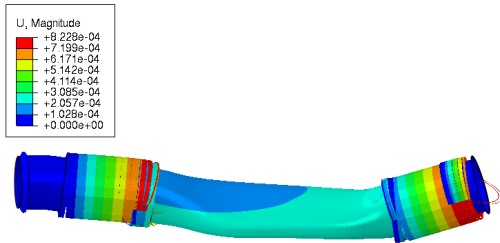
(a) **Second mode shape with excitation in Y-direction.**
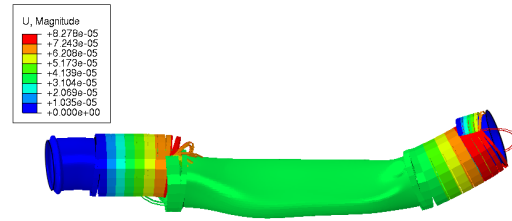
(b) **Second mode shape with excitation in X-direction.**

Figure 8.3.12: **Second mode shapes captured for complete pipe-assembly by thin-walled pipe elements model.**
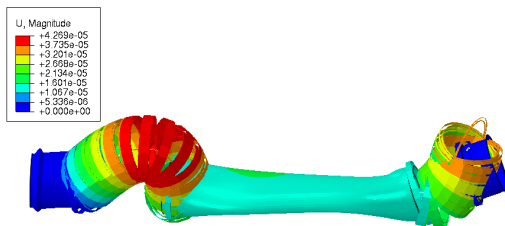
(a) **Third mode shape with excitation in Y-direction.**
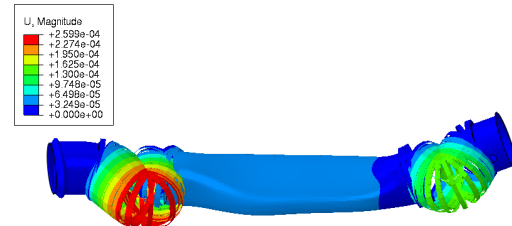
(b) **Third mode shape with excitation in X-direction.**

Figure 8.3.13: **Third mode shapes captured for complete pipe-assembly by thin-walled pipe elements model.**

(a) **Fourth mode shape with excitation in Y-direction.**

(b) **Fourth mode shape with excitation in X-direction.**
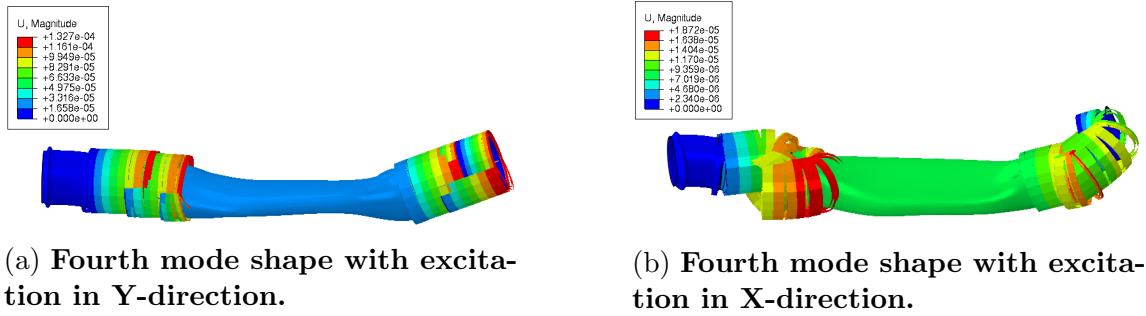
Figure 8.3.14: **Fourth mode shapes captured for complete pipe-assembly by thin-walled beam elements model.**

8.4   Flexible hose B

Lastly, at the end of the parametric study, by using thin-walled pipe elements (Fig. 7.2.4) on bellow B (Fig. 4.1.1c), the optimal values for bellow stiffness, interlock variables and end-cap mass are found, as shown in Tab. 8.12. The corresponding results and mode shapes can be seen in Figs. 8.4.1 and 8.4.2.

Property	Optimal parameter value
k_b [N/m]	10000
c_b [Nm/rad]	2872
ρ_i [kg/m^3]	8560
R_m, i [m]	0.085
k_i [N/m]	19801
c_i [Nm/rad]	17612
m_e [kg]	0.495

Table 8.12: **Best design obtained by parametric study on the beam element model for bellow B.**
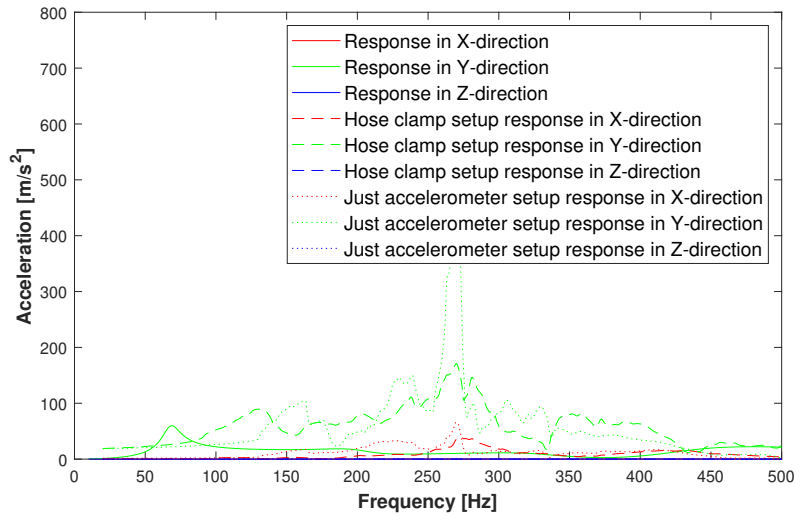
(a) **Frequency sweep in Y direction.**
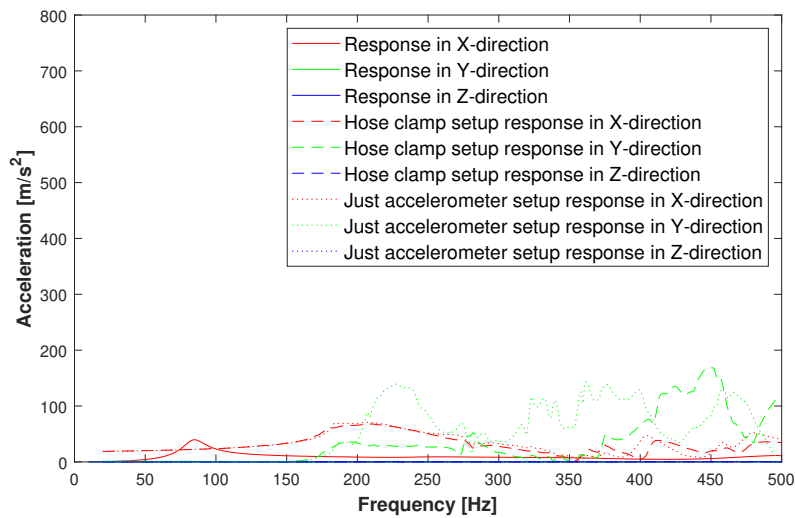
(b) **Frequency sweep in X direction.**

Figure 8.4.1: **Comparison between thin-walled pipe elements model and experimental measurements of the response in acceleration in individual directions for bellow B from frequency sweep in Y and X direction.**

(a) **First mode shape.**   (b) **Second mode shape.**
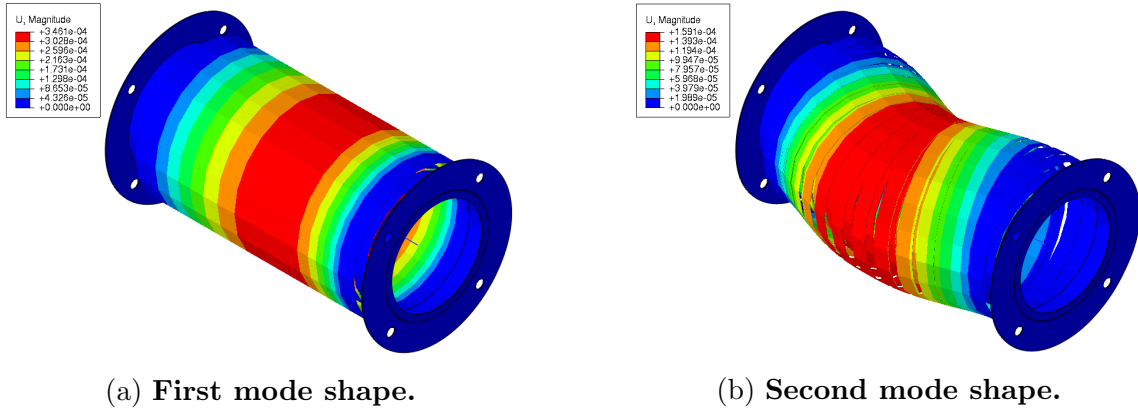
Figure 8.4.2: **First two mode shapes captured for bellow B by thin-walled pipe elements model with optimized parameters values.**

By applying static loads, the static stiffness values in Tab. 8.13 are obtained for the model.

Property	Computed	Experimental	Error [%]
k_T [N/m]	32042	5725	460
c_T [Nm/rad]	22160	17380	28

Table 8.13: **Static stiffness values of flexible hose B model obtained by static simulations.**

The results of the simulations on the bellow B by using thin-walled pipe elements model are summarised in Tab. 8.14.

Mode	Simulated eig. [Hz]	Experimental eig. [Hz]	Damp. [%]	Mode shape	Test direction
1	69	131-163	10	Axial	Y
2	85	207-211	10	Transverse	X

Table 8.14: **Eigenfrequencies and eigenmodes of bellow B by using thin-walled pipe model.**

Chapter 9

Discussion

9.1 Numerical simulation

9.1.1 Bellow A1

The results from different models are now compared, and the choice of the most efficient one is justified. Because of the presence of the first eigenfrequencies of fixtures, only the frequency ranges of $10 - 300$ Hz for different cases and $10 - 240$ Hz for new measurements in Sec. 6.3 are considered.

The shell elements model from the previous study came close to matching the first two eigenfrequencies and managed to simulate the direction of the first mode shape; the second one instead should be vertical, not transverse (Fig. 8.1.1, Tab. 8.1). As regards the amplitude of the first peaks, it can be further fitted by adjusting the damping ratio; in particular, it was not extracted in the X-direction so it has been assumed.
The model is not able to replicate the presence of other peaks at around 220 Hz.
It is worthy to mention again that the model has been fitted by changing the Young's modulus, which is decreased by 200 GPa to 7 GPa in order to match the first eigenfrequency.

As regards the connector elements approach, the original model, with static stiffness values from the supplier's data sheets, turns out to be too flexible, and the eigenfrequencies are significantly lower than experimental ones (Fig. 8.1.3, Tab. 8.3).
Through the parametric study, new parameter values from the best design are adopted, but they are much higher than the original ones (Tab. 8.2).
Despite the fact that the connector elements with optimized parameter values allow to get results quite close to the experimental measurements (Figs. 8.1.5), but, as

it for shell elements model (Fig. 8.1.1), the first peak for frequency sweep in the X-direction entails a main response in the direction of excitation, not in the vertical one.

No other peaks are identified in the frequency range of interest.

Further attempts at parametric study of the connector elements method by using different parameters for the connectors located at the ends or in the middle of the flexible pipe did not succeed.

From the parametric study on the bellow A1 thin-walled pipe elements model, a guess of the stiffness and mass distribution is obtained. The best design from optimization tends to be a bellow with a light but stiff inner structure and a more flexible outer part. The end-caps include more than one third of the total mass (Tabs.8.4, 4.1). Since the knowledge about the structure of flexible pipes agrees with a distribution of mass more concentrated at the two ends due to the presence of end-caps and inner sleeves, and it is likely that the inner sleeves and interlock together have a higher axial stiffness than the bellow, this result is retained as accurate.

Despite that, the total stiffness of the optimized model is slightly higher than expected, while the total torsion stiffness, computed by using a method whose accuracy is not certain, is strongly different compared to testing (Tabs.8.5, 4.2).

Looking at the corresponding results, the optimized model matches the first two eigenfrequencies with a low margin of error (Fig. 8.1.6, Tab. 8.6). In this case, the first peak for transverse excitation is found in the X-direction and the following peaks are not obtained.

All the simulation models are characterised by a response only in the direction of excitation (Figs. 8.1.1, 8.1.5, 8.1.6). It is excluded that it is related to the difference between the location of the accelerometer on the convolution and the response considered at the node on the axis in the 1D approximation because the result is also obtained in the shell elements model. A possible reason is identified in the lack of fixtures in the simulation.

Since the optimized shell (Fig. 7.1.1) and connector elements (Fig. 7.1.2) models have characteristics rather different from the original ones, the corresponding methodologies are not considered adequate for this type of application. Furthermore, the CAD model is not available for bellows A2 and B, making the use of shells not possible.

For these reasons, further case-studies have been conducted by adopting the only thin-walled pipe elements approach.

9.1.2 Bellow A2

For bellow A2, the thin-walled pipe elements model is considered. The best design from optimization generates a stiffer component than bellow A1, as expected comparing the experimental values (Tabs. 8.8, 8.5, 6.6). This time, most of the axial stiffness is concentrated in the inner part, while the torsion stiffness is equally distributed (Fig: 8.7). The mass of the end-caps is slightly less than one third of the total mass of flexible pipe (Figs. 8.7, 4.1). These optimal parameters are considered reliable on the basis of the structure of bellow A2, similar to the one of Bellow A1.

The optimal model is characterised by a dynamic response rather close to the experimental measurements for the first peaks in both directions of excitation (Fig. 8.2.1, Tab. 8.9). The amplitude of the peak can be adjusted by changing the damping ratios, although the experimental values are adopted in both cases. The following peaks are not obtained in the frequency range of interest, and the response is still limited to the direction of excitation.

9.1.3 Pipe-assembly

By substituting the bellow A1 shell elements model in the pipe-assembly (Fig. 7.2.2), an attempt at replicating its global behaviour was made. It was probably based on the assumption that the two bellows are not particularly different (Figs. 4.1.1a, 4.1.1b).
Looking at the results, only the third eigenfrequency is close to the corresponding experimental value (Tab. 8.10). As regards the mode shapes, the response is mainly in the direction of excitation at low frequencies, while at higher values the vertical vibrations become predominant, at least until 250 Hz; so its behaviour is similar to the tests (Figs. 8.3.1, 8.3.2 and 8.3.3).
Since the experimental damping ratios have been applied only for the first peak, while in the other cases a standard value is assumed, some difference in the amplitudes of the peaks compared to the measurement is justified. However, the use of the bellow A1 in place of the bellow A2 does not work very well.

By implementing the thin-walled pipe elements model in pipe-assembly (Fig. 7.2.3), the differences between the numerical and experimental peaks in the response are considerably reduced, especially for the first two peaks (Tab. 8.11).
For the first peak, the experimental damping ratio is adopted, and the response is rather similar to the test results (Figs. 8.3.8, 8.3.9, and 8.3.10). It does not occur for the following modes and could be due to the assumption made about the damping ratios.
The response seems to be mainly in the direction of excitation in the frequency

range of interest, although the third peak is characterised by a certain response in the vertical direction as well (Fig. 8.3.8).

The reasons behind the lower response in vertical directions, obtained by using the thin-walled pipe elements, are not clear.

Anyway, it seems that the new method manages to predict the peaks with higher accuracy than the previous one.

9.1.4   Bellow B

As regards the flexible hose B, the parametric study on the thin-walled pipe elements model (Fig. 7.2.4) did not succeed. From optimization, the model of flexible pipe is theoretically more rigid than the actual one (Tab. 8.13, 4.2), but the eigenfrequencies are still much lower than the measured ones (Tab. 8.14). Both axial and torsion stiffness are higher in the inner part, and the end-caps include approximately one-third of the mass of the entire component (Tab: 8.12, 4.1). This last characteristic seems to be exaggerated by considering the structure of the flexible pipe, because the two ends are less massive than previous cases (Fig. 4.1.1c, 4.1.1a, 4.1.1b).

Some contradictions arise from the comparison of the other components. According to measurements and data sheets (Tab. 4.2), the flexible hose B has a much lower stiffness than the other two bellows. Since it also has a higher mass, a lower first eigenfrequency is expected.

Although the measurement is not so accurate, it should be able to give a hint about the frequency range where the first peaks are found, and this range seems to be the same for the three components (Tab. 6.2, 6.3, 6.4).

Looking at the simulations, according to the thin-walled pipe elements model, the first eigenfrequencies are lower than experimental ones (Tab. 8.14), and then lower than in the other case-studies (Tab. 8.9, 8.6). At the same time, the simulated stiffness of the model is much higher than the experimental one but still lower compared to the other two components (Tab. 8.13, 8.5, 8.8).

More considerations for the simulation of this component are postponed until more reliable test results are obtained.

Chapter 10

Conclusion

This project has been conducted with the aim of developing a simple, yet reliable method for modelling the dynamic behaviour of flexible pipes.

By comparing the different methods, the thin-walled pipe elements approach turns out to be the most efficient way of modelling, guaranteeing both reliability and easier applicability, even if the CAD model or technical drawings are not available.

This model needs as input the geometry of the component, axial and torsion static stiffness values, and material properties, and, in the absence of knowing the characteristics of the different parts, an optimization process is performed to provide an estimation of them.

From the results, it seems to be suitable for simulating the dynamic behaviour of bellow A1 and, in particular, bellow A2, whose first two peaks and corresponding mode shapes show a high level of coherence to experimental results. The response is obtained mainly in the direction of excitation, and the following peaks in the frequency range of interest, limited by the influence of fixtures, are not captured.

When the model is implemented in the pipe-assembly, the eigenfrequencies are obtained with good accuracy, although the response is mainly limited to the direction of excitation and the difference in behaviour between low and high eigenfrequencies is not obtained.

As regards flexible hose B, the simulation does not match the experimental results. Simulation, experimental measurements on the shaker table, and data sheets from suppliers entail characteristics that are not compatible among themselves.

The possibility of applying this method to any flexible pipe in not operating conditions, including aged components, is not excluded since the only requirements regard the inputs used for building the equivalent model. It could also represent a starting point for studying operating conditions, although the contributions from high-temperature and pressure are not investigated.

The measurements on the flexible hose B are not retained as reliable due to the differences evidenced between different setups. The difference between the last results obtained and previous ones evidences that the damage to the few corrugations affects the response to excitation.

The comparison of frequency sweeps performed at different acceleration amplitudes shows the presence of non-linear dynamic behaviour. This softening phenomenon has a certain relevance and entails a decrease in the first eigenfreqeuncy value and the movement of the entire response downwards in relation to the frequency axis.

Chapter 11

Future work

This work aims to represent the starting point for further research about the dynamic behaviour of flexible pipes.

As regards the proposed method, it might be verified further. The static stiffness can be computed by static tests in order to check the values reported in data-sheets. By finding the actual characteristics of different parts, the results from optimization can be compared.

Different combinations of the beam elements could allow for a model with more similar stiffness characteristics compared to the theoretical values.
Since the response is mainly in the direction of excitation and the following peaks are not obtained in simulation, the fixture might be included in the model by using a coarse mesh, making the excitation in simulation more coherent to the testing one. Alternative methodologies for modelling should certainly be investigated. Among the approaches considered but not investigated for a short time, there is the possibility of using dynamic substructuring for flexible pipes and large pipe-assemblies in order to reduce the size of the simulations. In this case, CAD models are required.

As regards the test on flexible hose B, different setups might be considered. By turning down to get the local dynamic behaviour, the response of relative pipe-assembly could be tested with the accelerometer located on a flatter surface.
Evaluations of the tests robustness can be conducted in order to estimate the influence of measurement uncertainties on the results, even when they turn out to be unreliable.

The acceleration range of interest should be identified in order to be able to model the non-linear behaviour.
It is also recommended to verify the existence of harmonic distortion and amplitude

dependent FRFs for the other two case-studies by running frequency sweeps at different acceleration amplitudes on the shaker table.

Otherwise, alternative methods of detection can be used, such as random vibration excitations, sweeps with a linear increase in both frequency and amplitude on the shaker table, or hammer tests.

The model can be improved in order to include non-linear phenomena in the simulations, for example, by introducing a short elastic-plastic beam element as described by J. Wall[19]. Explicit dynamic simulations are required to be able to evaluate this capacity.

Although the effects of ageing and stiffening due to urea deposits were among the initial purposes of the thesis, it does not concern the influence of these phenomena on the vibration responses.

Furthermore, the operating conditions and the associated high-temperatures are not considered. These would influence the response, but it is thought that the model can be adjusted to be valid in those cases as well. Further research should examine these aspects in depth.

Bibliography

[1] Göran Broman, Madeleine Hermann, and Anders Jönsson. *Modelling flexible bellows by standard beam finite elements.* 1999.

[2] SD Wankhede and SH Gawande. Design and analysis aspect of metal expansion bellows: A review. *Forces in Mechanics*, page 100244, 2023.

[3] Johan Wall. *Simulation-driven design of complex mechanical and mechatronic systems.* PhD thesis, Blekinge Institute of Technology, 2007.

[4] Xiao Li, Xiaoli Jiang, and Hans Hopman. A review on predicting critical collapse pressure of flexible risers for ultra-deep oil and gas production. *Applied Ocean Research*, 80:1–10, 2018.

[5] Scania. Time to clear the air, 2017. URL `https://www.scania.com/content/dam/scanianoe/market/uk/brochures/bus-and-coach/brochures/clean-euro-VI-solutions-bus-and-coach.pdf`. [Accessed: 2024-02-11].

[6] ENVI Committee Press. Euro 7: Deal on new eu rules to reduce road transport emissions, 2023. URL `https://www.europarl.europa.eu/news/en/press-room/20231207IPR15740/euro-7-deal-on-new-eu-rules-to-reduce-road-transport-emissions`. [Accessed: 2024-02-11].

[7] Flextech Industries. Differences between flex connectors and bellows (expansion joints), 2023. URL `https://flextech-ind.com/news/differences-between-flex-connectors-and-bellows/#:~:text=Compared%20to%20flexible%20connectors%2C%20bellows,movement%20to%20tolerate%20pipe%20misalignment`. [Accessed: 2024-05-18].

[8] EJMA. *Standards of the Expansion Joint Manufacturer Association, ninth edition.* 2008.

[9] WESTFALIa Metal Hoses. Gastight hoses gth. URL `https://www.westfalia-mh.com/en/products/gastight-hoses-gth/`. [Accessed: 2024-06-13].

[10] Kelco industries. Expansion joints. URL `https://www.kelcoind.com/product/1407-series-5-ply-exhaust-capsules/`. [Accessed: 2024-06-13].

[11] RADCOFLEX. Stripwound metal hose. URL `https://www.radcoflex.com/products/stripwound-metal-hose/stripwound-metal-hose-range.html#:~:text=Stripwound%20flexible%20metal%20hoses%20are,within%20the%20two%20profiled%20locksections`. [Accessed: 2024-05-18].

[12] Lanfang Jiang, Yi He, Yaochen Lin, Shuyou Zhang, Yixiong Feng, Min Sun, and Xunzhong Guo. Influence of process parameters on thinning ratio and fittability of bellows hydroforming. *The International Journal of Advanced Manufacturing Technology*, 107:3371–3387, 2020.

[13] Ting-Xin Li, Bing-Liang Guo, and Tian-Xiang Li. Natural frequencies of u-shaped bellows. *International Journal of Pressure Vessels and Piping*, 42(1): 61–74, 1990.

[14] Feliksas Vaidutis Jakubauskas. Transverse vibrations of bellows expansion joints. 1995.

[15] William Weaver Jr, Stephen P Timoshenko, and Donovan Harold Young. *Vibration problems in engineering*. John Wiley & Sons, 1991.

[16] MP Paıdoussis and GX Li. Pipes conveying fluid: a model dynamical problem. *Journal of fluids and Structures*, 7(2):137–204, 1993.

[17] Thomas Englund, Johan Wall, Kjell Ahlin, and Göran Broman. Significance of non-linearity and component-internal vibrations in an exhaust system. In *Proceedings of the 2nd WSEAS International Conference on Simulation, Modelling and Optimization, Skiathos Island, Greece*. Citeseer, 2002.

[18] Johan Wall, Thomas Englund, Kjell Ahlin, and Göran Broman. Modelling of multi-ply bellows flexible joints of variable mean radius. In *NAFEMS World Congress 2003*. NAFEMS, 2003.

[19] TL Englund, JE Wall, KA Ahlin, and GI Broman. Dynamic characteristics of a combined bellows and liner flexible joint. *Proceedings of the Institution of Mechanical Engineers, Part D: Journal of Automobile Engineering*, 218(5): 485–493, 2004.

106

[20] JE Wall, TL Englund, KA Ahlin, and GI Broman. Influence of a bellows-type flexible joint on exhaust system dynamics. *Proceedings of the Institution of Mechanical Engineers, Part D: Journal of Automobile Engineering*, 218(12): 1473–1478, 2004.

[21] R. Wagman. Investigation of a simplified bellows model with fem, 2011.

[22] N. Björkblad. Verification method for flexible exhaust hose: A background study, 2015.

[23] B. Sharifimajd. *Internal report: 7047152 Method description: Durability assessment of flexible bellows.* 2017.

[24] A. Tchernov. *Internal report: 7044063 Best practice – Flex pipe stiffness documentation.* 2017.

[25] A.I. Ingvason. Fatigue investigations of flexible hoses, 2017.

[26] L. Gustavsson. *Internal report: 7077328 Modal analysis for LH exhaust pipe assembly.* 2022.

[27] E. Fredriksson. *Internal report: 7075778 Vibration test for LH exhaust bellows.* 2022.

[28] Alessandro Fasana, Stefano Marchesiello, et al. *Meccanica delle vibrazioni.* Clut, 2006.

[29] Khashaiar Noushin. Structural dynamics at higher frequencies using the finite element method: Assessment of solver algorithms and component mode synthesis for dynamic response analysis of large structures, 2022.

[30] Marcell Ferenc Treszkai, Balázs Vehovszky, and Dániel Feszty. Damping determination by the half power bandwidth method for a rectangular flat plate with bitumen damping layer application. *Journal of Vibroengineering*, 23(5): 1267–1277, 2021.

[31] Dario Anastasio. Nonlinear vibrations: an overview.

[32] Gui-Rong Liu and Siu Sin Quek. *The finite element method: a practical course.* Butterworth-Heinemann, 2013.

[33] Dassault Systems. Simulia user assistance 2024. URL `https://help.3ds.com/2024/english/dssimulia_established/SIMULIA_Established_FrontmatterMap/DSDocHome.htm?contextscope=all&id=0a82415e8fbd4d0eb5de90f6718bd625`. [Accessed: 2024-06-23].

[34] Laszlo P Kollar and Gabriella Tarján. *Mechanics of civil engineering structures*. Woodhead Publishing, 2020.

[35] Dan Zenkert. An introduction to sandwich structures, 1995.

[36] Siemens. About heeds mdo. URL `https://docs.sw.siemens.com/en-US/doc/266516929/PL20230405682489488.mdo/xid1624779`. [Accessed: 2024-06-28].

[37] R. Mohammadi. Verification method for flexible exhaust hose: Definition and modelling of damage, 2016.

[38] P. Bellieni. Flexible pipes equivalent thin-walled pipe elements model, .

[39] P. Bellieni. Heeds, .

[40] Tecquipment. Stroboscope. URL `https://www.tecquipment.com/stroboscope`. [Accessed: 2024-06-20].

Appendix A

Results from new measurements
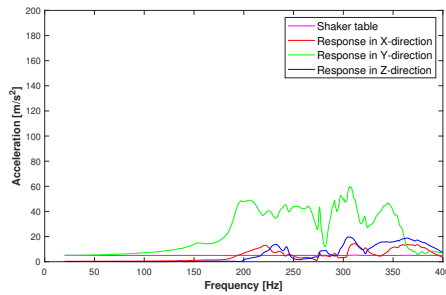
(a) **Acceleration amplitude at 5 m/s^2.**
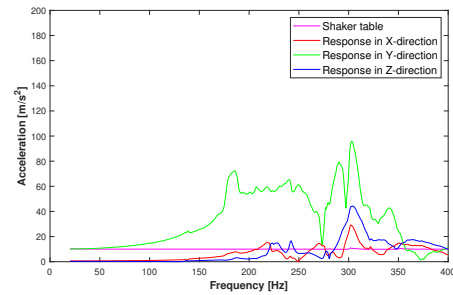
(b) **Acceleration amplitude at 10 m/s^2.**
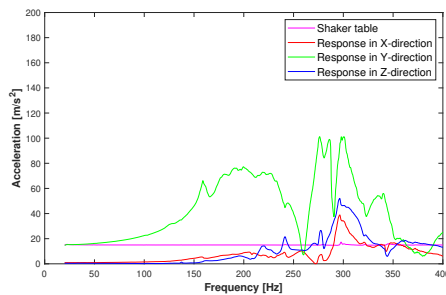
(c) **Acceleration amplitude at 15 m/s^2.**
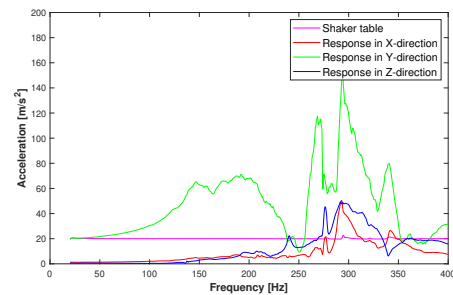
(d) **Acceleration amplitude at 20 m/s^2.**

Figure A.0.1: **Response in acceleration in individual directions for inlet flexible hose from frequency sweep in Y test direction.**

I
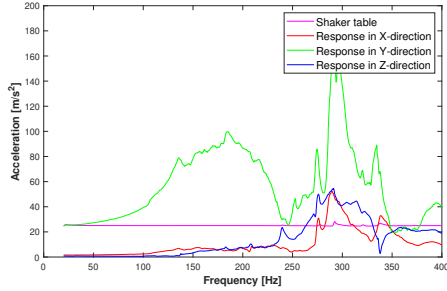
(a) **Acceleration amplitude at 25 m/s².**

(b) **Acceleration amplitude at 30 m/s².**
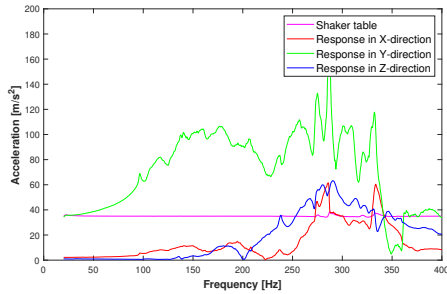
(c) **Acceleration amplitude at 35 m/s².**
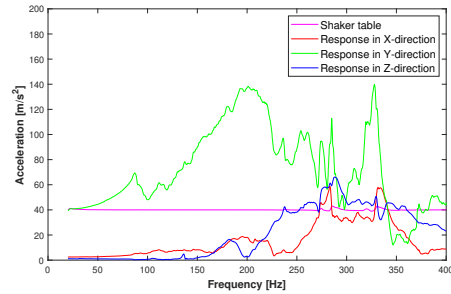
(d) **Acceleration amplitude at 40 m/s².**
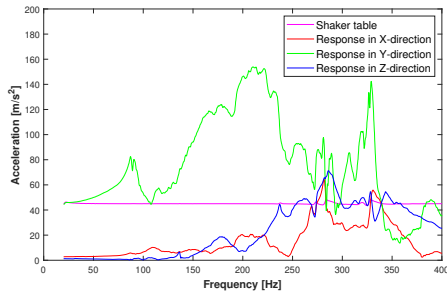
(e) **Acceleration amplitude at 45 m/s².**
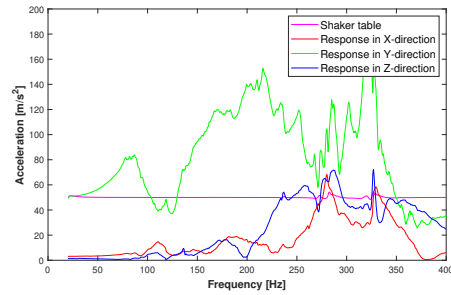
(f) **Acceleration amplitude at 50 m/s².**

Figure A.0.2: **Response in acceleration in individual directions for inlet flexible hose from frequency sweep in Y test direction.**
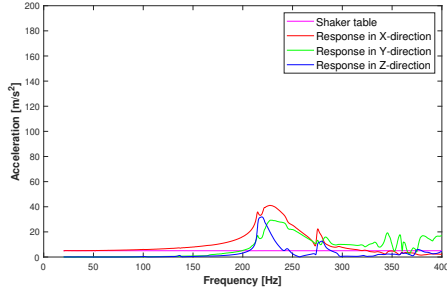
(a) **Acceleration amplitude at 5 m/s².**
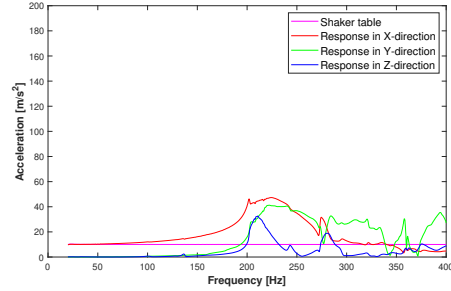
(b) **Acceleration amplitude at 10 m/s².**
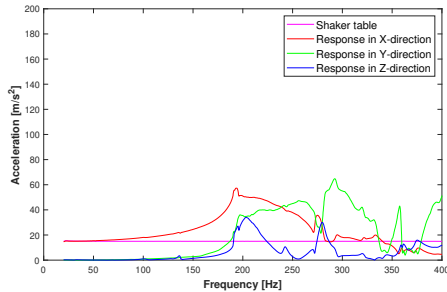
(c) **Acceleration amplitude at 15 m/s².**
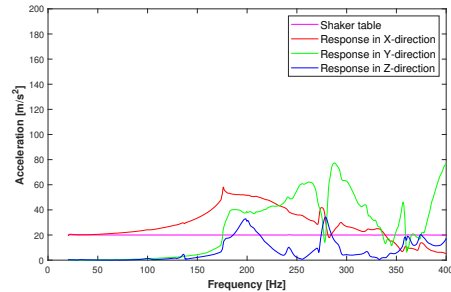
(d) **Acceleration amplitude at 20 m/s².**
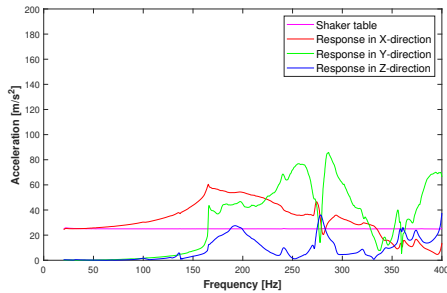
(e) **Acceleration amplitude at 25 m/s².**
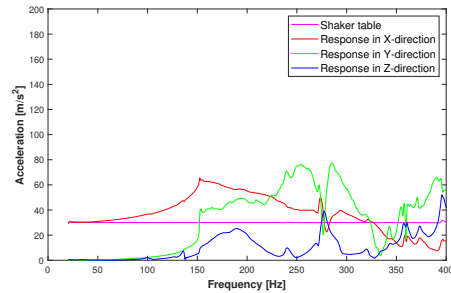
(f) **Acceleration amplitude at 30 m/s².**

Figure A.0.3: **Response in acceleration in individual directions for inlet flexible hose from frequency sweep in X test direction.**

III
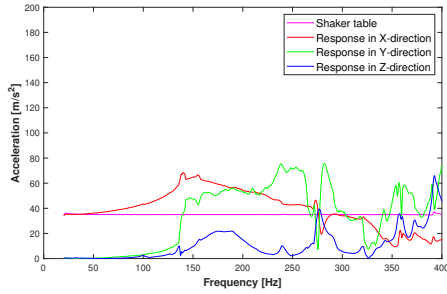
(a) **Acceleration amplitude at 35 m/s².**
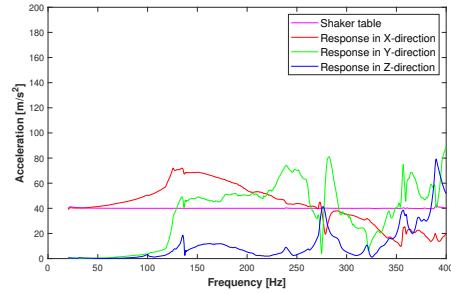
(b) **Acceleration amplitude at 40 m/s².**
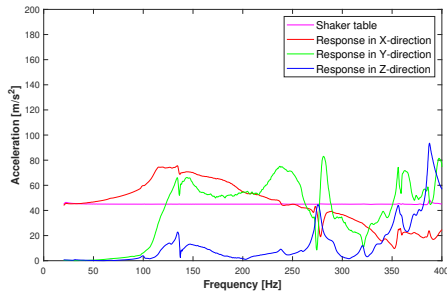
(c) **Acceleration amplitude at 45 m/s².**
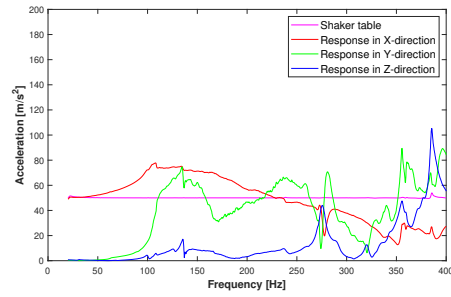
(d) **Acceleration amplitude at 50 m/s².**

Figure A.0.4: **Response in acceleration in individual directions for inlet flexible hose from frequency sweep in X test direction.**

Appendix B

ABAQUS Syntax[33]

This the Abaqus script related to the single flexible pipe simulation. In the pipe-assembly script, three different node outputs are defined and the base motion is set along DOF = 2 and DOF = 1 for axial and transverse response, respectively.

```
*=====================================================
* STEP 1. Eigenvalue analysis
*=====================================================
NSET, NSET=OUTPUT
"First node in the set","Last node in the set","Increment in node numbers between nodes in the set"
BOUNDARY, OP=NEW, FIXED
"Node number or node set label","First degree of freedom constrained","Last degree of freedom constrained"
STEP, NAME=frequency
*
FREQUENCY, EIGENSOLVER=LANCZOS, NORMALIZATION=MASS
"Number of eigenvalues to be calculated"," Minimum frequency of interest, in cycles/time","Maximum frequency of interest, in cycles/time"
END STEP
=====================================================
* STEP 2. Response analysis Axial direction
*=====================================================
AMPLITUDE, NAME=base
"Time or frequency","Amplitude value (relative or absolute) at the first point","Time or frequency","Amplitude value (relative or absolute) at the second point"
STEP, NAME=response
STEADY STATE DYNAMICS, INTERVAL=RANGE
```

"Lower limit of frequency range or a single frequency, in cycles/time","Upper limit of frequency range, in cycles/time","Total number of points in the frequency range at which results should be given, including the end points"
SELECT EIGENMODES, DEFINITION=FREQUENCY RANGE
"Lower boundary of the frequency range (in cycles/time)", "Upper boundary of the frequency range (in cycles/time)"
BASE MOTION, DOF=1, AMPLITUDE=base
MODAL DAMPING, MODAL=DIRECT, DEFINITION=FREQUENCY RANGE
"Frequency value (in cycles/time)","Damping factor"
"Frequency value (in cycles/time)", "Damping factor"
OUTPUT, FIELD
NODE OUTPUT
U
NODE OUTPUT, NSET=OUTPUT
A
NODE PRINT, NSET=OUTPUT
A
END STEP
*==
* STEP 3. Response analysis Transverse direction
*==
STEP, NAME=response2
STEADY STATE DYNAMICS, INTERVAL=RANGE
"Lower limit of frequency range or a single frequency, in cycles/time","Upper limit of frequency range, in cycles/time","Total number of points in the frequency range at which results should be given, including the end points"
SELECT EIGENMODES, DEFINITION=FREQUENCY RANGE
"Lower boundary of the frequency range (in cycles/time)", "Upper boundary of the frequency range (in cycles/time)"
BASE MOTION, DOF=3, AMPLITUDE=base
MODAL DAMPING, MODAL=DIRECT, DEFINITION=FREQUENCY RANGE
"Frequency value (in cycles/time)","Damping factor"
"Frequency value (in cycles/time)", "Damping factor"
OUTPUT, FIELD
NODE OUTPUT
U
NODE OUTPUT, NSET=OUTPUT
A
NODE PRINT, NSET=OUTPUT

A
END STEP

Appendix C

Correlation plots from optimization process in Heeds[36]
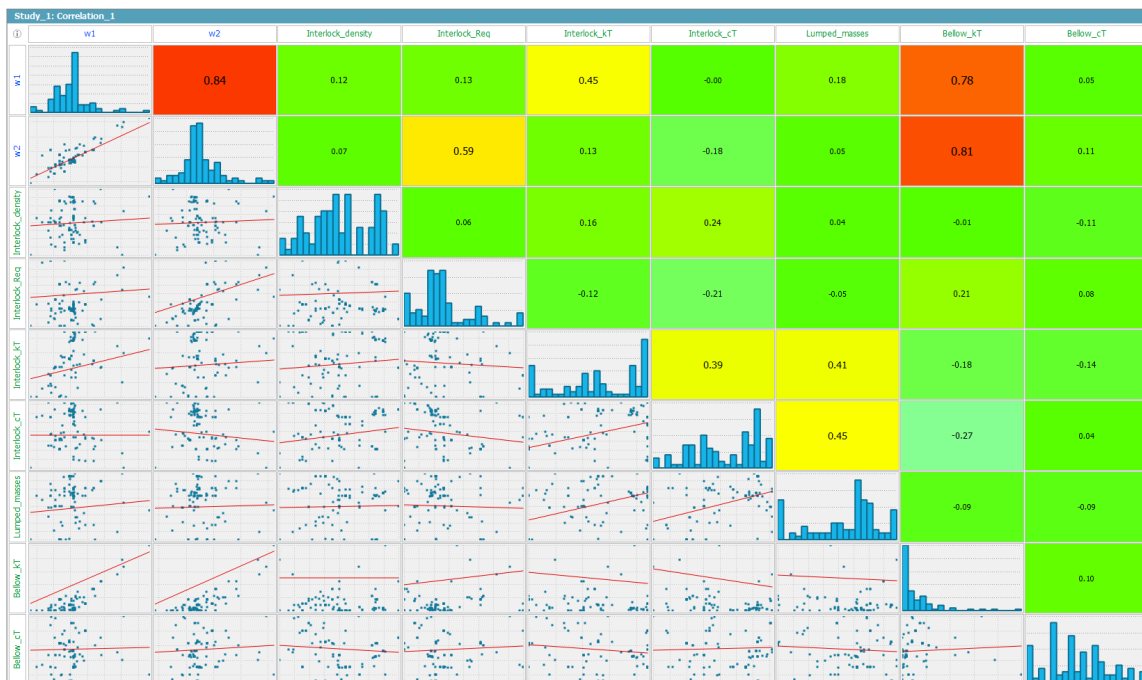
Figure C.0.1: **Correlation plot from optimization process on bellow A1.**

Figure C.0.2: **Correlation plot from optimization process on bellow A2.**
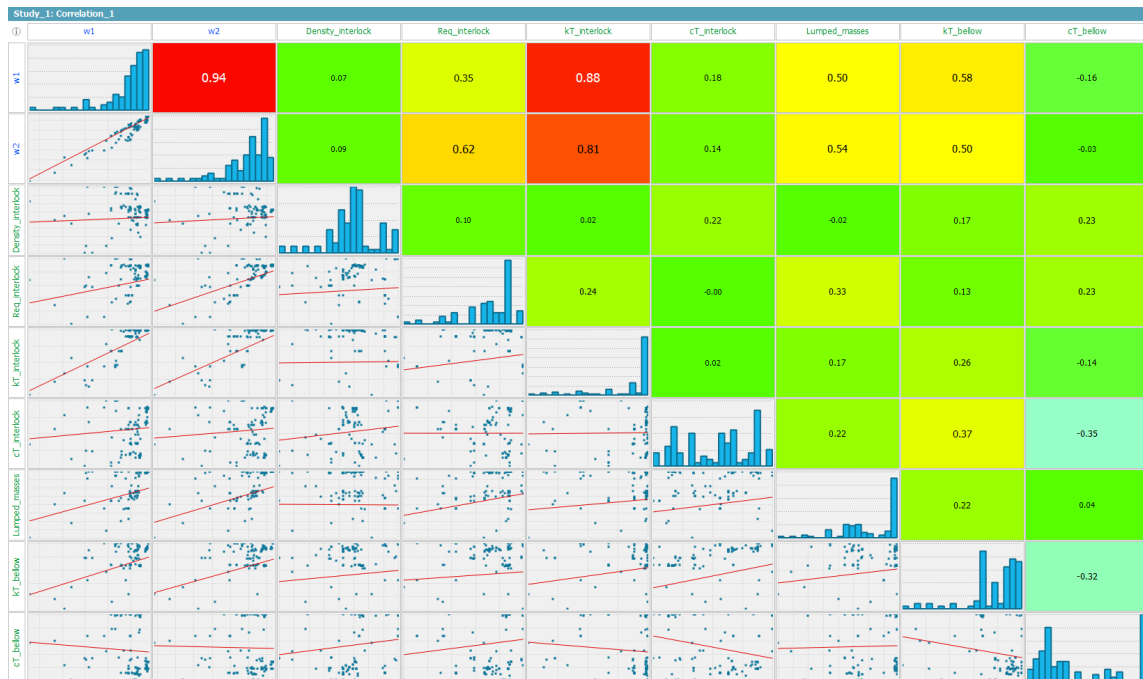
Figure C.0.3: **Correlation plot from optimization process on flexible hose B.**